Investigating the role of vaccinia virus binding proteins in host cell entry

Laura Pokorny

A dissertation submitted in partial fulfillment

of the requirements for the degree of

Doctor of Philosophy

of

University College London.

MRC Laboratory for Molecular Cell Biology

University College London

December 2020

I, Laura Pokorny, confirm that the work presented in this thesis is my own. Where information has been derived from other sources, I confirm that this has been indicated in the work.

Abstract

Poxviruses enter cells using the most complex binding and fusion machinery identified to date. Studies indicate that vaccinia virus fusion relies on eleven, and binding on at least four, distinct proteins. Understanding, and subsequently blocking, viral entry is the first and most effective line of defence we have against infection. Therefore, in-depth knowledge of this complex process is paramount.

The development of new and effective tools to aid the study of virus entry is important. To this end, I developed a minimal model system based on cell-derived membrane blebs. Blebs are advantageous due to their smooth surface, small size and the fact that they retain the original cell surface composition. Using this system, I found that VACV virions bind in a side-on orientation, and that this can be altered to become more tip bound by removing a subset of the binding proteins. Blebs also enabled the identification of a novel VACV, cellular membrane remodelling mechanism. Under low-pH conditions the binding protein D8 induces cellular membrane invagination. During virus entry via low-PH dependent macropinocytosis this membrane remodeling promotes productive infection by increasing the contact between the limiting membrane of the macropinosome and the viral fusion machinery which is found exclusively at the tips of the virion. From these findings, I conclude that VACV binding and fusion are more intimately linked than first thought.

Furthermore, I characterised VACV binding to an unprecedented degree revealing hierarchies and redundancies between the four binding proteins. The high level of redundancy and the ability of the virus to adapt to the binding environment presented on target cells is likely to account for the cell-type and host promiscuity displayed by VACV.

Impact Statement

Viral disease represents one the world's greatest socio-economic burdens. Increased international travel, population growth and climate change resulting in shifting viral vectors all contribute to the emergence of new, and often deadly, viruses. What's more, the deliberate introduction of viral disease through bioterrorism remains a large threat. At the same time, viruses are becoming increasingly important in biotechnology as vaccine vectors and in gene and cancer therapies. Therefore, detailed understanding of the complexity of viral particles and the development of new model systems to study them is important.

Poxviruses are highly significant in terms of both disease burden and biotechnology. Variola virus, the causative agent of smallpox, remains the deadliest in human history accounting for more than 500 million deaths worldwide. To date, it is the only viral disease to be successfully eradicated thanks to a mass vaccination campaign by the World Health Organisation (WHO) (World Health Organization, 1980; Barquet et al., 1997). Vaccinia virus (VACV) was used as the immunological agent of the smallpox vaccine and, in more recent times, has gained clinical significance as a promising anti-cancer therapy. Its relative safety has lead it to be used as the model poxvirus in the lab. Due to the ongoing threat of smallpox re-emergence through bioterrorism and outbreaks of zoonotic poxviruses, the study of VACV remains vital.

Due to host cell complexity, minimal membrane systems are widely employed to study viral binding and fusion. These systems are easily generated, readily perturbed and, in comparison to cells, are very small enabling imaging of thousands of events in a single frame. Here, I developed a novel minimal model system based on

cell-derived membrane blebs to study viral binding and fusion and demonstrated its effectiveness with VACV. Blebs as a model system enabled me to study the binding orientation and membrane remodelling activity of the virus under biomimetic conditions. This system is expected to have impact in the wider virus research community through its use with other viral pathogens, leading to exciting and novel discoveries in their entry mechanisms.

In addition to the development of this new tool, this thesis also characterises VACV binding to an unprecedented degree. Using the Mercer lab's large toolbox of mutant viruses and cell lines, the interplay between the four known viral binding proteins and their association with the cell surface was thoroughly examined. These findings highlight the degree of complexity involved in VACV-cell surface association and will be highly informative in anti-viral drug design. Further, this study could provide insight into the binding patterns of other complex viruses.

Acknowledgements

Completing this PhD in 2020 obviously came with many unforeseen challenges. I am thankful to everyone who supported me, helped me navigate lab work during the pandemic and kept me positive. The LMCB has been a wonderful place to undertake a PhD and moving to the University of Birmingham for the last few months was an exciting change. So I would like to start by not exactly thanking SARS-CoV-2, but realising the new opportunities that arose because of it.

First and foremost, a huge thank you to Jason. Your support and unyielding positivity was instrumental in getting me through this PhD. Thank you for always having your door open for discussion (scientific or otherwise), for teaching me that you can always learn something from failed experiments and, most importantly, for showing me that research is, above all, to be enjoyed! What's more, thank you for instilling a 'work hard play hard' attitude in us all and for your generosity in the pub! I hope we will be able to get in one last G&T before I leave.

David - thank you entrusting me with this project and teaching me everything I know about microscopy. You are one of the most patient and kind people I have ever met and I was extremely lucky to have your guidance in the first year and a half of my PhD. I (almost) even miss your surprise science quizzes!

To the many Mercenaries past and present - thank you for making the lab such a fun place to be for the last 3.5 years. Everyone was so kind and helpful when I first joined (even though adding another person to the already huge lab was a contentious issue!). In particular, Hattie - I feel so lucky to have made such a close friend in you through this PhD. You are incredibly strong and I have learnt so much from you - in science and out of. Thank you for an unforgettable trip travelling around the

Philippines.

I would especially like to thank Mariann, Becky and Jerzy for the monumental task setting up the lab in Birmingham and making my time there so enjoyable.

Jemima - I cannot thank you enough for your patience and perseverance with the many EM samples we worked on together. This project would be no where near as complete without you. Thank you for never giving up on me even after the many terrible bleb samples I prepped!

Importantly, a huge thank you to my wonderful best friends and housemates throughout this PhD - Ellie, Lizzy and Molly. You honestly have no idea how much your support means to me. Writing a thesis in a global pandemic was never going to be easy and I don't know what I would have done without you all. And I hope that one day I can come back as a day user of Three Werk - the best office there ever has been! I really miss you all terribly.

Thank you to my whole family. To my parents, Helen and Mike, without your unconditional support and belief I would never have been able to start, let alone finish, this PhD. Sarah - you are an absolute inspiration and you will, without a doubt, make a fantastic scientist.

Finally, Rob - meeting you the single best thing to come out of this PhD. Thank you for still discussing vaccinia related issues with me two years after you left the lab. Thank you for being my biggest cheerleader and never letting me give up. And, of course, thank you for moving out to Birmingham with me. Without you, I honestly don't know how I would have got to this point.

Contents

List of Figures

List of Tables

Abbreviations

AFM	Atomic force microscopy
BBB	Blood brain barrier
CEV	Cell-associated enveloped virus
CPV	Canine parvovirus
CPXV	Cowpox virus
CS	Chrondroitin sulfate
CSPG4	Chondroitin sulfate proteoglycan 4
DAB	3,3-diaminobenzidine
dSTORM	(direct) stochastic optical reconstruction microscopy
EEV	Extracellular enveloped virus
EFC	Entry fusion complex
EM	Electron microscopy
EV	Extracellular virion
FFWO	Fusion from without
GAG	Glycosaminoglycan
GPMV	Giant plasma membrane vesicle

GUV	Giant unilamellar vesicle
HCV	Hepatitis C virus
HIV	human immunodeficiency virus
HRP	Horseradish Peroxidase
HRP	Horseradish peroxidase
HS	Heparan sulfate
HSV	Herpes simplex virus
IAV	Influenza virus A
IB	Intracellular buffer
IHD-J	International Health Department-J
IMV	Intracellular mature virion
IV	Immature virion
IV	Immature virions
IVN	Immature virions with a nucleoid
JAM-A	Junctional adhesion molecule A
LBs	Lateral bodies
LRC	Ligand Receptor Capture
MOCV	Molluscum contagisom virus
mPy	Mouse polyomavirus
MV	Mature virion
PFU	Plaque forming unit

PS	Phosphotidylserine
PSCR1	Phospholipid scramblase-1
RT-qPCR	Reverse transcription-quantitative polymerase chain reaction
RVFV	Rift valley fever virus
SIM	Structred illumination microscopy
Sindbis virus	SINV
SLB	Supported lipid bilayer
SPR	Surface plasmon resonance
SPT	Single-particle trafficking
SV40	Simian virus 40
TfR	Transferrin receptor
TIRFM	Total internal reflection microscopy
VACV	Vaccinia virus
VARV	Variola virus
VLPs	Virus like particles
VSV	Vesicular stomatis virus
WR	Western reserve
WV	Wrapped virion
XL-MS	Crosslinking mass spectrometry

Chapter 1

Introduction

1.1 A general overview of the poxviruses

Poxviruses represent some of the largest and most complex viruses known. They are divided into two subfamiles: the vertebrate infecting *Chordopoxvirinae* and the insect infecting *Entomopoxvirinae*. The *Chordopoxvirinae* contain eight genera: *Orthopoxvirus, Parapoxvirus, Avipoxvirus, Capripoxvirus, Leporipoxvirus, Suipoxvirus, Molluscipoxvirus* and *Yatapoxvirus*, with only the *Orthopoxvirus, Parapoxvirus, Molluscipoxvirus* and *Yatapoxvirus* able to infect humans. The *Orthopoxvirus* are the most well studied and contain several poxviruses capable of infecting humans: vaccinia virus (VACV) - the subject of this thesis, variola virus (VARV) - the causative agent of smallpox, monkeypox virus (MPXV), molluscum contagiosum virus (MOCV) and cowpox virus (CPXV) (Figure 1.1). Interestingly, although it was once thought that host and poxvirus have co-evolved (Fenner and Kerr, 1994), phylogenetic analysis based on the amino acid sequence of 29 conserved poxvirus genes suggests that transfer from one host to another has been a recurrent feature in the evolution of the *Chordopoxvirinae* (Hughes et al., 2010) (Figure 1.1).

Poxviruses contain linear, double stranded DNA genomes with the two strands connected at their termini (Geshelin and Berns, 1974; Baroudy and Moss, 1982). The DNA ranges from 130 to 350 kilobase pairs (kbp) and encodes for 130-328 genes (Fields et al., 2007). Among these, over 100 genes are conserved in the chor-

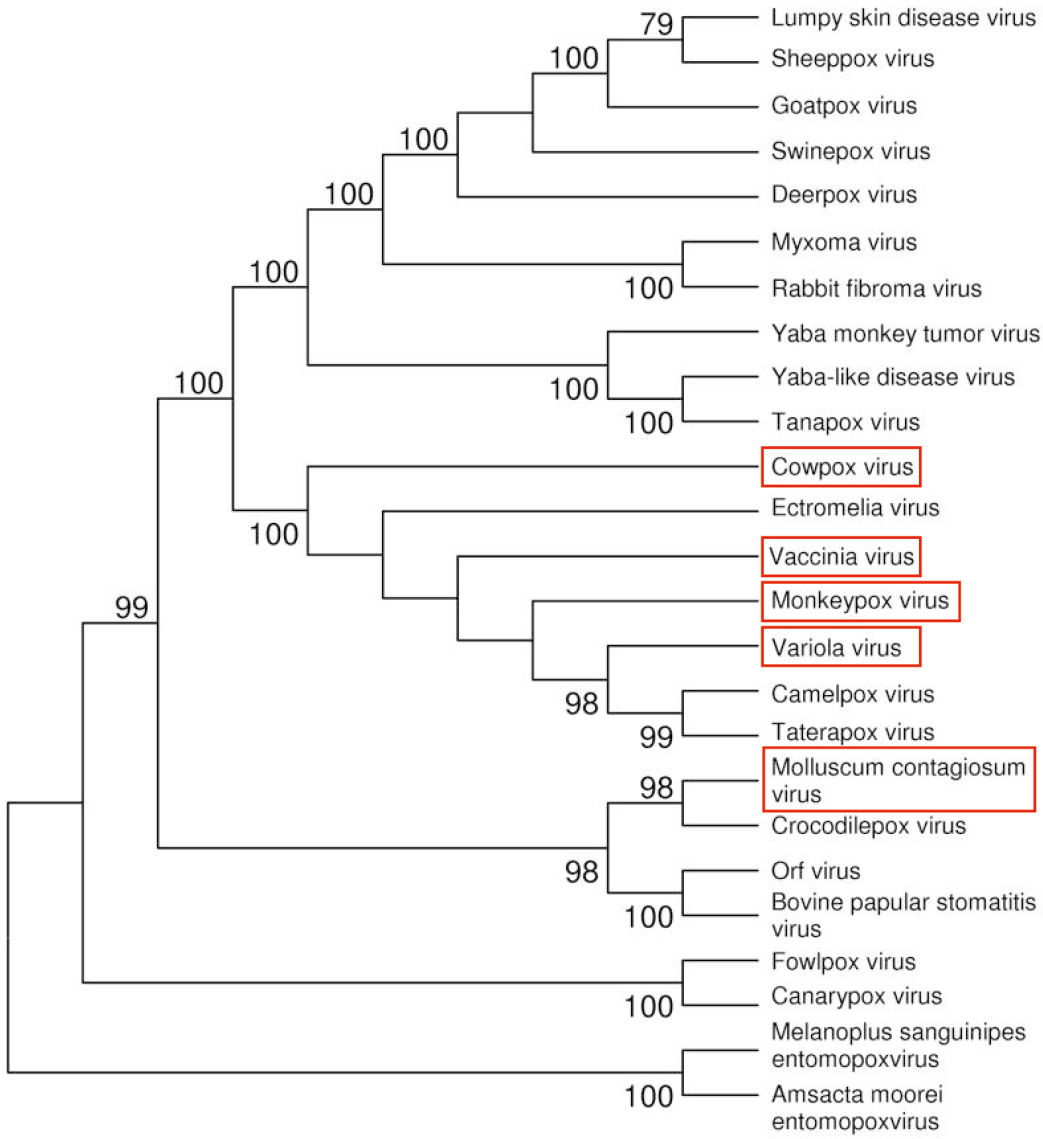

Figure 1.1: Phylogenetic tree of the poxvirus family. The phylogenetic tree based on concatenated amino acid sequences from 29 conserved genes. The numbers on the branches represent percentages of 1000 bootstrap samples supporting each branch. Red boxes signify the primary human pathogens. Adapted from (Hughes et al., 2010)

.

dopoxviruses and 66 genes are conserved in all poxviruses (Fields et al., 2007). Differing from most other DNA viruses, poxviruses replicate entirely in the cytoplasm independently of the nucleus. However, the host cell nucleus is still needed for productive infection, seemingly for the maturation stage and later (Prescott et al., 1971; Hruby et al., 1979b,a; Silver et al., 1979). Accordingly, the genome encodes for factors involved in both transcription and DNA replication (Fields et al., 2007).

Poxviruses are highly successful pathogens, due in part to their broad host range. They can infect many cell types from many different species (Hruby, 1990; McFadden, 2005). For vaccinia, exceptions appear to be natural killer cells and resting T cells (Chahroudi et al., 2005). In host organisms, poxvirus infection can occur through the airway (VARV), skin lesions (MOCV), or ingestion (entomopoxviruses) (Mitsuhashi et al., 2007; Fields et al., 2007). Further, the spread and pathogenesis caused depends on the immune response of the host which, in turn, is strongly manipulated through the many virus encoded immunomodulatory genes (Seet et al., 2003; Bidgood and Mercer, 2015). Interestingly, although many poxviruses show strict species specificity in terms of their zoonotic host, this can differ *in vitro* - in cell culture some poxviruses show a host-cell specificity unique from its *in vivo* host range (McFadden, 2005). An example of this is the rabbit-specific poxvirus, myxoma, which replicates well in transformed human cell lines (Stanford et al., 2007).

VARV, the causative agent of smallpox, is the most notorious member of the *Poxviridae*. Smallpox is regarded as the most deadly infectious disease known, causing the death of over 300 million people in the 20th century alone (Geddes, 2006; Li et al., 2007). The breakthrough in combating smallpox came in the 18th century when Dr. Edward Jenner found that inoculation with CPXV could protect against smallpox infection. Subsequently, smallpox was eradicated by vaccination in 1977 following the most successful global eradication program in history (World Health Organization, 1980; Barquet et al., 1997). Eradication was enabled by the fact that there is no animal reservoir, the time from exposure to the appearance of the first symptoms is fairly short and infection with the virus or with the smallpox

vaccine induced life long immunity.

Vaccinia virus is the immunological agent of the smallpox vaccine and is now widely used as the laboratory prototypic poxvirus. The origin of VACV has been controversial, however it is now thought to have been derived from horsepox (Esparza et al., 2017). The study of VACV remains relevant today due to the potential use of poxviruses in bioterrorism (Selgelid, 2004), the importance of poxviruses as therapeutic vectors (Sánchez-Sampedro et al., 2015) and the use of VACV as tool for technological advancements (Bidgood, 2019).

1.2 Vaccinia virus morphology

VACV, as with other poxviruses, produce two types of infectious particles: intracellular mature virions (MVs or IMVs) and extracellular virions (EVs). EVs can be released from the cells as cell associated (CEVs) or extracellular (EEVs). MVs are brick-shaped particles with the approximate dimensions of 360x270x250 nm (Cyrklaff et al., 2005). EVs are MV-like particles surrounded by a second membrane which contains at least 6 viral proteins unique to the EV (Figure. 1.2, (Payne, 1978, 1979; Smith et al., 2002)).

Vaccinia virus was the first animal virus to be visualised with electron microscopy (EM) (Nagler and Rake, 1948), with later studies revealing a more detailed view of the core, which houses the DNA, and the lateral bodies (LBs), small structures sitting adjacent to the core (Dales and Siminovitch, 1961; Peters and Muller, 1963) (Figure. 1.2). The MV membrane became a source of controversy with some studies claiming that it was in fact a double membrane (Roos et al., 1996) and others that the core itself was surrounded by a membrane (Sodeik et al., 1993) or palisade layer (Dubochet et al., 1994). Variations in the interpretation of the VACV structure most likely arose from the use of different preparation techniques. To this end, cryo-preparation began to be used as vitrification helps avoid artefacts. Cryo-EM methods were first used in 1994 (Dubochet et al., 1994) and, more recently, Cyrklaff *et al.* (2005) and Heuser *et al.* (2005) have used cryo-preparation to show a clearer picture of the structure (Cyrklaff et al., 2005; Heuser, 2005). Additionally, atomic

force microscopy (AFM) has been used to compliment the EM data as, although the resolution is theoretically lower, you gain topographical features of the surface and do not rely on homogeneous samples (Kuznetsov et al., 2008).

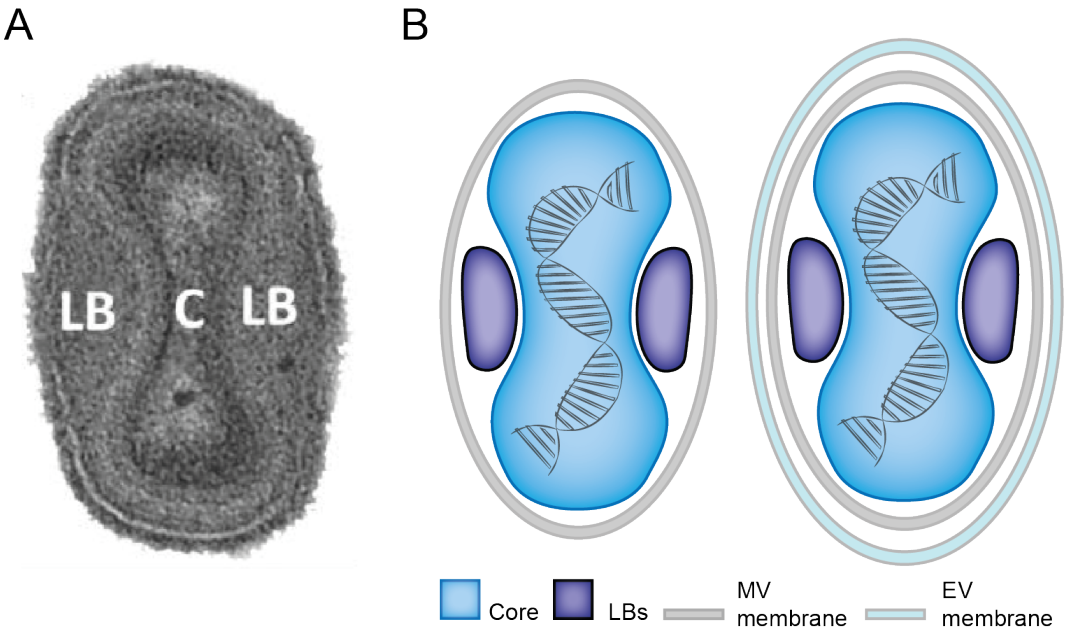

Figure 1.2: VACV structure. The structure of VACV as seen by A) electron microscopy (image courtesy of Dr. Jason Mercer) and B) as a graphical representation of an MV and EV particle.

Eventually it was established that the virion consists of a central, biconcave core in which the genome is densely packaged (Figure. 1.2, (Cyrklaff et al., 2005; Heuser, 2005; Condit et al., 2006)). The core contains multiple organised protein layers which, in the past, have been misinterpreted as a membranous layer (Sodeik et al., 1993).

The LBs are proteinacious structures (Ichihashi et al., 1984) which sit within two concavities in the core (Figure 1.2). Their full function still remains to be determined, however it has been shown that they deliver immunomodulators to the cytosol (Schmidt et al., 2013a). The particle is surrounded by a single lipid membrane containing at least 25 highly cross-linked proteins (Heuser, 2005; Szajner et al., 2005; Cyrklaff et al., 2005; Fields et al., 2007). The combined treatment of detergent and reducing agent is needed to solubilise them fully (Easterbrook, 1966).

Various methods have been used to analyse the composition of the virion. 1-D

and 2-D gel electrophoresis were the first techniques used (Holowczak and Joklik, 1967; Sarov and Joklik, 1972; Stern and Dales, 1976; Essani and Dales, 1979), which separated the polypeptides based on size and gave some basic information such as relative abundance. Later, fractionation studies made it possible to discern core and membrane proteins (Ichihashi et al., 1984; Jensen et al., 1996). Various mass spectrometry approaches have aided a more complete virion composition (Chung et al., 2006; Yoder et al., 2006; Resch et al., 2007) and immuno-EM has been used to confirm the broad localisation of various proteins (Roos et al., 1996; Schmidt et al., 2013a). To this end, super-resolution imaging techniques have been used to map viral proteins more accurately and this revealed a distinct polarisation of the fusion and binding proteins on the MV membrane (Gray et al., 2016, 2019). Additionally, the interactions between proteins in the virion have begun to be understood (Matson et al., 2014; Novy et al., 2018; Mirzakhanyan and Gershon, 2019). The consensus now is that particle contains upwards of 80 different viral proteins, as well as some 63 cellular proteins (Ngo et al., 2016).

1.3 A general overview of viral entry

1.3.1 Viral binding and uptake

The cellular membrane presents as the first barrier between the viral particle and the intracellular environment. The very first step in viral entry is binding and fusion, the overarching topic of this thesis. This section aims to deliver a general discussion on mechanisms toward viral entry using relevant examples and establishes principles that have shaped the interpretations of the data presented in this thesis.

Primary attachment of the virus to the cell surface is often mediated by non-specific binding with glycoconjugates or lipids (Young, 2001) and the requirements for this vary greatly between viruses. This primary attachment allows the viral particle to move toward the cell body using actin retrograde flow (such as in the case of herpes simplex virus (HSV) (Clement et al., 2006; Dixit et al., 2008), VACV (Mercer and Helenius, 2008), human papillomavirus-16 (Schelhaas et al., 2008), hepatitis C virus (HCV) (Coller et al., 2009) and human immunodeficiency virus (HIV)

(Lehmann et al., 2005)), or to just simply diffuse across the cell surface until it encounters its specific receptor(s) or is able to signal for endocytosis or fusion (Marsh and Helenius, 2006; Mercer et al., 2010b; Grove and Marsh, 2011; Yamauchi and Helenius, 2013; Boulant et al., 2015; Ketter and Randall, 2019). Therefore, this movement is highly important to the entry process of the virus. However, movement of virus on the cell surface is difficult to study. Single-particle tracking (SPT) with total internal reflection microscopy (TIRFM) has been used successfully in some cases. TIRFM uses an evanescent wave to selectively illuminate and excite fluorophores in a thin region, usually less than 200 nm from the coverslip. This functions to remove out-of-focus fluorescence and enhance the signal to noise ratio. Thus TIRFM is a good choice for single molecule studies. TIRFM and SPT have been used to study the movement of Mouse Polyomavirus (mPy) on the cell surface and it was found that mPY randomly diffuses on the plasma membrane for 5-10s before confinement in a cortical actin dependent manner (Ewers et al., 2005). This random diffusion was cholesterol dependent and essential for infectivity. After confinement, mPy signals to induce endocytosis. Confinement and endocytosis were not directly linked, as the tyrosine kinase signalling needed for endocytosis was not needed for confinement (Ewers et al., 2005).

The movement of viral particles on the plasma membrane can also function to bring the viral particle to the endocytic pit directly (Johannsdottir et al., 2009; Cureton et al., 2012). This was first shown with Vesicular stomatitis virus (VSV) (Johannsdottir et al., 2009). VSV was shown to utilise two methods of associating with clathrin coated pits: it could remain immobile on the surface and induce the formation of the pit beneath it, or it could move laterally along the membrane and become trapped in a preformed clathrin-coated membrane domain (Johannsdottir et al., 2009). Canine parvovirus (CPV) was shown to actively diffuse across the membrane before rapid interaction with a pre-formed clathrin coated pit. The interaction of CPV with the transferrin receptor (TfR) was essential to the highjacking of the preformed pit: weak binding of CPV to the TfR aided viral diffusion across the membrane and the interaction was broken prior to viral uptake by the pit (Cureton

et al., 2012).

In some cases, a co-receptor is also required alongside the primary receptor. HIV-1 displays transient interactions with the plasma membrane before immobilisation in a heparan sulphate dependent manner (Endreß et al., 2008). This is hypothesised to allow the virus to find its specific primary receptor CD4 (Endreß et al., 2008). The co-receptors, CCR5 or CXCR4, are then required to facilitate the conformational change leading to efficient virus-cell membrane fusion (Chen, 2019).

These examples demonstrate that the, often overlooked, primary attachment of virus is highly complex and can reveal novel and important information on viral entry. Moreover, studying entry with SPT is important as it collects real time, single virion data which can highlight dynamics lost in bulk measurements.

After primary attachment, the virus can bind to the cell surface via its specific receptor. Receptor binding may be multi-valent and lead to the formation of receptor rich domains that can activate cellular signalling pathways or cause structural rearrangements in the virus which directly facilitates endocytic uptake or direct penetration (Figure. 1.3) (Greber, 2002; Mercer et al., 2010b; Thorley et al., 2010; Grove and Marsh, 2011; Boulant et al., 2015). For direct penetration, enveloped viruses, such as HIV-1 (Stein et al., 1987), can fuse directly with the plasma membrane (Figure. 1.3) (HIV-1 has also been reported to enter by endocytosis (Fackler and Peterlin, 2000; Daecke et al., 2004; Maurin et al., 2007)), whilst non-enveloped viruses such as poliovirus, disrupt the plasma membrane or form a pore to gain entry (Dunnebacke et al., 1969; Bubeck et al., 2005). For endocytic entry, some viruses take advantage of receptors with known endocytic receptor function, such as HCV and the LDL receptor (Agnello et al., 1999), whilst many other viruses use receptors whose role in viral entry is still unknown (Boulant et al., 2015).

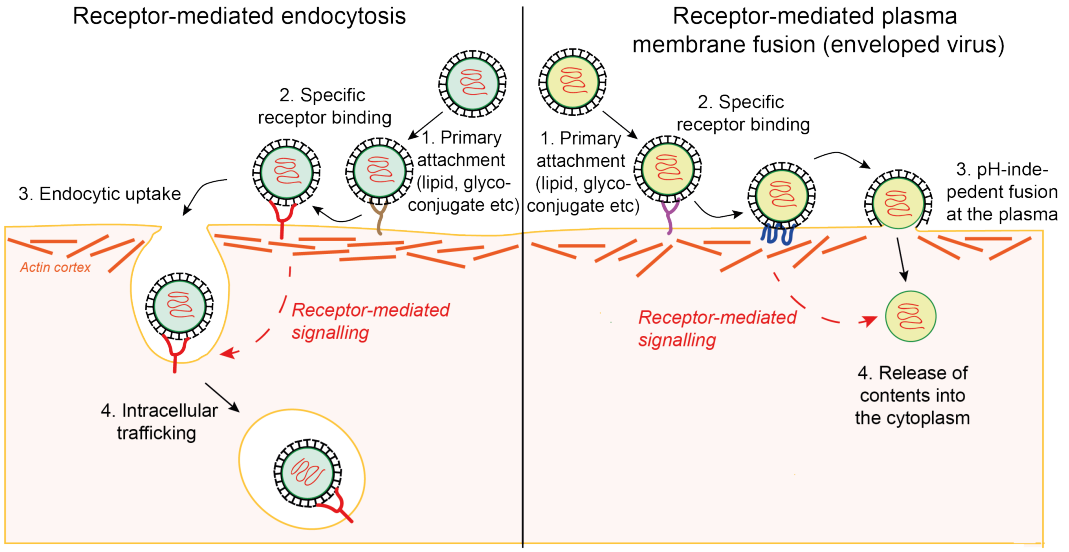

Figure 1.3: Strategies for viral entry. Viruses employ two main strategies for entry into the host cell: endocytic entry (left) and direct penetration of the plasma membrane (right; shown for an enveloped virus). Virus binds first to non-specific attachment factors and then to specific receptors which mediate cellular signalling, facilitating virus uptake.

Endocytosis appears to be the dominant route of viral entry, even if plasma membrane fusion is possible (Mercer et al., 2010b; Nicola et al., 2013). This is most likely because endocytosis offers many advantages to incoming pathogens: it allows the virus to bypass the actin cortex and cytoplasmic crowding whilst exploiting cellular molecular motors, the lowering of the pH within the endosome allows escape at specific locations and virus is protected from immunosurveillance within the endosome (Marsh and Helenius, 2006; Mercer et al., 2010b). Most, if not all, forms of endocytosis are exploited by viruses and, indeed, many were discovered by studying viral entry. Clathrin-mediated endocytosis, caveolar/raft-dependent endocytosis, phagocytosis and macropinocytosis are just a few examples of which multiple viruses take advantage (Mercer et al., 2010b).

1.3.2 Viral fusion

As discussed above, all enveloped viruses must fuse with the cellular membrane, either at the cell surface or within the endosome, in order to enter the cell. Catalysis of virus-cell membrane fusion is necessary as, although fusion is thermodynamically favourable, there is a high kinetic barrier to overcome (Chernomordik and Kozlov,

2003; Chernomordik et al., 2006). The cellular and viral membrane must overcome the repulsive 'hydration force' caused by the interaction of water layers with the polar heads of the lipids (Boden and Sixl, 1986). To this end, viruses must display on their surface a glycoprotein able to catalyse fusion - the fusion protein. The fusion protein is held in a native, prefusion conformation until being triggered in some way, most likely by engagement with a cellular receptor or in response to lowering of pH. In the case of low pH, the proton acts as a trigger. This triggering acts to expose the fusion peptide on the protein (Harrison, 2015). Unlike intracellular fusion proteins such as SNAREs which show reversible priming, viral fusion proteins are almost all 'suicide proteins' - their priming is irreversible. The G protein of VSV appears to be the exception to this rule. G protein can undergo an reversible conformational change (Roche et al., 2006). The pre-fusion and post-fusion states are in thermodynamic equilibrium, with the equilibrium shifted towards the post fusion state at low-pH (Roche et al., 2006).

The conformational change of the fusion protein liberates free energy which is then used to bring the membranes together. The widely accepted pathway toward the merging of viral and cellular membrane is as follows: the fusion protein is triggered and enters its 'active' conformation, the 'active' fusion protein forms a bridge between the cellular and viral membrane, a hemistalk is formed, the hemistalk opens to form a transient pore and the fusion protein then refolds to render the open pore state irreversible (White et al., 2008; Harrison, 2009; Cooper and Heldwein, 2015) (Figure. 1.4).

Viral fusion proteins fall into a number of structural classes. Class I fusion proteins are typified by influenza virus HA (Skehel and Wiley, 2000) and HIV gp41 (Chan and Kim, 1998). These proteins are trimers of a single chain precursor, and cleavage forms two fragments, one generating a hydrophobic fusion peptide characterised by an trimeric α-helical domain in the post-fusion complex. The second class of fusion peptide is found on flaviviruses, bunyaviruses and alphaviruses (Kielian, 2006). They are genetically and structurally different from class I proteins but use the same principle and topology to trigger fusions. Class II proteins are usu-

ally beta-sheets and primed by cleavage of a second viral protein (Guirakhoo et al., 1991; Lobigs and Garoff, 1990). Their conformation change involves a change in oligomeric state from prefusion dimers to postfusion trimers. The third class of fusion proteins are found on rhabdo-viruses (G protein), herpesviruses (gB), and group 1 alphabaculoviruses (gp64). This class combines features of the first two proteins: a central trimeric coiled-coil (a hallmark of class I proteins) and three beta-sheet domains with an internal fusion peptide (a hallmark of class II proteins) (Backovic and Jardetzky, 2009).

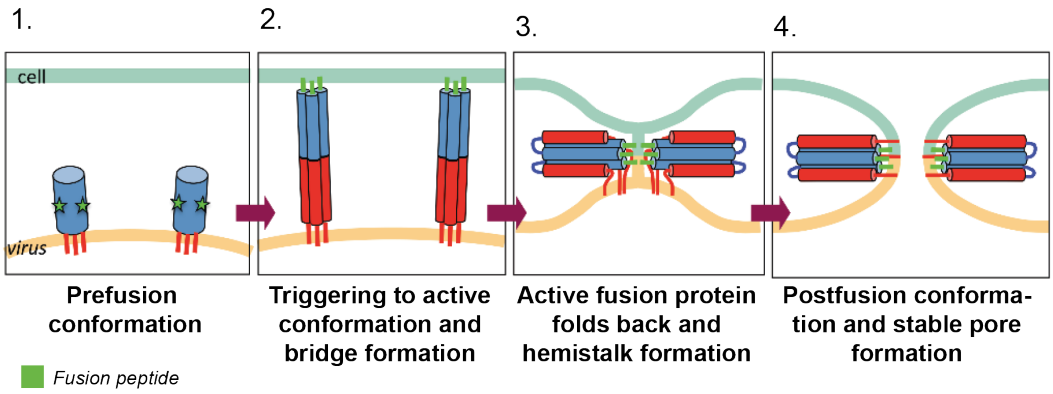

Figure 1.4: Steps of viral membrane fusion. 1. The fusion protein is triggered and fusion peptide exposed. 2. The fusion peptide inserts into the cellular membrane. 3. The fusion peptide folds back on itself bringing the opposing membranes together and a hemifusion intermediate is formed. 4. The fusion protein refolds to its most energetically stable conformation and a pore is formed. Adapted from (Cooper and Heldwein, 2015)

Viruses vary greatly in the number of separate glycoproteins encoded on their surface needed for fusion. Many encode only one protein, which is the fusion peptide. For example, the HIV Env protein (Doms and Moore, 2000). In other cases accessory proteins are essential, such as in the case of the HSV. Four of the twelvec HSV surface glycoproteins are essential for fusion. gB, the fusion protein, is activated by accessory proteins gH and gL, which in turn are activated by the receptor binding protein gD (Cooper and Heldwein, 2015). VACV also requires many proteins for fusion - at least 11 with none known to be the specific fusion protein (Moss, 2012). This will be discussed in more detail in Section 1.4.

1.3.3 Cellular membrane remodelling activity of viruses

As discussed above, the requirements for the receptors involved in binding and fusion are fairly well understood. However, less well studied is the remodelling of the cellular membrane topology, composition and shape in response to viral binding and fusion. It is known that, in some cases, viral binding can alter the lipid and glycoprotein availability as well as the physical membrane curvature of the cellular membrane. In the following section, this remodelling is explored and the emerging understanding that viral binding is a highly active process leading to large-scale cell surface modification to support entry is highlighted.

HSV-1 provides an example of viral induced cellular lipid remodelling. HSV-1 binding activates phospholipid scramblase-1 (PSCR1) to flip cellular phosphatidylserine and Akt from the inner to outer leaflet (Cheshenko et al., 2018). This induces the Akt1 signalling cascade needed for HSV-1 endocytosis. HSV-1 gL protein then binds PSCR1 to promote the relocalisation of phosphatidylserine to the inner membrane, preventing the cell from being marked as apoptotic and subsequent phagocytic uptake (Cheshenko et al., 2018).

Virus binding can also remodel the plasma membrane through the recruitment of secondary, specific receptors. However, its very difficult experimentally to show whether virus binding to the primary receptor recruits the specific secondary receptors, or if the secondary receptors move toward the virus/primary receptor complex (Boulant et al., 2015). The model suggested for reoviruses is that the virus binds its primary receptor, sialic acid, allowing it to bind its specific receptor $\beta 1$ integrin. This binding reaction then recruits and induces the clustering of the junctional adhesion molecule A (JAM-A). JAM-A mediates the internalisation of the reovirus particle (Barton et al., 2001; Maginnis et al., 2006; Cera et al., 2009; Boulant et al., 2015).

Remodelling of the membrane to induce curvature to support viral entry is common, both in endocytosis and in supporting fusion. The curvature induction can be negative or positive. Positive curvature induction has been studied in detail with influenza A virus (IAV) using cryo-EM (Lee, 2010; Gui et al., 2016). Cryo-

EM is the only technique at present which allows high resolution of membrane leaflets, fusion proteins and other features of virus ultrastructure under near-native conditions. Using liposomes as a membrane model system that supports fusion, four separate intermediates leading to fusion were visualised. One of these steps involves the puckering of the target membrane in response to low-pH, drawing the dimple toward the unperturbed viral membrane through the refolding action of a small number of clustered HA spikes (Figure. 1.5A) (Lee, 2010; Gui et al., 2016). Localized dimpling is hypothesised to minimise the initial penalty from dehydration of the two membranes, allowing a small contact zone to form (Gui et al., 2016).

Negative curvature induction is more common and well studied. Simian virus 40 (SV40) was shown to induce dramatic membrane curvature on the plasma membrane (Figure. 1.5B) as well as on artificial membranes (Figure. 1.5C) (Ewers et al., 2010). This directly induces its endocytic uptake, which differs from viruses which rely on cell driven processes. The invagination depends on the multivalent interaction between capsid VP1 pentamers and the GM1 receptor molecule, leading to the clustering of GM1 on the membrane (Ewers et al., 2010). In a similar manner, human norovirus binds and clusters glycosphingolipids to induce tubular invaginations on artificial membranes (Figure. 1.5D) (Rydell et al., 2013).

Both of these pieces of work demonstrate, using minimal systems, that cellular factors (e.g receptors) are not always needed for curvature induction leading to endocytic internalisation. In these cases, the interactions leading to curvature occur on the external side of the membrane, differing from receptor-mediated endocytosis where the intracellular domains of trans-membrane proteins provide sites for coatomers to bind to and to deform membrane (Ewers and Helenius, 2011). Therefore, the virus must generate the force to deform the membrane itself. This is likely to arise from the binding energy generated from the multi-valent interactions between the coat protein and the membrane lipid (Ewers and Helenius, 2011). The virus can ‘wrap’ itself in the membrane using a zipper-like mechanism. Moreover, it is likely that the viral induced clustering of lipids on the membrane creates a lipid domain with a distinct composition from the bulk membrane. This creates line

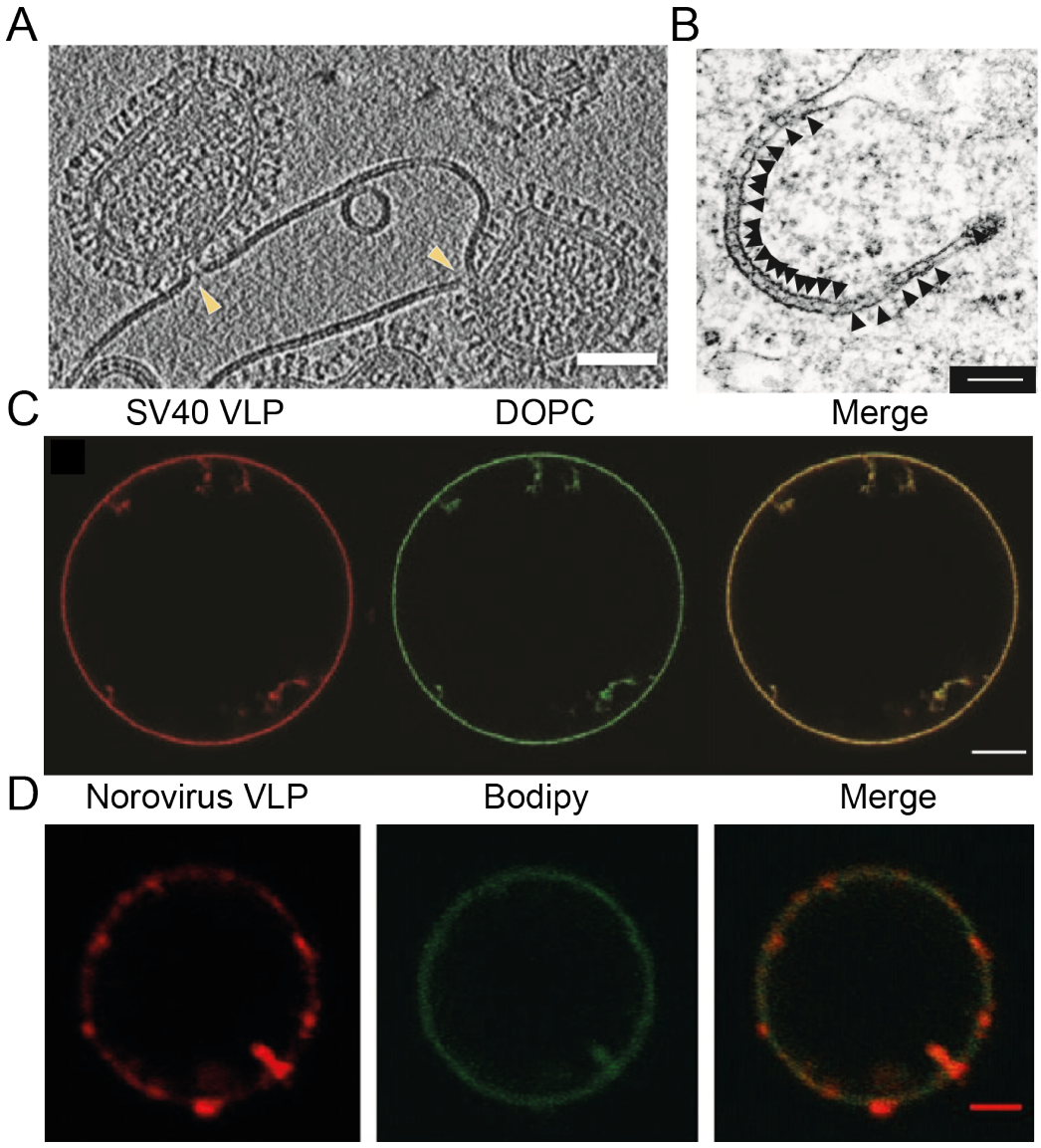

Figure 1.5: Viral remodelling leading to cellular membrane curvature. A) 3.2 nm think computational slice of a cryo-EM tomograph of IAV induced invagination with liposomes at pH 5.5 for 30 min. Yellow arrows point to pinching of liposome membrane. Scale bar, 50 nm. Adapted from (Gui et al., 2016). B) Electron micrograph showing SV40 virus like particles (VLPs) inducing caveolin-independent invagination in the plasma membrane of CV-1 cells after 30 min incubation. Black arrows show viral particles. Scale bar, 200 nm. Adapted from (Ewers et al., 2010). C) Confocal section showing tubule invaginations induced by SV40 VLPS bound to GUVs. Scale bar, 5 µm. Adapted from (Ewers et al., 2010). D) Confocal sections showing tubule invagination produced by human norovirus VLP on GUVs. Scale bar, 2 µm. Adapted from (Rydell et al., 2013)

tension which can lead to membrane invagination (Ewers and Helenius, 2011).

Despite these examples highlighting the importance of viral-induced cellular membrane remodelling in infection, its role in many cases is lacking and understudied. This step of entry must be studied to fully understand viral entry. It is important to revisit the information we have on the entry processes of specific viruses and re-examine these first steps with cellular membrane remodelling in mind. Key to this will be the use of minimal systems and state-of-the-art high-resolution microscopy techniques. Moreover, SPT at high temporal and spatial resolution of virus and lipid on the plasma membrane will be indispensable to dynamic information on the nanoscale level.

1.4 Vaccinia virus life cyle

Having described a general overview of viral entry, I will now focus on the specifics of VACV MV binding, uptake and fusion - the topics of this thesis. Post-fusion steps will then be outlined. The majority of this section will focus specifically on MV entry, as opposed to EV entry.

The complex life cycle of VACV takes place entirely in the cytoplasm of infected cells and, accordingly, the VACV genome encodes for factors involved in both transcription and translation (Fields et al., 2007). In terms of VACV infection, a single-virion single-cell study has shown that 52% of viral particles are blocked at the entry stage of infection and 90% are arrested prior to early gene expression (Stiefel et al., 2012), highlighting how critical the early steps in infection are. In addition to this, VACV was shown to display cooperative behaviour in the early stages of infection, likely acting to increase the chance of productive infection (Stiefel et al., 2012).

1.4.1 Binding

The replication cycle starts with binding of VACV to the host cell surface (Figure **??**) through the interaction of cellular glycosaminoglycans (GAGs) and viral membrane proteins. The degree of interaction with specific GAGs appears to vary with cell type, virus strain and experimental condition (Carter et al., 2005; Bengali et al.,

2009; Whitbeck et al., 2009).

The viral proteins known to be involved in binding are A27, H3, D8 and A26. A27, the first VACV binding protein to be identified, binds to the GAG heparan sulfate (HS) (Figure. 4.1) (Chung et al., 1998). This was evidenced by the fact that soluble A27 could bind to BSC40 (Chung et al., 1998; Hsiao et al., 1998) and HeLa cells (Ho et al., 2005); that soluble HS specifically inhibited VACV binding to BSC40 cells (Chung et al., 1998) and that soluble HS can compete with soluble A27 for binding to the cell surface (Chung et al., 1998). However, this data does not categorically prove that the A27-HS interaction is important in VACV binding. For example, there has been no published data showing that A27(-) virions bind less well to cells than WT, or that A27(-) virions show reduced heparan binding activity.

In addition to its role in viral binding, A27 was first thought to be a viral fusion protein. A27(-) virus was reportedly unable to induce syncytia when bound to cells and treated with low-pH (Vázquez et al., 1999). What's more, the co-expression of A27 protein and its membrane anchor, A17, in both mammalian and insect cells triggered cell-cell fusion (Kochan et al., 2008). However, the contradictory observations that virus lacking A27 had no defect in MV production (Vázquez et al., 1999; Gray et al., 2019) and the discovery of 12 distinct proteins needed for VACV fusion (Moss, 2012) led to the conclusion that A27 does not have a direct role in fusion.

A27 is also needed for the microtubule dependent transport of MVs from viral factories to the trans-golgi network (Sanderson et al., 2000) and subsequently for the wrapping of the intracellular mature virion (IMV) (Ward, 2005). More recently, Gray *et al.* (2019) have shown that A27 is needed for the polarisation and clustering of the fusion proteins and suggest that it is this role in protein organisation which aids the efficient fusion of the virus, explaining why A27(-) virus cannot induce syncytia to the levels of WT (Gray et al., 2019).

The protein H3 is a VACV membrane protein, inserted into the membrane post-translationally and tethered by the C-terminal hydrophobic domain during particle maturation (da Fonseca et al., 2000a). It was shown to bind to HS (Figure. 1.6) (Lin et al., 2000). Evidence for this is that soluble H3 was shown to inhibit binding and

infection of VACV in a dose dependent manner (Lin et al., 2000); soluble H3 was shown to bind to BSC40 cells and that competition with heparin, but not chondroitin sulfate (CS), inhibited this binding. Additionally, soluble H3 bound poorly to gro2c cells which lack HS on the cell surface, although it should be noted that there was some binding (Lin et al., 2000). Although Lin *et al.* (2000) suggested that H3 plays key a role in binding, da Fonseca *et al.* (2000) suggested that its role as a binding protein was not so important. They showed that ΔH3 virus and WT had similar rates of binding in an infectious-centre assay. However, this assay only compares binding of infectious particles so, arguably, does not fully assay binding capacity. This is especially true for the ΔH3 virus which, in the same paper, is reported to have a defect in maturation (da Fonseca et al., 2000b).

In addition to a role in viral binding, virus lacking H3 shows a small plaque phenotype (Lin et al., 2000; da Fonseca et al., 2000b), growth after 24 hours was shown to be about 10-fold less and EV yield was reduced, suggesting H3 has an important role in infection. This was shown to be during conversion of immature virion (IV) to IMV (Lin et al., 2000; da Fonseca et al., 2000b). Moreover, H3 is highly immunogenic in mice, rabbits and humans (Wilton et al., 1986; Zinoviev et al., 1994; Housawi et al., 1998; Davies et al., 2005; Meng et al., 2011; Crickard et al., 2012). H3 also plays a role as a central hub for a sub network of binding and fusion proteins, as determined by protein-protein crosslinking mass spectrometry (XL-MS) (Mirzakhanyan and Gershon, 2019).

D8 binds to the GAG CS (Figure. **??**) (Hsiao et al., 1999). Hsiao *et al.* (1999) demonstrated this by showing soluble D8 bound to BSC40, HeLa and L cells and acted as a competitor of VACV binding. Additionally, the authors showed that virus lacking D8 had a higher particle to plaque forming unit (PFU) ratio than parental virus, which was attributed to reduced cell binding capacity (Hsiao et al., 1999). D8 has been crystalised and shows a carbonic anhydrase fold which houses a positively charged crevice, hypothesised to be the CS binding pocket (Matho et al., 2012). It exists as a non-covalent hexamer, with dimerisation mediated through a C-terminal cysteine (Matho et al., 2014). The optimal CS ligand for D8 binding

was shown to be CSE (Matho et al., 2014). Moreover, chondroitin sulfate proteoglycan 4 (CSPG4) was shown to be one of the most statistically significant binding partners of VACV western reserve (WR) strain using ligand-receptor capture (Frei et al., 2012).

VACV also encodes membrane proteins implicated in virus-cell attachment but do not bind GAGs. The best characterised of these is A26, which binds extracellular laminin (Figure. **??**): WT virus is inhibited by soluble laminin and this effect is not seen when virus lacks A26 (Li et al., 2007). Soluble A26 was also shown to bind soluble laminin by surface plasmon resonance (SPR) analysis (Li et al., 2007). A26 does not have a transmembrane domain and attaches to the virus through binding to A27 (Howard et al., 2008). A26 acts a fusion suppressor bound to the A16-G9 subcomplex and dissociates from the virus at low-pH (Chang et al., 2010, 2012, 2019), however this fusion suppression mechanism seems to be cell type specific (Chang et al., 2010; **?**). In addition to A26, the entry fusion complex protein L1 has been shown to bind to an unknown, non-GAG receptor on cells (Foo et al., 2009) and soluble H3 and A27 can bind to GAG-deficient cells (Lin et al., 2000; Foo et al., 2009) suggesting additional affinity for non-GAG receptors.

Despite understanding a GAG dependence of VACV binding, few studies have looked directly at specific binding receptors. It seems that cholesterol containing lipid rafts are critical for entry (Chung et al., 2005), as well as the association with integrin $\beta 1$ (Izmailyan et al., 2012; Schroeder et al., 2012). VACV also appeared to bind lung surfactant phospholipid DPPG (Perino et al., 2011). Preincubation with DPPG significantly reduced binding of virus to cells and showed a protective effect in mice (Perino et al., 2011). Moreover, the epidermal growth factor receptor may or may not be utilised in virion binding (Eppstein et al., 1985; Orynbayeva et al., 2007). More specifically, on keratinocytes the scavenger receptor MARCO is used for attachment (Macleod et al., 2015). However, the main study toward understanding VACV receptors comes from Frei *et al.* (2012), who utilised ligand receptor crosslinking to show that the cell surface proteins AXL, M6PR, DAG1, CSPG4 and CDH13 are all VACV binding factors on HeLa cells (Frei et al., 2012).

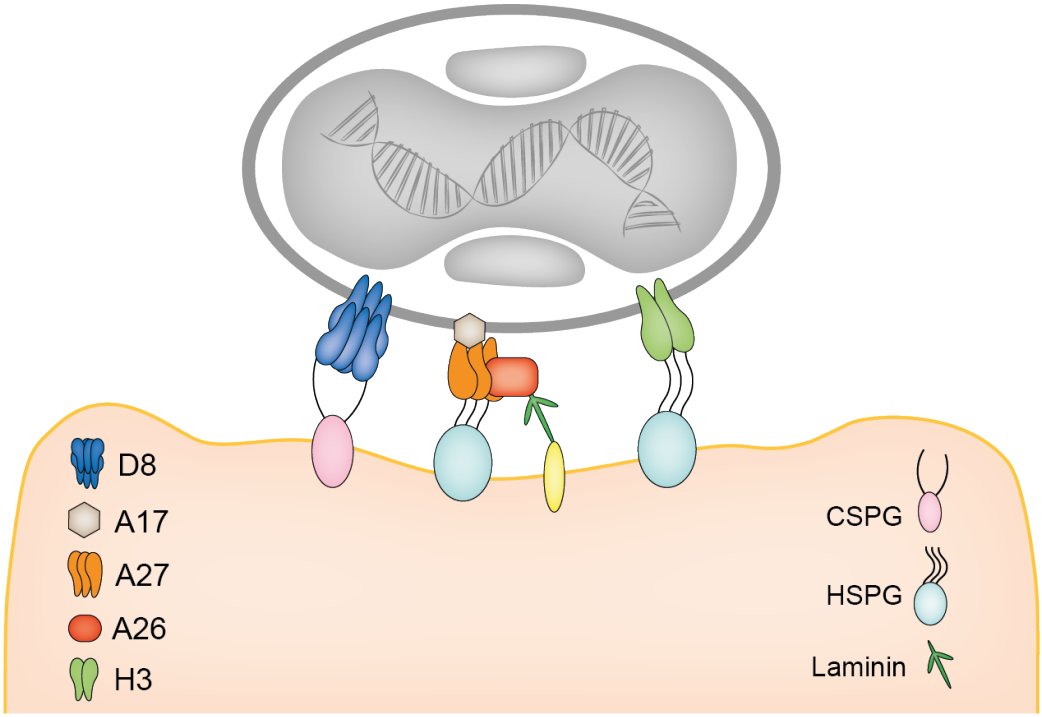

Figure 1.6: Vaccinia virus binding interactions. VACV utilises 4 known interactions for plasma membrane binding. D8 binds chondroitin sulfate proteoglycans (CSPG). A27 and H3 binds heparan sulfate proteoglycans (HSPG) and A26 binds extracellular laminin.

Thus, there appears to be a high level of redundancy in the MV binding proteins and their cellular counterparts. This is thought to partially account for the ability of VACV to infect many different cell types and organisms. Much detail around VACV binding remains unknown: the effect of each individual binding protein on entry should be elucidated to build a picture of how they work together. The strong GAG-dependence of binding suggests that movement of the virus on the plasma membrane may be highly important as GAGs are highly abundant. Moreover, the interplay between the differently polarised binding and fusion proteins must be studied.

1.4.2 Uptake

VACV binds to filopodia and undergoes retrograde flow, moving the MVs toward the cell body (Mercer and Helenius, 2008; Huang et al., 2008). The entry pathway of VACV has been controversial, and may be strain dependent (Bengali et al., 2009;

?), with both endocytic entry (Huang et al., 2008; Mercer and Helenius, 2008; Mercer et al., 2010a; Laliberte and Moss, 2009; Moser et al., 2010; Schmidt et al., 2011) and direct plasma membrane fusion (Armstrong et al., 1973; Chang and Metz, 1976; Doms et al., 1990; Carter et al., 2005) suggested. It is now widely accepted that the main and most physiological route of entry for both MVs and EVs is macropinocytosis (Townsley et al., 2006; Mercer and Helenius, 2008; Sandgren et al., 2010; Mercer et al., 2010a; Schmidt et al., 2011) (Figure. 1.8).

Macropinocytic entry involves large scale actin rearrangements and is primarily used by cells for the non-selective internalisation of fluid, membranes and particles (Mercer and Helenius, 2010). For VACV strain WR, these actin rearrangements are in the form of large, transient plasma membrane blebs (Mercer and Helenius, 2008). Alternatively, the strain International Health Department-J (IHD-J) induces filopodia (Mercer et al., 2010a). Phosphotidylserine (PS) on the MV membrane activates receptors which trigger the downstream cascade leading to these actin rearrangements (Ichihashi and Masayasu, 1983; Mercer and Helenius, 2010). PS marks apoptotic bodies for clearance via macropinocytosis in many cell types (Henson et al., 2001; Albert, 2004) and, importantly, does not lead to an immmune response. Therefore, it seems that VACV utilises apoptotoc mimicry for its uptake (Mercer and Helenius, 2008; Laliberte and Moss, 2009; Mercer and Helenius, 2010).

1.4.3 Fusion

VACV WR strain fusion is pH dependent: when MVs are bound to cells both direct plasma membrane fusion and syncytia formation can be driven by lowering the pH of the media. Inhibitors of endosomal acidication inhibit entry (Townsley et al., 2006; **?**). The A25-A26 complex has been shown to mediate the pH dependence on some cell lines (Li et al., 2007; **?**; Chang et al., 2019). Additionally, as the treatment of MVs with low-pH before binding accelerates entry but virions remain bafilomycin sensitive, there are two pH dependant steps leading to VACV entry (Townsley and Moss, 2007). More recently, it was shown that the MV membrane is proton permeable - low-pH treatment quenched A4-EGFP fluorescence and fluorescence was able to recover at physiological pH (Schmidt et al., 2013b). This

suggests that low-pH treatment may be important in core activation, separate from low-pH activation of the EFC.

The macropinosome undergoes maturation, resulting in VACV being released from the late stage macropinosome or lysosome in response to the low-pH environment (Rizopoulos et al., 2015) (Figure. 1.8). The fusion of VACV is thought to be one of the most complex mechanisms in the virus world. This is because it requires at least 11 distinct fusion proteins which make up the entry fusion complex (EFC). These are: A16 (Ojeda et al., 2006a), A21 (Townsley et al., 2005a), A28 (Senkevich et al., 2004), F9 (Brown et al., 2006), G3 (Izmailyan et al., 2006; Senkevich and Moss, 2005), G9 (Ojeda et al., 2006b), H2 (Senkevich et al., 2005), J5 (Wolfe et al., 2012), L1 (Bisht et al., 2008), L5 (Townsley et al., 2005b) and O3 (Satheshkumar and Moss, 2009). Mutants in any of these 11 proteins fail to infect cells due to a lack of full fusion, however A28(-), L1(-) and L5(-) mutants are still able to hemifuse (Laliberte et al., 2011), suggesting that these function in pore formation. There are 3 known sub-complexes within the EFC: A28 and H2 (Nelson et al., 2008), A16 and G9 (Wagenaar et al., 2008) and G3 and L5 (Wolfe and Moss, 2011). The fusion suppressors, A26 and A25, bind to the A16-G19 subcomplex (Chang et al., 2012). Figure. 1.7 shows a diagrammatic depiction of all the known interactions between the binding proteins, fusion suppressors and EFC proteins. Data for these interactions come from immunoprecipitation studies and whole virion protein-protein XL-MS (Wagenaar et al., 2008; Nelson et al., 2008; Howard et al., 2008; Ching et al., 2009; Laliberte et al., 2011; Wolfe and Moss, 2011; Chang et al., 2012; Mirzakhanyan and Gershon, 2019). Understanding these interactions can help our understanding of the organisation of the EFC and membrane protein architecture.

The work in this thesis considers only MVs, therefore EV binding and entry is not studied. The EV membrane contains at least 6 viral proteins unique to the EV (Smith et al., 2002) and thus EV binding differs from MV binding. EV entry, however, follows a similar route to MV entry: the EV is taken up into a macropinosome, acid-activated membrane rupture within the macropinosome re-

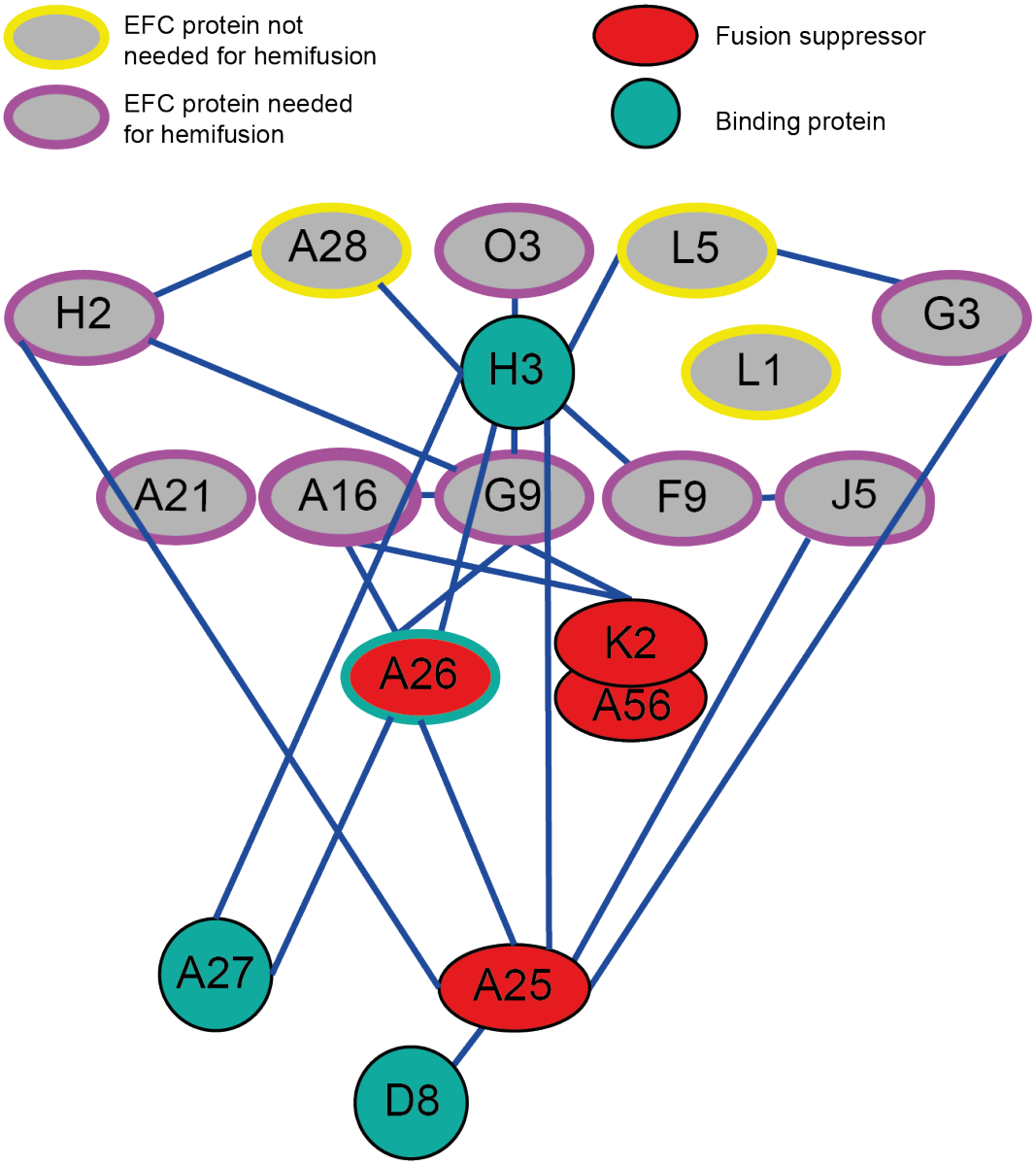

Figure 1.7: VACV membrane protein interactions The known interactions between the EFC proteins, fusion suppressors and binding proteins on the VACV membrane. Blue lines represent interactions. Experimental evidence comes from protein-protein XL-MS and immunoprecipitation studies (Wagenaar et al., 2008; Nelson et al., 2008; Howard et al., 2008; Ching et al., 2009; Laliberte et al., 2011; Wolfe and Moss, 2011; Chang et al., 2012; Mirzakhanyan and Gershon, 2019).

moves the outer membrane revealing the MV membrane and EFC, the MV-like particle can then fuse and the core is released into the cytoplasm (Schmidt et al., 2011). The inner, MV-like particle of the EV differs slightly from the MV membrane in that it lacks the MV fusion regulatory complex A25-A26 (Howard et al., 2008). Therefore, this may act as a mechanism to regulate EV formation. EVs contain their unique fusion suppression machinery in the form of the A56-K2 complex (Turner and Moyer, 2008) which binds the A16-G9 sub-complex (Wagenaar et al., 2008). This prevents syncitia formation of infected cells. The A56-K2 complex also prevents superinfection by its expression on the cell surface and binding to A16-G9 of incoming MVs, inhibiting fusion of the viral membrane and the cellular membrane (Moss, 2006; Turner and Moyer, 2008).

1.4.4 Post-fusion

After fusion, the core separates from the lateral bodies, which remain associated with the macropinosomal membrane and are degraded in a proteasome-dependent manner (Figure. 1.8) (Schmidt et al., 2013a), and is released into the cytoplasm. The core expands taking on an ovoid shape and the disulphide bonds are reduced (Locker et al., 2000; Cyrklaff et al., 2007; Schmidt et al., 2012). The core houses its own transcription machinery (Kates and McAuslan, 1967), thus early gene transcription begins immediately after core release. Approximately 80 different early proteins are translated on host ribosomes in the cytosol (Zhang et al., 1994; Yang and Moss, 2009). The core is then disassembled (Schmidt et al., 2012) and the viral DNA genome is released to the cytoplasm (Joklik and Becker, 1964) where it is accessible to viral DNA replication machinery. Electron micrographs have been observed showing VACV DNA adjacent to remnants of open or empty cores, suggesting that the core does not need to be completely disassembled for DNA release (Dales et al., 1978; Pedersen et al., 2000).

For viral DNA replication to happen the genome must be uncoated. This requires the early protein D5, a multifunctional AAA+ ATPase (Kilcher and Mercer, 2014). Although the virus encodes its own DNA replication machinery, it appears that VACV also recruits host proteins during the replication process, such as ATR

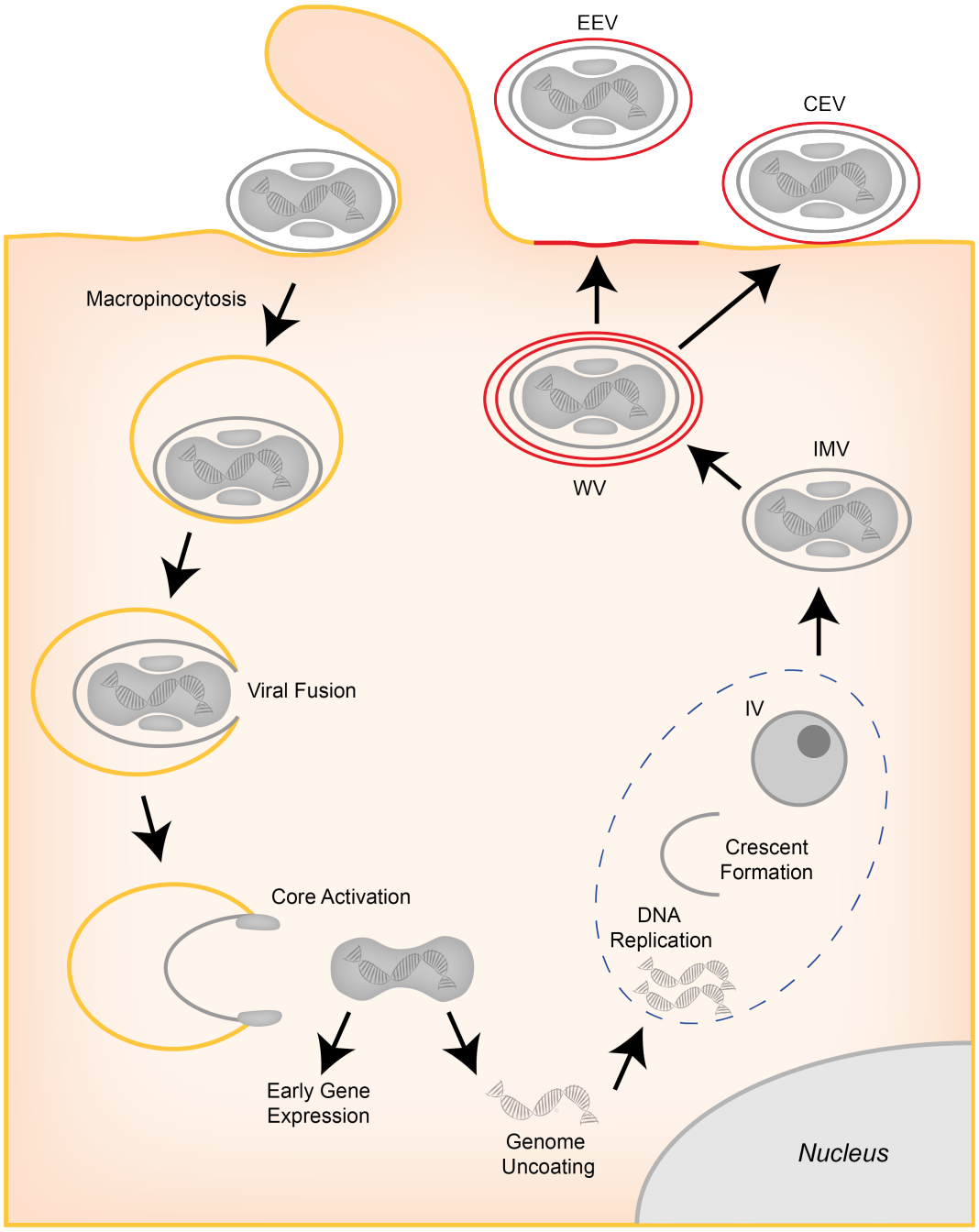

Figure 1.8: VACV life cycle VACV binds the cellular membrane and is taken up by macropinocytosis. The MV/IMV membrane then fuses with the macropinosome membrane under low-pH conditions. The core enters the cytoplasm, is uncoated and the DNA is replicated and IVs formed in replication sites. MVs/IMVs are formed after morphogensis. Wrapped virions (WVs) can then be generated and can fuse with the plasma membrane forming extracellular enveloped virions (EEVs) or cell-associated enveloped virions (CEVs).

and RPA (Oh and Broyles, 2005; Postigo et al., 2017). The successfully replicated DNA genome then provides the template for intermediate and late gene expression, accounting for 93 open reading frames (Fields et al., 2007).

1.4.5 Morphogenesis

MVs are assembled in a highly complex process that is still relatively unknown (Condit et al., 2006). After infection is established, viral factories are formed. Viral factories are highly electron-dense, organelle free areas of the cytoplasm transiently surrounded by cellular endoplasmic reticulum (ER)-derived cisternae (Tolonen et al., 2001; Cepeda and Esteban, 2014), where viral DNA and late proteins accumulate. The first morphologically distinct structures are crescents (Figure. 1.8), which are comprised of a smooth inner layer and an external layer of D13 trimers, the crescent scaffold protein (Dales and Mosbach, 1968; Hollinshead et al., 1999; Risco et al., 2002; Szajner et al., 2005; Bahar et al., 2011). It has recently been established that crescents derive from ER (Weisberg et al., 2017; Moss, 2018) and are not synthesised *de novo* (Dales and Mosbach, 1968).

Crescents eventually close on themselves to form spherical immature virions (IVs) (Figure. 1.8) (Condit et al., 2006). The viral DNA is packaged into the IV before its closure, along with viroplasm which contains viral core proteins (Morgan, 1976; Chlanda et al., 2009). Once the DNA is packaged, the IVs become immature virions with a nucleoid (IVNs). Although the details around how the viroplasm and DNA is incorporated into the IV are unclear, it is known that the seven-protein complex and protein E9 are essential (Liu et al., 2014).

IVNs then mature into MVs (Figure. 1.8). The viral core and lateral bodies are formed within the membrane. The transition from IVN to MV requires proteolytic cleavage of many core and membrane proteins by the viral protease I7. This includes the proteolytic processing of A17, the protein which binds D13 to the IV membrane, resulting in the loss of the D13 scaffold (Bisht et al., 2008). Additionally, the viral redox proteins A2.5, E10 and G4 are essential for maturation and control the disulphide bond formation in many of EFC proteins (Senkevich et al., 2000; White et al., 2002; Senkevich et al., 2002).

During the maturation process, additional surface proteins are added to the MV membrane. These are mostly involved in attachment and in mediating infection. For example, A17 acts as the anchor for the addition of A27 and A26 (Howard et al., 2008). MVs accumulate in the cytoplasm and are released when the cell lyses around 72 hours post infection.

A subset of MVs go on to form EVs. These MVs are transported out of the viral factory using the microtubule network, and are wrapped in two additional membranes derived from the trans-golgi or early endosome. At least 6 unique EV membrane proteins are incorporated during this process. Virion wrapping is known to require the viral proteins A27, B5 and F13 (Roberts and Smith, 2008). These virions are wrapped virions (WVs) (Figure. 1.8). The WVs are transported to the plasma membrane where they fuse their outer envelope, releasing the double-membraned EVs. Here, they can be released as extracellular enveloped virion (EEV) or maintained on the cell surface as cell-associated extracelluar enveloped virion (CEV) (Figure. 1.8). Signalling of viral proteins induces the formation of actin tails beneath CEVs, which function to drive them into neighboring cells (Smith et al., 2002).

1.5 Cell free systems in virus research

Having described in detail viral binding and entry in section 1.3, it is important now to look toward the techniques useful in studying this. As the work described in this thesis utilises a minimal model system based on cell-derived membrane blebs, I will briefly introduce alternative model systems used in virus research and explain the rationale behind utilising cell-derived membrane blebs for this project.

Artificial membrane systems have been used widely to study the earliest interactions between virus and host. They provide a platform to explore the host requirements for viral binding and fusion without the complexities found in cellular assays, where decoupling the contribution of the cell surface factors from the multitude of other cellular factors is difficult. Moreover, due to their smaller and more defined size and shape, many artificial membranes can provide a system amenable

to quantifying significant numbers of events in imaging studies.

The most simple way to investigate virus-cell receptor interactions is via the immobilisation of a cellular receptor on a sensor surface and characterisation of the interaction kinetics. These biosensor assays rely on SPR technology, which measures refractive index changes of photons hitting a metal surface (Figure. 1.9). The change in refractive index is proportional to the mass on the surface. Therefore, the cellular receptor can be captured on the surface, the viral binding partner flowed over (or vice versa) and the specificity, affinity and kinetic parameters between them determined. This is very powerful in characterising binding interactions and has been used widely in the virus field. For example, the binding sites of both influenza HA and HSV gD have been determined and the kinetics to different cellular binding partners characterised using SPR technology (Bertucci et al., 2003; Takahashi et al., 2013). In the VACV field, SPR has been used to determine the binding kinetics of A26 to laminin (Chiu et al., 2007) and mutated forms of A27 to heparin to determine functionality behind the structure (Ho et al., 2005).

SPR has many advantages: it gives label-free, specific and accurate information on the kinetics of binding using very little sample. However, removing the cellular receptor from its natural lipid environment can alter its functionality (Dowhan and Bogdanov, 2012). In addition, SPR platforms rely on the prior knowledge of the components involved in virus binding and are not well suited to studying the multivalent and complex interactions which are common to virus-cell membrane interactions (Mammen et al., 1998; Rankl et al., 2008; Grove and Marsh, 2011).

In this direction, supported lipid bilayers (SLBs) are model membranes in which one can incorporate receptors of interest, allowing for mobility of the receptor in the membrane (Figure. 1.10A). SLBs allow for control of the surface properties, whilst providing structural similarities to the cell membrane. SLBs can be used in combination with TIRFM to study binding kinetics, allowing the binding kinetics of individual proteins or virions to be established, as opposed to only the ensemble measurements of SPR. For example, binding kinetics of IAV to α2,3 sialic acid (SA) glycolipids were investigated using single-particle tracking and SLBs (Lee

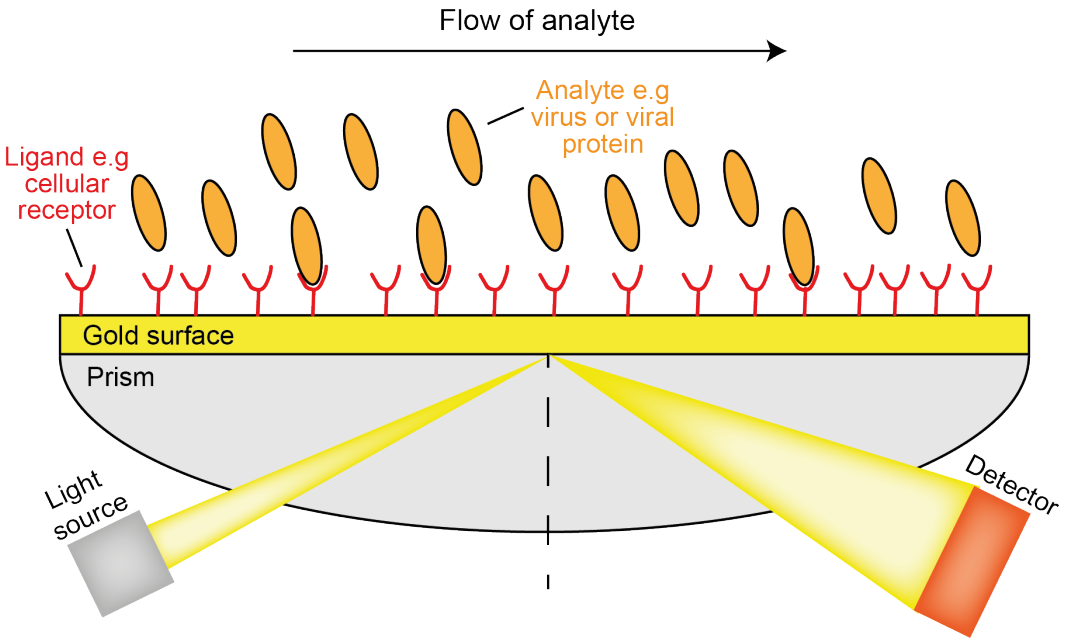

Figure 1.9: SPR schematic. One binding partner (the ligand) is immobilised on the metal surface of the chip, and the other (the analyte) is flowed across it. SPR detects changes in the refractive index in the immediate vicinity of the surface layer of the chip. The refractive index changes upon binding of analyte to ligand and this shift is the basis of the SPR signal.

et al., 2016), as well as HSV-1 binding to heparin (Peerboom et al., 2018). Similar experiments have measured single particle kinetics of fusion (Wessels et al., 2007). Although SLBs offer an important and widely used tool, the substrate that the bilayer sits on is known to impact the diffusion of the membrane components (Przybylo et al., 2006; Hsieh et al., 2014) thereby hampering its use as a entirely accurate cell model. Giant unilamellar vesicles (GUVs) are thought to be an improved cell mimic in this respect. GUVs consist of a lipid bilayer and have sizes and curvature comparable to that of eukaryotic cells (Figure 1.10B). GUVs make good cell mimics as they display curvature, have a finite surface area and the membrane is flexible (Fenz and Sengupta, 2012). The simple nature and precise control over lipid composition creates an advantage when studying the role of one protein or lipid in membrane remodelling activities. It is also possible to capture a cytoskeleton within the GUV (Tsai et al., 2011), making it a potential model for studies on the cytoskeletal contribution to cell shape. GUVs have been used as important tools in studying virus binding (Nikolaus et al., 2010; Ewers et al., 2010; Rydell et al.,

2013; Ho et al., 2016; Olety et al., 2016) and fusion (Kamiya et al., 2010; Rossman et al., 2010; Haldar et al., 2019). For example, influenza M2 was shown to induce curvature and lipid ordering in a cholesterol dependent manner on GUVs, revealing its ESCRT independent role in membrane scission (Rossman et al., 2010; Martyna et al., 2017). Although GUVs present with many advantages, it is known that VACV does not bind to GUVs (Schmidt et al., 2013a) implying that cell surface constituents are required for VACV binding and, therefore, a more complex minimal model system, which better mimics the cell-surface, is required.

Giant plasma membrane vesicles (GPMVs) are cell-derived, chemically induced vesicles (Figure 1.10C). Compared to GUVs, GPMVs maintain the membrane composition of the cell, although slightly higher levels of cholesterol and sphingomyelin were shown (Scott, 1976). In the virus field, GPMVs have been used to study the cholesterol dependence of HIV binding and entry (Yang et al., 2017) and raft association of influenza hemagglutinin (Nikolaus et al., 2010) due to the capability of GPMVs to form microscopic, lipid driven domains without the many variables of live cells. However, due to the covalent modifications induced by the chemical cross-linkers and vesiculants (notably formaldehyde (FA) and dithiothreitol (DTT)) used in the preparation of GPMVs, the lipid bilayer may not best mimic that of the living cell. Indeed, it has been shown that in FA and DTT induced GPMVs, the orientation of PS is flipped and the amount of various proteins expressed on the membrane are reduced as compared to cells (Liu et al., 2017).

Toward this end, we utilise a minimal model system based on cell-derived membrane blebs. Blebs are naturally produced in cells during apoptosis (Mills et al., 1998), cytokinesis (Fishkind et al., 1991) and migration of some embryonic cells (Trinkaus, 1973). They are cell-derived, spherical, cytosol filled membrane protrusions which reach diameters of 1 μM to 10 μM. Blebs arise from an actomyosin-driven increase in intracellular pressure, which causes detachment of membrane from the actin cortex (Charras, 2008). Blebbing can also result as a consequence of a tension induced breakage in the cortex and subsequent influx of cytosol (Paluch et al., 2005). Once the bleb is formed, the actin cortex reassembles

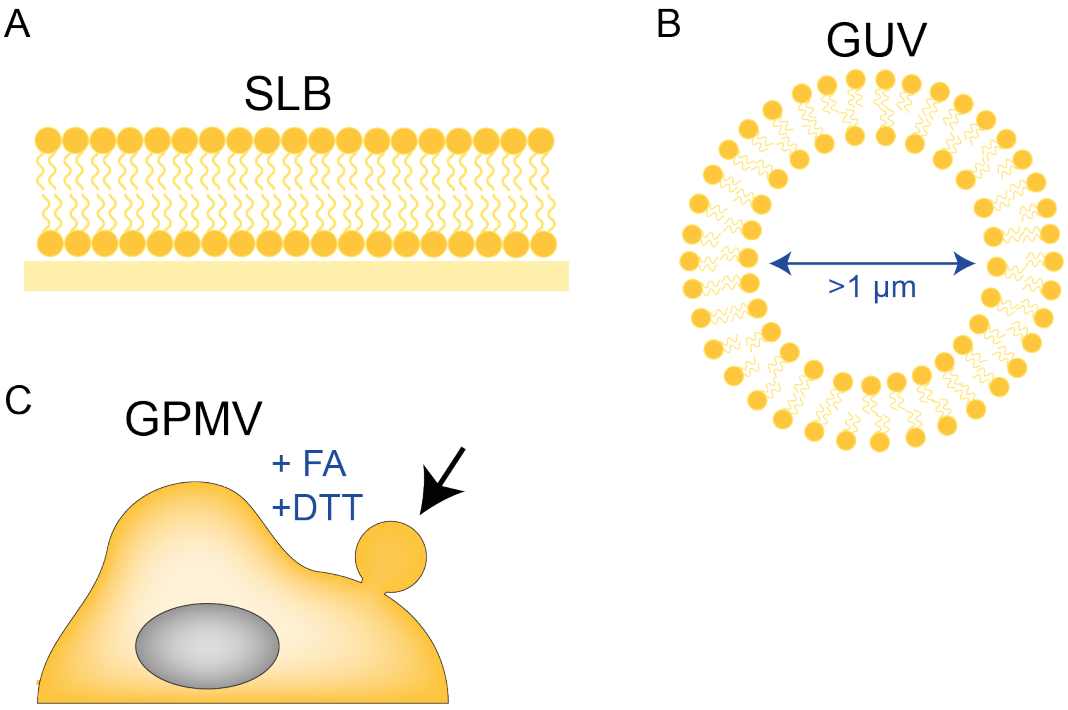

Figure 1.10: Examples of minimal model systems. A) Supported Lipid Bilayer (SLB), B) Giant Unilamellar Vesicle (GUV), C) Cell showing the formation of a Giant Plasma Membrane Vesicle (GPMV) in response to FA and DTT.

beneath the retracting bleb and stays stable, with actin turnover becoming very slow (Charras et al., 2006). The process of blebbing itself has been used to dissect the cortex assembley pathway. First, actin-membrane linker proteins are recruited to the bleb. Subsequently, actin, actin-bundling proteins and myosin motor proteins bind to form the reassembled cortex (Charras et al., 2006). Moreover, the retracting bleb displays high membrane rigidity explained in full by the assembly of the actin cortex (Charras et al., 2008).

Blebs have indeed been used as biomimetic systems. Mechanical sheering can remove blebs from the cell body (Davies and Stossel, 1977; Pick et al., 2005; Biro et al., 2013) and purified blebs have been used to study the celluar cortex (Biro et al., 2013). As blebs maintain the original membrane topology and composition of the cell (Pick et al., 2005; Grasso et al., 2013), they provide us a physiologically relevant minimal system to study the earliest stages of viral entry.

1.6 Aims

The two overarching aims of this thesis were to develop a minimal model system for the study of VACV binding and fusion and to understand the intricacies involved in VACV binding. As discussed in Section 1.4, the process of VACV binding is distinctly more complex than that of many other viruses. Four known proteins are involved and present varying degrees of redundancy. A large oversight in the VACV field thus far is that the interplay between these proteins during cellular binding has never been fully explored, with the majority of studies utilising only the purified virus or cellular protein in question. In this work, I ask essential questions on the interaction of these proteins in viral binding. Are any of these proteins more important than the other in binding? What, if any, redundancies and hierarchies are at play between them? Are there alternative roles for any of the viral proteins? Only this way can we begin to understand VACV binding fully.

In the same manner, this thesis also seeks to understand the recently published data detailing the polarisation of the fusion and binding proteins on the viral membrane (Gray et al., 2019) in the context of infection. Specifically, exploring the functionality behind this polarisation. To this end, I have utilised a minimal system based on cell-derived membrane blebs (Biro et al., 2013). The small size of blebs allows for the quantification of large numbers in imaging experiments, their smooth surface allows for accurate quantification of VACV binding orientation and their reduced complexity as compared to cells allows blebs to act as a simplified model of a cell. This system provides a completely novel way to study VACV binding and allowed me, using advanced imaging techniques, to correlate binding protein polarisation and virus-cell interaction and infection.

Lastly, the cellular membrane remodelling activity during the binding and fusion of VACV is almost completely unknown. Our minimal system in combination with high resolution microscopy lead to the discovery of VACV induced membrane curvature and I subsequently correlated this to productive infection.

Together, this thesis demonstrates the advantages of using blebs as a novel system to study VACV infection. It addresses enigmatic and understudied areas of

VACV biology with pioneering methodology allowing an alternative approach to study viral entry.

Although smallpox has thankfully been eradicated, the population today is left unvaccinated and at risk of poxvirus infection from bioterrorism or zoonosis. As I sit here writing this, now in the seventh week of the government enforced lockdown due to the SARs-CoV-2 virus, the importance of studying emerging viral disease has never seemed more significant. A complete understanding of the poxvirus entry mechanism is vital. Not only will this aid the development of novel and improved anti-viral drugs and vaccines, but understanding this highly complex virus may give us clues into the workings of other viruses, large or small.

Chapter 2

Materials and Methods

2.1 General Materials and Methods

2.1.1 Cell Culture

BSC40, HeLa, L929, Gro2c and Sog9 cells were cultivated in Dulbecco's modified Eagle's medium (DMEM, Life Technologies) supplemented with 10% heat-inactivated fetal bovine serum (FBS, Life Technologies), 2 mM Glutamax (Life Technologies), 100 units/ml penicillin and 100 µg/ml streptomycin (Life Technologies). This will henceforth known as full medium. Gro2c and sog9 cells are variants of L929 cells, selected by their relative resistance to HSV infection (Gruenheid et al., 1993; Banfield et al., 1995). Gro2c cells lack heparan sulfate proteoglycans (Gruenheid et al., 1993) and sog9 cells lack heparan and chondroitin sulfate proteoglycans (Banfield et al., 1995). Cells were grown at 37°C and 5% CO_2. Cells were routinely maintained and passaged using Phosphate-Buffered Saline (PBS) and Trypsin/EDTA (2.5g Trypsin/litre, 0.2g EDTA/litre). Cell counts were determined using a Cellometer (Nexelcom).

2.1.2 Viruses

All the viruses used in this project are based on the Western Reserve (WR) strain and are listed in Table 2.1 along with a reference if generated elsewhere, or the parental virus, if generated for this project. Inducible viruses are referred to as the inducible protein followed by +/-. Virus produced in the presence of inducer, and so containing the inducible protein is denoted as '+'. These viruses are very similar to

Virus	Reference or Parental Strain
WT	Dr Jason Mercer
EGFP-A4	(Schmidt et al., 2011) as A5-eGFP
mCherry-A4	(Schmidt et al., 2011) as A5-mCherry
ΔD8	(Townsley and Moss, 2007) as ΔD8vFire
ΔD8 EGFP-A4	ΔD8
ΔA26 EGFP-A4	EGFP-A4
A27+/- EGFP-A4	(Gray et al., 2019)
H3+/- EGFP-A4	(da Fonseca et al., 2000b) as vH3i
ΔA26ΔD8 EGFP-A4	ΔD8 A4-EGFP
A28(+/-) mCherry-A4	(Gray et al., 2019)
O3(+/-)	(Satheshkumar and Moss, 2009) as vO3-HAi
A26-HA EGFP-mCherry	A4-mCherry
HA-H3 EGFP-A4	EGFP-A4
E EGFP	WT

Table 2.1: List of the viruses used or referred to in this thesis. With each virus is the reference or the parental strain used to generate it.

WT. Virus produced in the absence of inducer, and so not containing the inducible protein, is denoted as '-'. Viruses with a protein completely knocked out are denoted with Δ followed by the deleted protein.

2.1.3 Antibodies

Anti-L1 mouse monoclonal antibody (clone 7D11) was purified from a hybridoma cell line kindly provided by Bernard Moss (NIH) with permission of Alan Schmal john (University of Maryland). Anti-D8 rabbit polyclonal antibody was made by immunising a rabbit with puried D8 protein and adjuvant. Anti-A26 was produced by GenScript USA inc. The peptide NKKGIAKVTEDKPD corresponding to residues 295-308 of A26 was was used to immunise one rabbit and anti-A26 antibody was anity puried after three immunisations. Antibodies against viral protein A27 (VMC39) was produced by the Cohen lab using puried recombinant baculovirus-expressed proteins as previously described (Aldaz-carroll et al., 2005). Anti-HA polyclonal rabbit and mouse antibodies were purchased from BioLegend. Anti-laminin rabbit antibody was purchased from novus biologicals. Anti-CSPG4 was purchased from ThermoFisher. AlexaFluor-488, AlexaFluor-594 AlexaFluor-647 coupled goat anti-rabbit secondary antibodies and the membrane stains Cell-

Mask Deep Red and Orange Plasma membrane stains were purchased from Life Technologies. Anti-rabbit and anti-mouse IgG HRP-linked antibodies were purchased from Cell Signaling Technology and used at 1:2000.

2.2 Virus Methods

2.2.1 Virus Generation

New recombinant viruses were generated as follows. All recombinant viruses were generated using plasmids based on pBluescript II KS (pBSIIKS).

For WR ΔA26 EGFP-A4 and WR ΔA26ΔD8 EGFP-A4, A26 at its endogenous locus was replaced within WR EFGP-A4 or WR ΔD8 EGFP-A4 respectively. Primers 5'-TTGGGTACCGGGCCCCCCCTCGAGGTCGACCCTAAA ATCTGTACTTTAAATGGACGGA-3' and 5'-ACTAGTGGATCCCCCGGGCTG-CAGGAATTCTCTGACT TAATGAGTCGTAGTTC-3' were used to amplify the A26 gene and the 300 bp flanking. This was inserted into the pBluescript II KS backbone (+) using Gibson assembly. The A26 gene was then replaced by the mCherry gene (for WR ΔA26 EGFP-A4) or lacZ gene (for WR ΔA26ΔD8 EGFP-A4) using Gibson assembly. For WR HA-H3 or WR A26-HA, the N- and C-terminus were HA tagged respectively and recombinant virus selected for by an E/L EGFP. Firstly, A26 or H3 were inserted into pBluescript II KS backbone (+). For A26 see above. Primers 5'-TTGGGTACCGGGCCCCCCCTCGAGGTCGACCTCAAATATTATTATTCTAA-CTCC-3' and 5'-ACTAGTGGATCCCCCGGGCTGCAGGAATTCCGCTGGTAA-GGATGATAT-3' were used to amplify the H3 gene and the 300 bp flanking. This was inserted into the pBluescript II KS backbone (+) using Gibson assembly. HA was then inserted through primer design. Lastly, E/L EGFP was inserted using Gibson assembly within the flanking regions.

A 60 mm dish of BSC40 cells was infected with the parental virus strain at an MOI of 0.03 in DMEM. After 3 hours, infected cells were transfected with 5-8 μg of the linearized plasmid. For this, 15 μL Lipofectamine 2000 (Invitrogen) in 0.5 mL DMEM was incubated at room temperature (RT) for 5 min and mixed with

linearized plasmid in 0.5 mL DMEM and incubated at RT for 20 min. The DNA-Lipofectamine solution was added to cells for 1 hour at 37°C before the addition of full medium. 48 hours post infection (hpi) cells were harvested by scraping, resuspended in 100 µl 1 mM Tris pH 9 and disrupted by freeze-thawing in liquid nitrogen three times.

Viruses with the desired phenotype were selected by plaque purification. The phenotype was either the display of fluorescence or by the synthesis of β-galactosidase upon the addition of 0.06 mg/mL 5-bromo-4-chloro-3-indolyl-b-D-galactopyranoside (x-gal) in an agar overlay, resulting in blue plaques. In the first round, 10 cm dishes of BSC40 cells were infected with the infection-transfection cell lysate solution diluted 10^4, 10^5 and 10^6 times in DMEM. In subsequent rounds, 6-well dishes were infected with the previous plaque solution diluted 10^2, 10^3 and 10^4 times in 500 µl of DMEM. In all cases inoculum was removed after 30 min incubation at 37°C and replaced with full medium. 48 hpi plaques were desired for the desired phenotype and picked into 100 µl 1 mM Tris pH 9 by scraping with a P20 pipette tip. Viruses were purified through 4-5 rounds of plaque purification or until all observed plaques displayed the desired phenotype.

2.2.2 Virus Purification

Viruses were purified as described previously (Mercer and Helenius, 2008). Breifly, crude extract was produced by infecting two 15 cm dishes of BSC40 cells grown with virus from plaque purification or a previous crude extract. Virus was diluted in DMEM, cells were infected and the inoculum was replaced after 1 hr with full medium. After 48 hours cells were harvested by scraping, lysed by freeze-thawing three times in liquid nitrogen, resuspended in 1 mL 1 mM Tris pH 9 and cell debris was pelleted by centrifugation at 4000 rpm for 10 min. The supernatant was collected and stored at -80°C as crude extract.

To produce purified virus for use in experiments, 10x 15 cm dishes of BSC40 cells were infected with crude extract (10 µL per plate) diluted in DMEM. Infection medium was added to cells, incubated at 37°C for 30 min and replaced with full medium. 48 hpi, cells were harvested by scraping, pelleted by centrifugation at

300 x g for 5 min, washed with PBS and stored at -80°C. Cell pellets were then resuspended in 12 mL 10 mM Tris pH 9 for 5 min to swell cells and then disrupted in a tight-fitting doucer. Cell nuclei were removed by pelleting at 2000 x g for 10 min and the supernatant retained.

Supernatant was loaded onto a 36% sucrose in 10 mM Tris pH 9 and purified by ultracentrifugation at 43,000 x g for 80 min. Sedimented virus was either resuspended for use in 1 mL 1 mM Tris pH 9 or further purified by banding. In this case, sedimented virus was resuspended in 200 µL 1 mM Tris pH 9, loaded onto a 25-40% sucrose gradient and ultracentrifuged at 12,000 x g for 40 min. The band within the gradient formed by virus was extracted and sucrose removed by dilution in 1 mM Tris pH 9 followed by ultracentrifugation at 43,000 x g for 40 min. Resultant pellets were resuspended in 1 mM Tris pH 9 and stored at -80°C.

2.2.3 Plaque Assay

BSC40 cells were grown to confluency in 6-well plates. Virus was serially diluted to varying concentrations below 1 pfu/mL in DMEM. 500 µL of virus in DMEM was added to wells and incubated for 1 hr at 37°C, after which it was replaced with full medium. 48 hrs after infection, media was removed and cells fixed with 0.1% crystal violet in 4% formaldehyde. Plaques were counted in the wells with between 10 and 100 plaques and the viral titre in pfu/mL calculated.

2.3 Super Resolution Imaging

2.3.1 Sample Preparation

High performance coverslips (18 mm, 1.5H, Zeiss) were washed in 100% ethanol (Sigma) and deionised water. Purified banded virus was diluted in 20 µL 1 mM Tris pH 9 and pipetted into the center of the coverslip. After 30 min at RT, virus was removed and 1 mL 4% EM-grade formaldehyde (EMS) was added for 20 min. Autofluorescence was quenched by brief incubation in 0.25% NH_4Cl in PBS. Samples were washed 3 times in PBS and blocked for 30 min with 5% BSA, 1% FCS in PBS (blocking buffer). Membrane proteins were stained with primary antibody diluted 1:1000 or 1:100 (depending on antibody) in blocking buffer overnight at 4°C. Cov-

erslips were then washed 3 times in PBS and Alexa Fluor 647-conjugated secondary antibodies (Invitrogen) diluted 1:1000 in blocking buffer were added for 1 hr at RT. Coverslips were washed 3 times in PBS and mounted on to Secure-Seal incubation chambers in BME buffer (1% b-mercaptoethanol (Sigma), 150 mM Tris, 1% glucose, 1% glycerol, 10 mM NaCl, pH 8) for dSTORM or in PBS for structured illumination microscopy (SIM).

2.3.2 Single-molecule localization microscopy

Imaging was performed on a Zeiss Elyra PS.1 inverted microscope with a Plan-Apochromat 100x / 1.46 NA oil DIC M27 objective with a 1.6x tube lens and in iXon 897 EMCCD camera (Andor). Images were acquired at 20 ms exposure time with 642 nm excitation at 100% laser power and a 655 nm LP filter. Fluorophore activation was dynamically controlled with a 405 nm laser at 0-1.5% laser power. Images were processed in Fiji (Schindelin et al., 2019) using ThunderSTORM (Hagen et al., 2014). Localisations were fitted with a maximum-likelihood estimate, lateral drift corrected by cross-correlation, localisations $<$20 nm apart from within $\leq$1 frame merged, and images rendered using a Gaussian profile with the NanoJ-Orange LUT (NanoJ). Lateral resolution was 25 nm, determined by Fourier ring correlation (FRC).

2.3.2.1 SR-Tessler analysis

Cluster analysis was performed using SR-Tesseler (Levet et al., 2015). Localization tables from ThunderSTORM were imported and Voronoi diagrams were created. Individual virions were selected as regions of interest and segmented as single objects with a density factor δ of 1–2. Within individual objects, clusters were identified with δ = 3 that yielded less than 5% clustering in the nonclustered reference probe A13–EGFP.

2.3.3 Structured Illumination Microscopy

SIM imaging was performed using Plan-Apochromat 100x/1.4 oil DIC M27 objective in an Elyra PS1 microscope (Zeiss). Images were acquired using 5 phase shifts and 3 grid rotations, with the 561 nm and 488 nm lasers (32 µm grating period) and

filter set 3. 2D images were acquired using a CMOS camera and processed using the ZEN software (Zeiss).

2.4 Electron Microscopy

2.4.1 Sample Preparation

2.4.1.1 Blebs and Virus

Virus was bound to blebs at 4°C, with each sample containing $\frac{1}{6}^{\text{th}}$ of a bleb prep from three T75 flasks. Virus bound blebs were pelleted at 1000 x g for 10 min and resuspended in 50 µL of low-calcium, high-potassium buffer mimicking the intraceulluar ionic composition henceforth referred to as intracellular buffer (IB; IB; 10 mM NaCl, 280 mM k-glutamic acid, 14 mM Mg_2SO_4, 13.34 mM $CaCl_2$, 5 mM Hepes) pH 7.4. Samples were centrifuged at 175 x g for 7 min onto fibronectin coated CELLview glass bottom cell culture slides (Greiner Bio-One). Supernatant was removed, replaced with IB at pH 5.0 or 7.4 and incubated at 37°C for 10 min, before fixation in 1.5% formaldehyde 2% glutaraldehyde in IB for 30 min.

2.4.1.2 Infected cells

For samples capturing virus in macropinosomes, HeLa cells were grown to confluency on 13 mm coverslips and virus bound at RT at MOI 100 for 1 hr. Unbound virus was removed and full medium supplemented with 10 mg/mL horseradish peroxidase (HRP; Sigma). Samples were then shifted to 37°C for 1 hr before fixation in 1.5% FA and 2% glutaraldehyde in 0.1 M cacodylate for 30 min.

Samples were osmicated for 1 hr in 1% osmium tetraoxide/1.5% potassium ferricyanide at 4°C and treated with 1% tannic acid in 0.05 M sodium cacodylate for 45 min in the dark, RT. Samples were dehydrated in sequentially increasing concentrations of ethanol solution and embedded in Epon resin. Prepolymerised Epon stubs were pushed onto each well containing the sample, or when coverslips were used, coverslips were inverted onto the stub, and polymerised by baking at 60°C overnight. The 70 nm thin sections were cut with a Diatome 45°diamond knife using an ultramicrotome (UC7, Leica). Sections were collected on 1x2 mm

formvar-coated slot grids and stained with Reynolds lead citrate.

2.4.2 Imaging

All samples were imaged using a transmission electron microscope (Tecnai T12, FEI) equipped with a charge-coupled device camera (SIS Morada, Olympus). All electron microscopy sample preparation from osmication was kindly done by Dr Jemima Burden, LMCB electron microscopy leader.

2.4.3 Image Analysis

For invagination depth of bleb bound virions was quantified using the Olympus SIS iTEM software. A straight line was drawn from the two edges of the invagination and the perpendicular distance from the inner leaflet of the bleb membrane to the virion membrane was found as invagination depth. For macropinosome curvature analysis, the Kappa plugin (Mary and Brouhard, 2019) in Fiji (Schindelin et al., 2019) was used. In brief, an initialisation curve was traced using a point-click method along the macropinosome membrane in contact with the virion membrane. This was then fit to the underlying data using an iterative minimization algorithm. The Bezier curve was extracted and the mean curvature along the entire curve reported.

2.5 Fusion from Without

BSC40 cells, L cells or Gro2c cells were grown to confluency in fibronectin coated CELLview glass bottom cell culture slides (Greiner Bio-One). Virus diluted in DMEM was added to wells at the WT MOI of 100 or 25. ΔA26 and ΔA26ΔD8 virus was bound at an equal particle count to WT virus. Virus was bound for 1 hour on ice before cells were washed twice with PBS and incubated for 5 min at 37°C with PBS adjusted with 100 mM MES to pH 7.4 or pH 5. Cells were then washed once with PBS and incubated with full medium for 2 hours, 37°C. Cells were fixed with 4% formaldehyde for 10 min and then blocked and permeabilized with 5% BSA, 0.05% saponin in PBS for 30 min. Cells were stained with Alexa Fluor 594-phalloidin (1:1000, Invitrogen) and Hoechst 33258 (1:5000, Invitrogen) for 1 hr. Samples were washed twice with PBS before imaging.

Imaging was performed on a VT-iSIM microscope (VisiTech) with a Plan Apo lambda 100X oil objective. Alexa Fluor 594 fluorescence was excited with the 564 nm laser and Hoechst with the 405 nm laser. 5x5 images were stitched together using the 564 channel to align. The fusion index was calculated from maximum intensity projections of the stacks using the formula

$$f = [1 - (\frac{C}{N})]$$

where f is the fusion index, C is the number of cells and N is the number of nuclei (White et al., 1981; Mercer et al., 2010b).

2.6 Bulk Fusion

Bulk fusion experiments were adapted from the protocol in (Schmidt et al., 2013b). Purified MVs were labeled by incubating with 22.5 μM octodecyl rhodamine (R18, ThermoFisher) in 1 mM Tris pH 9 at RT for 1 hr. Labelled virus was pelleted by centrifugation at 16,000 x g for 10 min at 4°C and washed in 1 mM Tris pH 9 twice to remove excess R18. Labeled virus was added to 7x10^5 HeLa cells at an MOI of 10 or 30 and bound at RT for one hour. Virus bound cells were pelleted by centrifugation at 300 x g for 5 min and resuspended in 100 μL PBS. The cell suspension was kept at RT before 630 μL of prewarmed PBS was added and the solution pipetted into a quartz cuvette. The cuvette was placed into a prewarmed spectrofluorometer at 37°C.

Samples for R18 dequenching measurements with blebs were performed similarly. Labeled virus was added to $\frac{1}{6}^{\text{th}}$ of a bleb prep from three T75s and bound on ice for 1 hour. Virus bound blebs were pelleted by centrifugation at 1,000 x g for 5 min and resuspended in 20 μL IB. 140 μL prewarmed IB was added and the suspension, pipetted into a 200 μL quartz curvette and placed into a prewarmed spectrofluormeter.

R18 dequenching was measured with an excitation wavelength of 560 ± 5 nm and an emission wavelength of 590 ± 5 nm. After 1 min, 100 mM MES was added to reduce the pH to 5.0 or keep it at 7.4. R18 fluorescence was measured up to

20 min when all R18 was dequenched by the addition 10% Triton X-100 to a final concentration of 1%. R18 fluorescence was normalised to the signal intensity after Triton X-100 addition.

2.7 Western Blot

2.7.1 Sample preparation

Cell lysates or purified virus were added to SDS PAGE buffer with 40 mM DTT, sonicated for 10 min, heated to 95°C for 10 min and centrifuged at 20,000 x g for 5 min.

2.7.2 Western blot analysis

Samples were separated on 4-12% Bis-Tris polyacrylamide gels and ran with MES SDS buffer (ThermoFisher) at 120 V, 1 hr 20 min. Transfers onto 0.2 µM nitrocellulose membranes were carried out using the semi-dry transfer system (Biorad) at 15 V for 45 min. Membranes were blocked with 5% milk in Tris-buffered saline with 0.1% Tween-20 (TBST) (Sigma Aldrich) for 1 hr at RT. Primary antibody was diluted in 5% milk in TBST and added to membranes overnight, rolling at 4°C. Membranes were washed 3 times in TBST, incubated with HRP-conjugated secondary antibody diluted in 5% milk in TBST for 1 hr at RT. Membranes were washed 3 times with TBST and imaged on with ImageQuant LAS 4000 Mini (GE Life Sciences) and Luminata Forte Western HRP Substrate (Merck) was used for detection. Western blot quantifications were done using Fiji (Schindelin et al., 2019).

2.8 Flow Cytometry

2.8.1 Sample Preparation

2.8.1.1 Binding Assay

L929 cells, gro2c cells and sog9 cells were seeded to 50,000 cells per well. The amount of virus per mL was measured using the A_{260} reading on a Nanodrop 1000 Spectrophotometer (ThermoFisher scientific) and calculated using the reference:

$$A_{260} = 1 = 1.2x10^{10} particles/mL$$

3x10^7 particles were added per well and bound at 4°C for 1 hr. Cells were then washed with PBS twice and scraped into 4% PFA, 5% FBS in PBS.

2.8.1.2 Treatment with soluble glycosaminoglycans and laminin

L929 or Gro2c cells were seeded to 50,000 cells per well in a 96 well plate. 3x10^6 particles/well were treated with 100 µg/mL soluble glycosaminoglycan/laminin in 1 mM Tris, pH 9 or mock treated in 1 mM Tris, pH 9 for 1 hr at 4°C. Virus and glycosaminoglycan/laminin solution was then diluted in DMEM and added to cells for binding at 4°C for 1 hr. Cells were washed with PBS twice and scraped into 4% PFA, 5% FBS in PBS.

2.8.1.3 Early Gene Expression

Confluent 96-well dishes of L929 or Gro2c cells were infected for flow cytometry with virus expressing EGFP under a viral early promoter (WR E EGFP) diluted to an MOI of 2 in DMEM. Virus was bound for 1 hr at RT before media removed and replaced with full medium for 4 hrs at 37°C. Cells were then washed in PBS, detached with trypsin and fixed with 4% PFA.

2.8.2 Flow Cytometry Analysis

Flow cytometry was performed on the Guava EasyCyte HT flow cytometer, recording the EGFP fluorescence with the 488 nm laser. Analysis of the flow cytometry data was performed with the GuavaSoft 3.3 analysis package (FlowJo).

2.9 RT-qPCR

HeLa cells were grown to confluency in 6 well dishes and infected with virus at MOI 10. Cells were left for 30 min at RT for virus binding. Dishes were then incubated for 2 hrs and DNA extracted using the RNeasy Plus Mini kit (Quiagen), with the homogenization of the cell lysate carried out with a 21G needle. RNA was eluted in 30 µL RNase-free water and the concentration measured on a NanoDrop 1000 Spectrophotometer (ThermoFisher Scientific).

First-strand cDNA synthesis was carried out with the Oligo(dT)$_{12-18}$ Primer (Invitrogen), dNTPs (ThermoFisher Scientific) and approximately 400 ng RNA extract per sample for 5 min at 65°C. RNaseOUT Recominbinant Ribonuclease Inhibitor and the Superscript II 5 x First Strand buffer (Invitrogen) were added alongside 0.1 M DTT before incubation for 2 min at 42°C. Superscript II Reverse-Transcriptase was added and sample incubated for 50 min at 42°C followed for 15 min at 70°C. 96-well PCR plates and the flat 8-cap strips (Biorad) were used for running of the qPCR samples. Amplification of cDNA of the early gene C11 and the house-keeping gene glyceraldehyde-3-phosphate dehydrogenase (GAPDH) was performed using the Mesa Blue qPCR MasterMix Plus for SYBR assay (Eurogenetec) using primers designed previously (Yakimovich et al., 2017) on a CFX Connect (Biorad). The run cycle consisted of 5 min at 95°C, 40 cycles of 15s 95°C 1 min 60°C, then hold at 50°C. Viral mRNA threshold cycle (CT) values were calculated and expression relative to GAPDH housekeeping gene determined.

2.10 Papain treatment of virus

WT virus was incubated with PBS adjusted to pH 7.4 or pH 5 with 100 mM MES for 3 min at 37°C. Papain was then diluted in 5 mM L-cysteine in PBS at either pH 7.4 or pH 5 to varying concentrations. The resulting papain dilution was added to virus and incubated at 37°C for 30 min. Papain was then inactivated by the addition of 40 mM *N*-ethlyl maleimide, virions pelleted, resuspended in SDS PAGE buffer with 40 mM DTT and analysed by western blotting (see section 2.7).

2.11 Biotinylation of Chondroitin Sulfate E

2 mg of chondroitin sulfate E (CosmoBio USA) was solubilised in 1 mL oxidation buffer (0.1 M sodium acetate, pH 5.5). 1 mL of cold sodium meta-periodate was added and the solution was incubated on ice for 30 min. Excess periodate was removed by gel filtration through a Zeba-Spin column (ThermoFischer Scientific) equilibrated with coupling buffer. EZ Link Hydrazide LC Biotin solution (ThermoFisher Scientific) was added to 5 mM and mixed for 2 hour at RT. Biotinylated chondroitin sulfate E was separated from non-reacted material by gel filtration

through a Zeba-Spin column and the resulting biotinylated chondroitin sulfate E was stored at -20°C.

2.12 Immunoprecipitation

Soluble D8 protein (MyBioSource) at increasing concentration was incubated for 3 hrs at RT with 0.5 μM or 5 μM biotinylated chondroitin sulfate A (Creative PEG-works) or biotinylated chondroitin sulfate E (see section 2.11). Dynabeads M280 streptavadin (ThermoFisher) were vortexed for 30 sec and washed with PBS. 0.5 mg/reaction of beads were incubated with chondroitin sulfate and D8 solution with gentle rotation. Beads were washed 4 times with PBS and resuspended in SDS PAGE buffer with 40 mM DTT for western blot analysis (see section 2.7).

Chapter 3

Characterising cell-derived membrane blebs as a minimal model system

3.1 Introduction

The first contact between an invading virus and its host is cell surface binding. This interaction is highly complex, multi-faceted and likely to involve many proteins, lipids and glycans on both the cell and the viral surface. In many cases, due to this complexity, viral binding remains fairly enigmatic and none more so than within the poxvirus family. As explained in Section 1.4.1, VACV binding involves at least four viral proteins, which bind a variety of cellular GAGs and proteins. Moreover, it seems that there are other, yet uncharacterised, interactions between VACV and the cell (Foo et al., 2009). Therefore, it remains important to continue to study and understand this early interaction.

One method of studying virus cell binding and fusion is to use a minimal system. As described in Section 1.5, many researchers have used methods to achieve a simplified model of the cell surface. This is advantageous as the complexity of the cell can lead to misinterpretations of data. For example, if the aim is to study a single cell surface receptor, the availability of many different receptors and the redundancies of the living cell obscures this. Moreover, due to recent finding that

the VACV binding and fusion proteins are polarised on the VACV membrane (Gray et al., 2019), important questions have arisen on how this corresponds to the orientation of virion binding. The irregular surface of the cell prevents accurate quantification of this.

Although lipid bilayer based systems (liposomes, GUVs, small unilamellar vesicles (SUVs)) are a popular choice in virus research, VACV does not efficiently bind to artificial membranes (Schmidt et al., 2013b), presumably due to the requirement of glycosaminoglycans in binding. Therefore, a system which maintains the native biological membrane is needed.

In this chapter, I sought to characterise cell-derived membrane blebs as a simplified system for studying the complex process of VACV binding and fusion. Blebs are cell-derived, spherical, cytosol filled membrane protrusions that arise from an actomyosin-driven increase in intracellular pressure, which causes detachment of membrane from the actin cortex (Charras, 2008). Blebs have been utilised as a system for the study of the cellular actin cortex (Charras et al., 2006; Biro et al., 2013; Bovellan et al., 2014).

For our purpose, the spherical nature of the bleb allows accurate quantification on the orientation of viral binding, the small size allows many events to be quantified and the presence of GAGs allows viral binding. Moreover, blebs reform the actin cortex (Charras et al., 2006; Biro et al., 2013). The cortex of the cell has been shown to regulate cell surface tension (Vicente-Manzanares et al., 2009; Clark et al., 2014; Chugh et al., 2017). Therefore, in this respect, blebs are a more accurate cell model than other membrane models (see Section 1.5). This cellular mimicry in terms of cell surface tension will aid more accurate results when studying VACV binding on blebs.

In this chapter I adapt the protocol for the separation of cellular blebs outlined in Biro *et al.* (2013) and characterise our system in regard to size, shape, the reformation of the actin cortex and the ability for endocytic uptake.

3.2 Purification methods

A protocol for the isolation and purification of a cell-derived membrane bleb system has already been established in Biro *et al.* (2013). I therefore adapted and optimised this protocol for use with HeLa, L929, Gro2c and Sog9 cells. I tested increasing concentrations of the actin depolymerising agent Latrunculin B and found the optimum concentration to induce blebbing without cell death, as assessed by visualisation, on HeLa cells to be 1.6 μM (Figure. 3.1) and 2 μM on L, Gro2c and Sog9 cells.

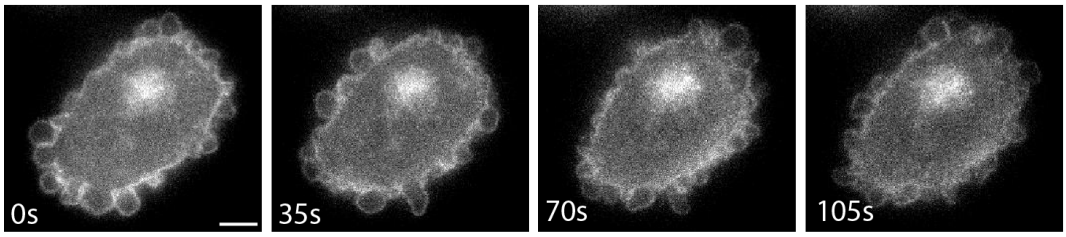

Figure 3.1: Blebbing HeLa cell. Timelapse confocal imaging of a HeLa cell treated with 1.6 μM Latrunculin B. The time of each still is shown in white. The cell is labelled with the plasma membrane stain CellMask. Scale bar, 10 μM.

I then tested different methods of collection and purification of blebs from cells. As in Biro *et al* (2013), I utilised cell shaking to detach blebs from the cell body. I then collected the supernatant and tested different purification techniques. First, an Optiprep^{TM} density gradient was used. Optiprep^{TM} is a density gradient medium consisting of 60% w/v iodixanol in distilled water with a density of 1.32 g/mol. Optiprep^{TM} gradients of 5-40% have been used to separate extracellular vesicles from cells (Greening et al., 2015), therefore I utilised this gradient and protocol for our bleb purification. After a 100,000 x g spin for 15 hours, 4 °C, two bands and a pellet appeared. To determine how effective this isolation protocol was, I removed the top band, middle, bottom band and pellet (Figure. 3.2) and viewed each fraction by brightfield microscopy. The observations are summarised in table 3.1.

As this procedure was time-consuming and as none of the fractions seemed to provide a high density of blebs without contaminating cellular debris, I looked to alternative purification techniques. I experimented with using a combination of spin

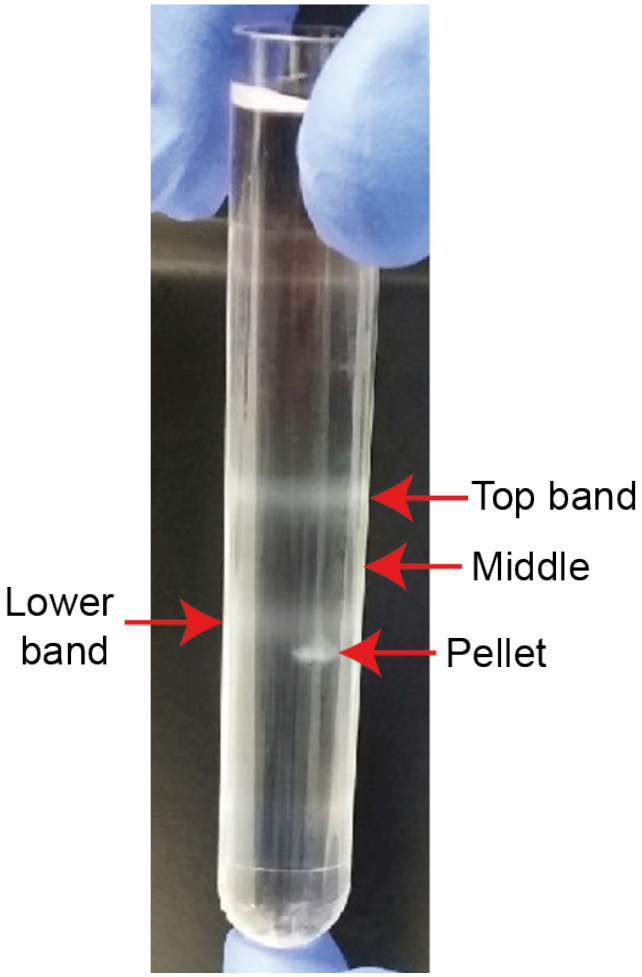

Figure 3.2: Optiprep™ gradient for bleb purification. Density gradient purification of bleb system. The bands labelled were collected and viewed by brightfield.

Top band	Middle	Bottom band	Pellet
Cellular and membrane debris, very few blebs	Very low density, mainly small blebs	Large cellular debris, very few blebs	Low concentration of blebs. Very sticky, assumed to be DNA

Table 3.1: Observation table of Optiprep™ gradient. Observations made with brightfield microscopy of each pulled fraction.

steps and filtration. I collected the supernatant after 15 min shaking in blebbing buffer (full medium, 1.6 µM), spun at 300 x g to pellet large cellular debris and spun the resulting supernatant at 4,000 x g to collect blebs. I then resuspended the pellet in 1 mL of a low-calcium, high-potassium buffer mimicking the intraceulluar ionic composition, henceforth referred to as intracellular buffer (IB). At this stage,

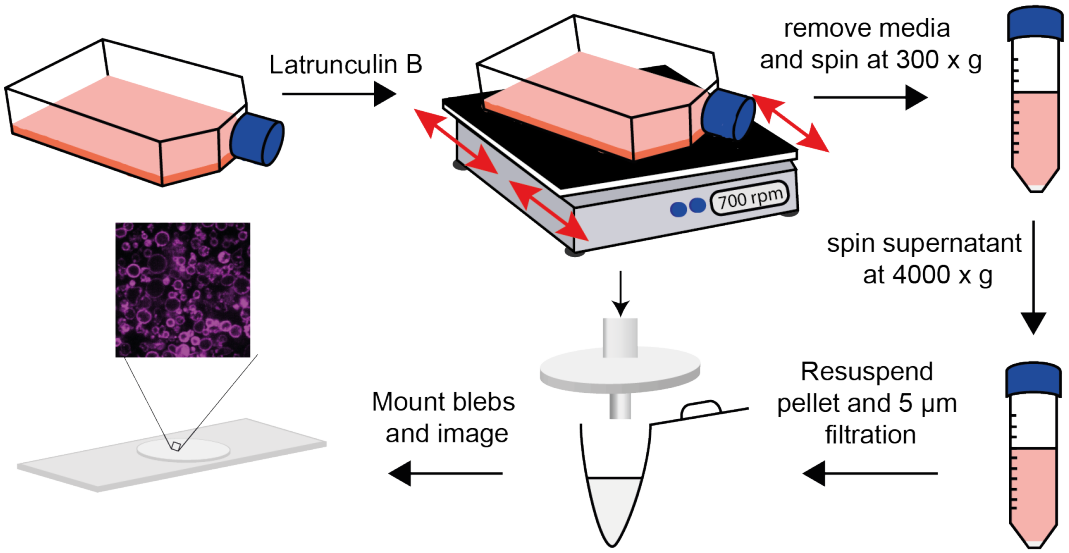

Figure 3.3: Protocol for cellular bleb isolation and purification. Latrunculin B is added to cells to induce blebbing. Cells are shaken to detach blebs, cellular debris removed by a slow spin step, blebs collected by a fast spin step, and remaining large debris removed by filtration through a 5 µm pore size filter.

I filtered the solution through a 5 µm filter to remove debris small enough to have not been removed by the 300 x g spin (Figure. 3.3). This technique worked well and provided a high concentration of blebs with very little contaminating cellular debris.

I purified blebs using this methodology from HeLa, L929, Gro2c and Sog9 cells as these are the cell types used in the subsequent research and chapters. I imaged with transmission electron microscopy (TEM) and showed that all four cell types produced circular blebs with heterogeneous material encapsulated within (Figure. 3.4). There was a large heterogeneity of encapsulated material between blebs within each cell type.

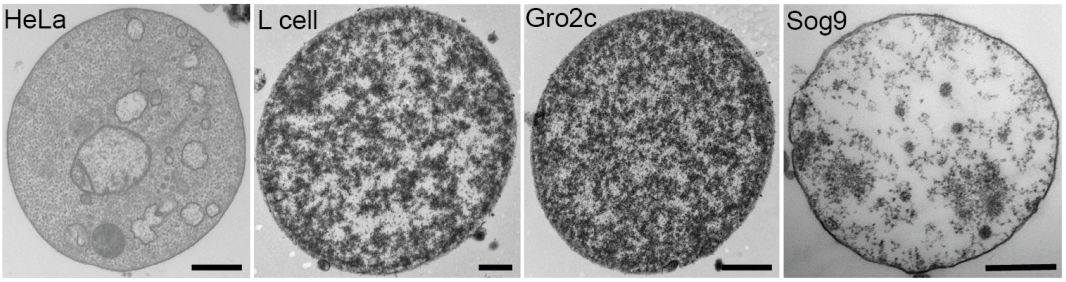

Figure 3.4: TEM images of blebs from multiple cell types. Blebs were purified from HeLa, L929, Gro2c and Sog9 cells following the protocol outlined in Section 3.2. TEM images were taken of example blebs. Scale bars, 500 nm.

3.3 Characterisation of the bleb system

3.3.1 Size and shape analysis

A key reason for utilising blebs as a system for VACV study is that their small size allows for significant numbers of events to be quantified in imaging studies very quickly. Therefore, I first characterised the range of bleb sizes attained with our current filtration protocol. To do this, I labelled blebs with CellMask plasma membrane stain, imaged and measured the diameter using Fiji (Schindelin et al., 2019) (Figure. 3.5A). As shown in Figure. 3.5B, the majority of blebs were 2-3 μm in diameter with very little under 1 μm. Moreover, the vast majority of blebs were circular, with a small minority displaying a bi- or multi- lobed appearance (Figure. 3.5C).

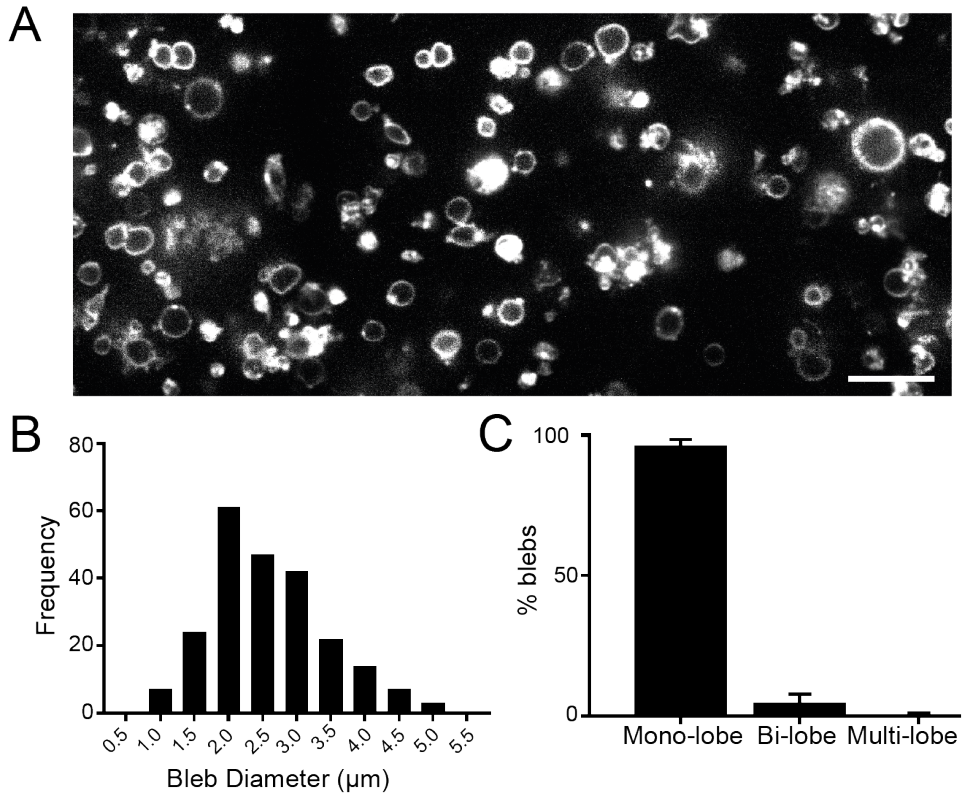

Figure 3.5: Bleb size and shape analysis. Blebs were isolated from HeLa cells as in Figure. 3.3 A) Blebs were labelled with CellMask plasma membrane stain. Scale bar, 10 µm. B) Histogram of bleb diameter distribution. C) Blebs were scored for mono-, bi- and multi- lobulation. Data are means ± standard deviation (SD) of three experiments.

3.3.2 ATP regeneration

VACV enters cells by macropinocytosis (Mercer and Helenius, 2008; Mercer et al., 2010a; Schmidt et al., 2011) which involves large scale cortical actin rearrangements. Moreover, the cellular cortex generates cell surface tension (Vicente-Manzanares et al., 2009; Clark et al., 2014; Chugh et al., 2017). Thus, to act as an accurate cell model for the study of viral binding and fusion, it is important that our minimal system possess an actin cortex. Actin is progressively recruited to the bleb membrane during retraction on the blebbing cell (Charras et al., 2006). To ensure maintenance of an actin cortex in blebs, Biro *et al.* (2013) use an exogenous source of ATP to preserve ATP dependant processes such as actin turnover. To allow the ATP molecules to cross the plasma membrane, blebs were permeabilised with *Staphylococcus aureus* α-Hemolysin (Biro et al., 2013). However, permeabilisation

of the membrane may interfere adversely with its integrity and, as the aim of this bleb system is the study of viral binding and fusion, this could effect our results. Therefore, the reformation and stability of the actin cortex in blebs treated with (reconstituted) or without (non-reconstituted) exogenous ATP was compared. Both the plasma membrane and actin were stained (Figure. 3.6A) and the percentage of blebs with an intact cortex determined. There was no significant difference between reconstituted or non-reconstituted blebs (Figure. 3.6B). Next, the stability of the cortex was assessed. Reconstituted and non-reconstituted blebs were incubated at 37°C for 1 or 5 hours, fixed, stained for actin and intensity measurements compared. There was no significant difference in actin intensity between non-reconstituted and reconstituted blebs, or between 1 and 5 hour timepoints.

The data presented here shows that the actin cortex reforms in the majority of blebs and maintains stable for up to 5 hours without the addition of exogenous ATP. Therefore, in all following experiments blebs were not treated with *Staphylococcus aureus* α-Hemolysin and exogenous ATP.

3.3.3 Endocytic ability of blebs

As the main route of entry for VACV is macropinocytosis (Mercer and Helenius, 2008; Mercer et al., 2010a; Schmidt et al., 2011), I asked whether blebs have macropinocytic ability. Macropinocytosis can be directly monitored by fluorescent dextran uptake (Jones, 2007). As smaller dextrans can be taken up by both micro- and macropinocytosis and larger ones only by macropinocytosis (Li et al., 2015), I used 20 and 150 kDa dextrans to probe both forms of uptake. Additionally, the small 20 kDa dextran was also used to ask whether the blebs contained any small pores or discontinuities of the membrane. Plasma membrane stained blebs were incubated with 20 kDa or 150 kDa dextran for 20 min at 37°C, washed and incubated with IB, pH 5.0 for 5 min to quench external fluorescence. In the case of both dextrans, there appeared to be four distinct subsets of blebs. These were blebs that were completely full of dextran, blebs that were partially full, blebs with puncta of dextran and blebs containing no dextran (Figure. 3.7A). Completely full, partially full and empty blebs were labelled by measuring the average intensity of dextran

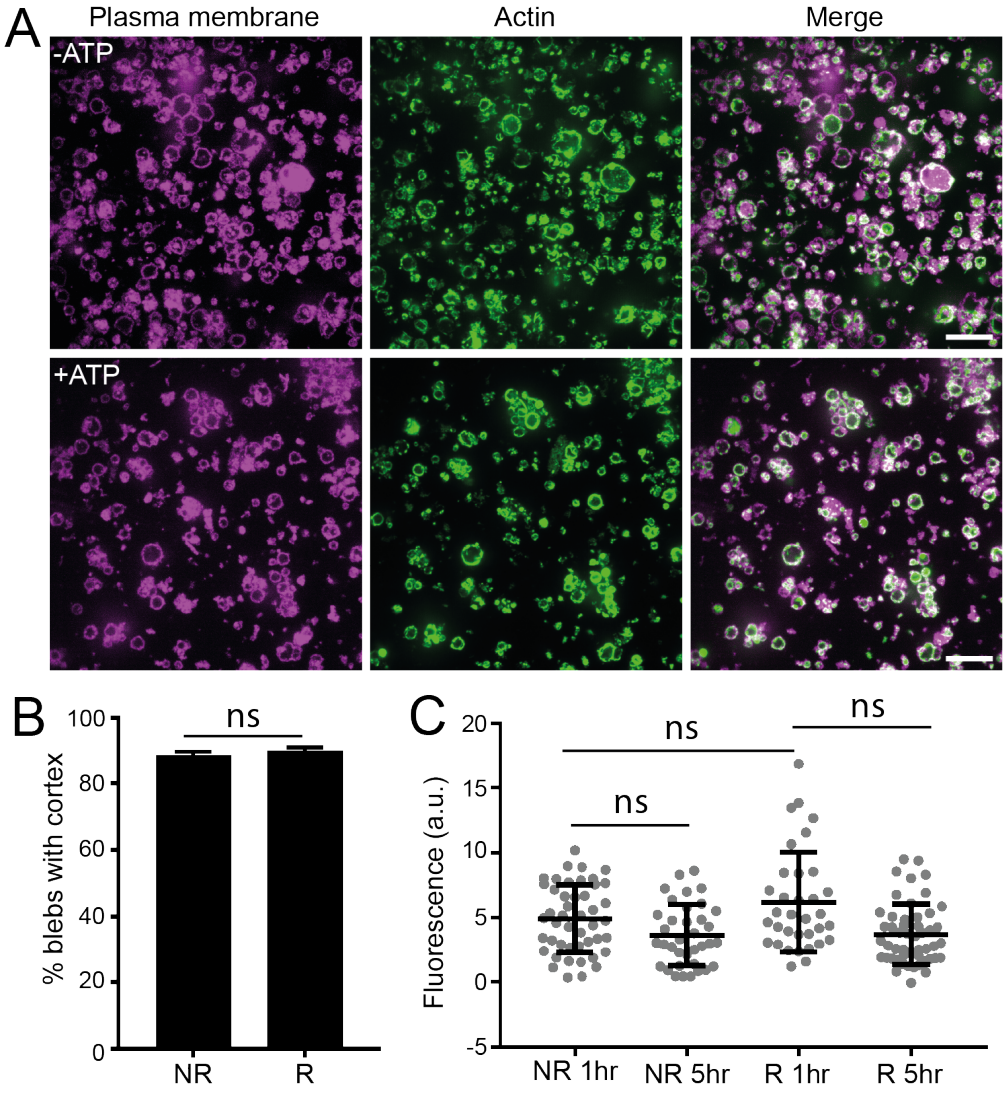

Figure 3.6: Comparison of the actin cortex with and without exogenous ATP. A) Blebs from HeLa cells were treated with or without exogenous ATP, labelled with CellMask and phalloidin and imaged by fluorescence microscopy. Scale bar, 10 µm. B) Percentage of blebs with an actin cortex, comparing non-reconstituted (NR) and reconstituted (R) blebs. C) Blebs were incubated at 37°C for 1 or 5 hrs. Stability of the actin cortex over time was determined by intensity measurements of the phalloidin stain on z-projections. Data are means ± SD of three experiments.

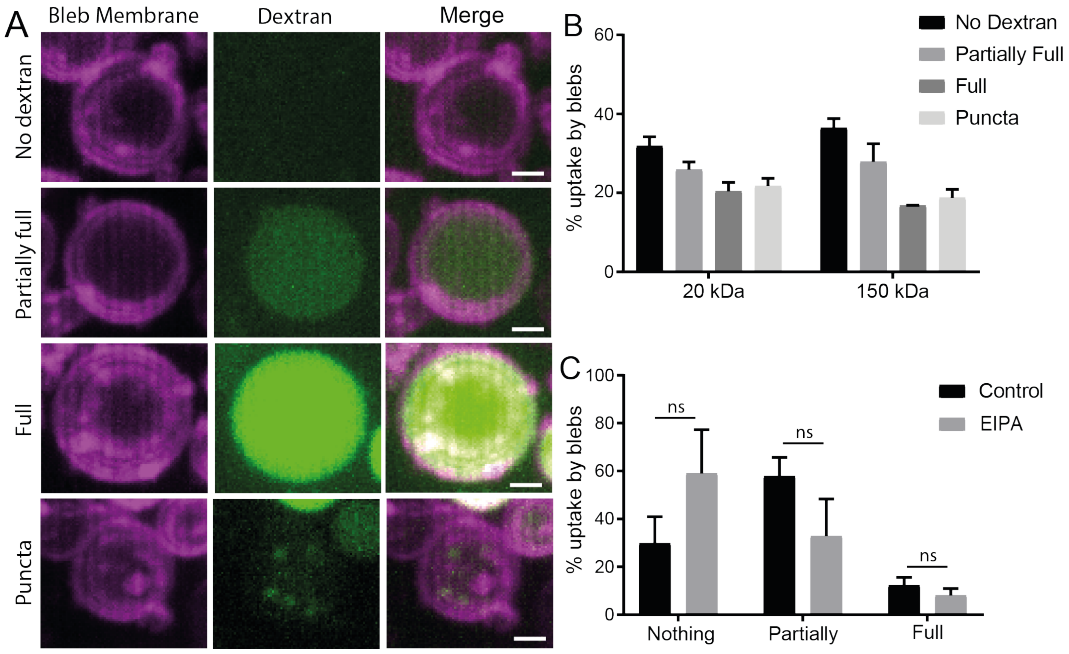

Figure 3.7: Macropinocytic potential of blebs. A) Blebs were incubated with 20 kDa or 100 kDa FITC-dextran at 37°C for 20 min, washed briefly with low pH and fixed. Blebs were scored into 4 categories: no dextran, partially full, full and those displaying puncta of dextran. Representive images with for 100 kDa dexran treatment. Scale bar, 1 µM. B) The percentage of blebs in each catergory was determined. C) Blebs were pretreated with 100 µM EIPA for 20 min before the addition of FITC-dextran and scored for dextran subsets. Data are means ± SD of three experiments. Two-tailed unpaired t-test was used for statistical comparison, ns $P>0.05$.

across the whole bleb and implementing cut offs for each category. Both 20 kDa and 150 kDa dextan showed similar percentages in each category, with empty blebs being most abundant in both cases (Figure. 3.7B). As this data suggests that blebs may have macropinocytic activity, I then utilised the drug 5-(N-ethyl-N-isopropyl)-amiloride (EIPA). EIPA is a selective Na+/H+ antiport inhibitor known to inhibit macropinocytosis. Blebs were pretreated with or without 100 µM EIPA before the addition of 100 kDa dextran. EIPA treatment resulted in a non-significant increase in the percentage of blebs unable to take up dextran and a slight but non-significant decrease in those partially full and full of dextran (Figure. 3.7B). This suggests that at least a subset of our blebs may display some macropinocytic activity.

To further probe this result, I used VACV as a tool to increase the macropinocytic activity of blebs (Mercer and Helenius, 2008). VACV was in-

cubated with blebs at 4°C for 30 min before the addition of 20 kDa or 150 kDa and shift to 37°C. As shown in Figure 3.8, VACV did not significantly alter the uptake of 20 kDa (Figure. 3.8A) or 150 kDa (Figure. 3.8B) dextran. The addition of virus actually appeared to increase the proportion of empty blebs in the case of the 100 kDa macropinocytic marker. Taken together, the data presented here signifies that, with regard to macropinocytosis, blebs do not fully mimic intact cells.

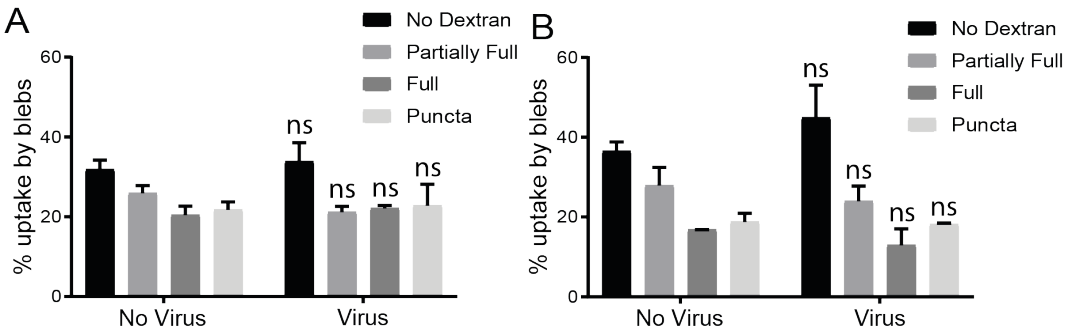

Figure 3.8: VACV incubation does not effect dextran uptake of blebs. Blebs were incubated with $5x10^7$ particles of WT virus per sample at 4°C for 30 min, before the addition of 20 kDa (A) or 150 kDa (B) dextran and shift to 37°C for 20 min. Data are means ± SD of three experiments. Two-tailed unpaired t-test was used for statistical comparison, ns $P>0.05$.

3.4 Discussion

In this chapter, I adapted the protocol from Biro *et al.* (2013) to develop a minimal cell system for the study of VACV binding and fusion. Blebs are generated by the addition of the actin depolymerising agent Latrunculin B and are detached from cells by gentle agitation (Figure. 3.3). I found that a protocol of spin steps in combination with 5 µm filtration the most effective way to achieve a concentrated and pure bleb preparation. I showed that this is applicable to many cells types, with HeLa cells, L cells, gro2c cells and sog9 cells exhibited here (Figure. 3.4).

The bleb system was then characterised for size, shape, cortical actin and endocytic ability. Blebs up to 5 µm in diameter were collected, with the majority 2-3 µm in diameter and most appeared to be spherical (Figure. 3.5). Biro *et al.* (2013) use exogenous ATP to preserve ATP dependant process. However, this utilitses the pore forming molecule α-hemolysin which disrupts the integrity of the

plasma membrane. As the aim of our system is to investigate the binding and fusion of VACV which relies heavily on cell surface components (Vázquez et al., 1999; Hsiao et al., 1999; Lin et al., 2000; Li et al., 2007), I wanted as little damage to the membrane as possible. The actin cortex is important for VACV virus entry due to the role of large-scale actin rearrangement in macropinocytosis (Mercer and Helenius, 2008). Moreover, an intact actin cortex in our bleb system would allow blebs to serve as a more accurate minimal cell model in terms of the tension generated at the plasma membrane (Vicente-Manzanares et al., 2009; Clark et al., 2014; Chugh et al., 2017). There was no significant difference in the percentage of blebs reforming an actin cortex when comparing regenerated and non-regenerated blebs and, when assessing the intensity of actin within blebs, the cortex remained intact over a 5 hour timespan (Figure. 3.6). These data suggest that blebs contain enough encapsulated ATP during the detachment process to reform and maintain an intact actin cortex. This aids the maintenance of bleb shape and allows the bleb to act as a more accurate cell surface model.

The endocytic potential of blebs was then investigated using fluorescent dextrans. A subset of blebs were filled completely with dextran in both the 20 kDa and 150 kDa case. A small percentage of blebs appeared to take up puncta of dextran (Figure. 3.7). These puncta are unlikely to be endosomes as they display no plasma membrane labelling signifying that the dextran was not membrane encapsulated. It is unlikely that dextran is entering the blebs through large pores or membrane discontinuity as the blebs maintain their spherical shape. Moreover, our protocol for the dextran uptake assay involves a low-pH wash to quench any external fluorescence. It is assumed that if blebs displayed large pores in the membrane then the low-pH buffer would enter the interior of the blebs and quench the internal dextran fluorescence. To investigate macropinocytic activity further, the drug EIPA was used which is known to inhibit macropinocytosis. Treatment with this drug increased the proportion of empty blebs and decreased the proportion of partially full and full blebs. However, none of these changes were significant. I then used VACV as a tool to manipulate the macropinocytic uptake of blebs as the virus was shown

to induce macropinocytosis of the cell (Mercer and Helenius, 2008). There was no significant increase the uptake of dextran between blebs incubated with or without virus with either size dextran (Figure. 3.8) suggesting that any dextran uptake is not due to macropinocytosis. Taken together, it is not clear if blebs can undergo endocytosis but, as the addition of virus does not significantly increase bleb dextran uptake, I propose that blebs are not a good cell mimic for studying the macropinocytic uptake of VACV. Therefore, this system will only be used for the study of viral binding and fusion.

The bleb system is advantageous over alternative minimal systems for VACV binding and fusion for multiple reasons. Firstly, the original cell surface is maintained. Other artificial membrane systems, such as liposomes, SLBs and GUVs, are constituted of only lipids. For VACV binding, it is known that proteoglycans are used and therefore binding and fusion to lipidic systems is neither efficient (Schmidt et al., 2013a) nor biologically relevant. What's more, for viruses where the host cellular membrane requirements are unknown, the biological membrane of blebs is particularly helpful. The efficiency for fusion of some viruses, for example IAV and HIV, has been shown to rely, in part, on the cholesterol content of the target membrane (Lai et al., 2012; Domanska et al., 2013; Yang et al., 2016; Meher et al., 2019; Liu and Boxer, 2020). It is thought that cholesterol acts to stabilise the hemifusion stalk and fusion pore (Churchward et al., 2005, 2008). Indeed, when studying single virus hemifusion kinetics of VACV and IAV on the cellular membrane (Schmidt et al., 2013b), a discrepancy was seen between that and the kinetics recorded on artificial membranes (Wessels et al., 2007; Floyd et al., 2008; Costello et al., 2012) - hemifusion on the artificial membrane was faster than on the cellular membrane. Therefore, important kinetic information on physiological fusion can be lost using artificial membranes and a simplified cellular mimic, such as blebs, would give more accurate results.

Secondly, blebs maintain the actin cortex which is known to be important in VACV entry (Mercer and Helenius, 2008; Mercer et al., 2010a; Sandgren et al., 2010). Again, this aids biological relevance and also membrane rigidity.

Lastly, their small size and high curvature (unlike GUVs and SLBs) allow many events to be imaged in one frame, gaining statistically significant numbers. This makes them ideal for investigating nanoscale changes in virus architecture using single particle averaging. Indeed, membrane systems have been used in cryo-EM studies to investigate conformational changes in viral structure during binding and fusion (Lee, 2010; Cardone et al., 2012; Cao and Zhang, 2013; Gui et al., 2016; Chlanda et al., 2016). This would be particularly informative for VACV, as very little is known about the structural organisation of conformational changes of the EFC. The high curvature of blebs would also emphasises membrane remodelling activity of the virus, making it easier to identify and quantify.

In conclusion, this chapter outlines a protocol for the efficient purification of cell-derived membrane blebs that maintain an actin cortex and original cellular membrane. I propose that this system can be used for the study not only of VACV binding and fusion, but also for other viral pathogens.

Chapter 4

Blebs as a model system for studying VACV binding and fusion

4.1 Introduction

VACV binding and fusion is highly complex due to the large number of proteins involved (Moss, 2012). VACV binding involves at least four separate proteins (Vázquez et al., 1999; Hsiao et al., 1999; Lin et al., 2000; Li et al., 2007), with the possibility that more interactions utilising unknown binding partners on both the cell and viral surface may exist (Foo et al., 2009). Moreover, it is known that most of the binding proteins also have alternative roles: A27 is involved in wrapping (Ward, 2005) and in EFC polarisation (Gray et al., 2019), A26 acts as a fusion suppressor (Chang et al., 2010, 2012, 2019) and H3 may be involved in IV to IMV transition (Lin et al., 2000; da Fonseca et al., 2000b). Therefore, an alternative system to study viral binding, such as with the minimal model based on cell-derived membrane blebs outlined in the previous chapter, may reveal novel information on VACV binding.

VACV is a large and asymmetric virus. Its size means that it is amenable to imaging with fluorescence microscopy. Recently published data from our lab show that the fusion and binding proteins are polarised into distinct domains: binding proteins to the sides of the virus and fusion proteins to the tips (Gray et al., 2019). It is now important to study this polarisation with respect to the cell surface. How

does polarisation affect the orientation of viral binding and fusion? Is viral binding a static or dynamic process in this respect? How does each binding protein regulate binding orientation? Blebs are a good system for this due to their smooth surface and small size, allowing easy quantification with significant numbers using structured illumination microscopy (SIM).

In this chapter, I first confirm that VACV can bind and fuse with blebs, before assessing VACV binding orientation. Utilising a library of VACV mutants and cell types with GAG production mutations, I investigate the role of each binding protein in binding orientation and begin to dissect redundancies and hierarchies between them.

I then visualise VACV binding on blebs at high resolution with TEM. This reveals pH dependant VACV induced invagination of the cellular surface. Due to their smooth shape, blebs allow us to capture this remodelling activity which is masked by the irregular surface of the cell. The invagination induction appears to involve D8, thereby highlighting a novel role of the D8 binding protein.

4.2 VACV binding and fusion with cell-derived membrane blebs

4.2.1 VACV can bind to blebs

The ability for VACV to bind and fuse to blebs was first assessed. Blebs were purified from HeLa cells and centrifuged onto poly-L-lysine (PLL) coated coverslips. Blebs were then incubated with A4-EGFP virus at 4°C for 1 hr, washed with IB and imaged. It was confirmed that virus could bind to blebs (Figure. 4.1).

I then assessed the ability for VACV to bind to blebs derived from parental L cells and the daughter cell lines gro2c and sog9. Gro2c cells are deficient in HSPG and sog9 cells are deficient in both HSPG and CSPG. For simplicity, from here on in, I will refer to L, gro2c and sog9 cells as HS+/CS+, HS-/CS+ and HS-/CS- cells respectively. Due to the GAG dependence of VACV binding (Vázquez et al., 1999; Hsiao et al., 1999; Lin et al., 2000), these cell lines offer a useful tool for studying the redundancies and hierarchies between the different binding proteins. In the same

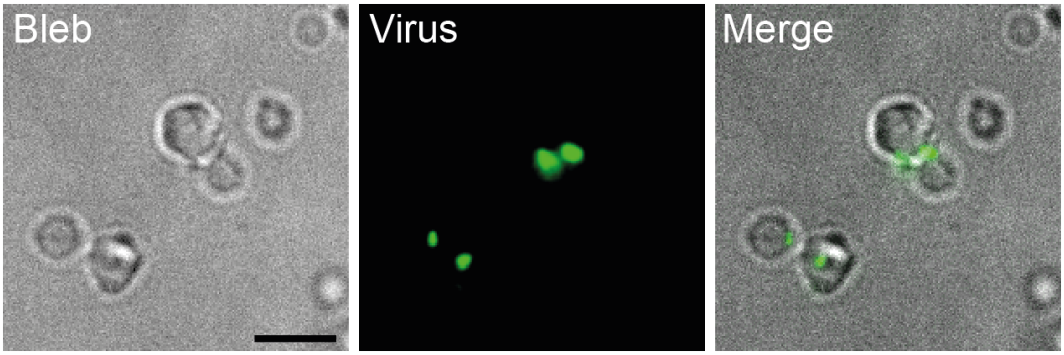

Figure 4.1: VACV can bind to blebs. Blebs from HeLa cells were spun onto PLL coated coverslips, incubated with $3x10^7$ particles of WR A4-EGFP for 1 hr at 4°C and washed with IB. Blebs and virus were imaged on a Zeiss Elyra PS.1. Scale bar, 5 µm.

way as with HeLa cells, EGFP-A4 virus was incubated with blebs derived from the three cell lines at 4°C for 1 hr. Figure 4.2 confirms that VACV can bind to blebs derived from HS+/CS+, HS-/CS+ and HS-/CS- cells.

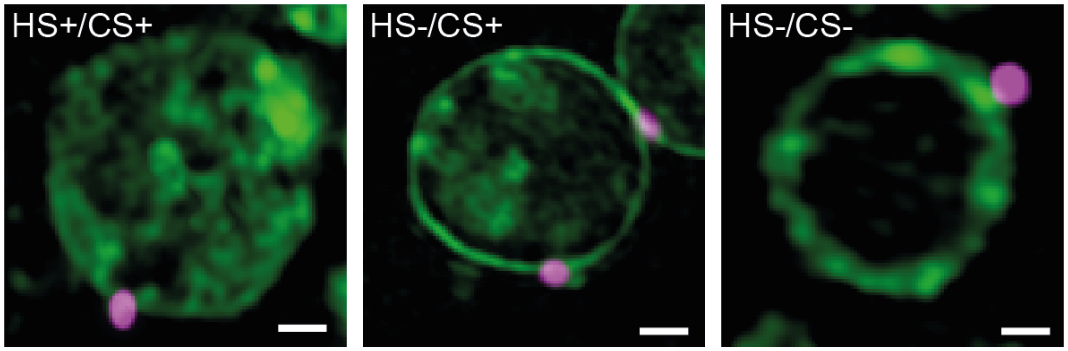

Figure 4.2: VACV can bind to HS+/CS+, HS-/CS+ and HS-/CS- cells derived blebs. Blebs derived from HS+/CS+, HS-/CS+ and HS-/CS- cells were stained for the plasma membrane (green) and incubated with A4-EGFP virus (magenta) at 4°C for 1 hr. Samples were then fixed and imaged. Scale bar, 1 µm.

4.2.2 VACV can fuse with blebs

The ability for VACV to fuse with blebs was then assessed. WT virus was labelled with self-quenching quantities of the lipophilic dye R18 and bound to blebs at 4°C for 1 hr. When hemifusion between virus and cellular membrane is induced by lowering the pH of the surrounding media, the R18 dye diffuses into the cellular membrane resulting in a measurable increase in fluorescence (Figure. 4.3A). An increase in fluorescence was seen at pH 5.0 (red line) compared to pH 7.4 (black line),

and fusion with blebs followed similar bulk fusion kinetics as that seen with cells (Schmidt et al., 2013a) (Figure. 4.3B). To test whether R18 dequenching was the consequence of genuine fusion or just non-fusogenic lipid dye transfer, two controls were carried out. In the first, virus was preincubated with the neutralising anti-L1 antibody 7D11, which is known to inhibit fusion (Doms et al., 1990). R18 fluorescence did not increase over time at pH 5.0 in this case, following very similar kinetics to that at pH 7.4 (blue line) (Figure. 4.3B). Next, equal quantities of blebs were labelled with CellMask Green plasma membrane stain or R18 lipid dye and incubated together for 1 hr at pH 5.0. We monitored lipid dye transfer microscopically and no blebs containing both dyes were seen (Figure. 4.3C). The results of these two controls confirm that VACV can fuse with our minimal system.

4.3 Binding orientation

4.3.1 Binding protein distribution

As VACV can bind and fuse with blebs, binding orientation of the virus was next assessed. The VACV binding and fusion proteins have recently been shown to be polarised on the viral membrane (Gray et al., 2019). As outlined in Section 4.1, this polarisation now needs to be assessed in regards to the cellular membrane and blebs are the perfect system for this.

I first sought to characterise the localisation of the two remaining binding proteins not visualised by Gray *et al.* (2019): A26 and H3. For this, I constructed recombinant viruses with an HA tag at the extra-virion end of the protein in question (N-terminal for H3 and C-terminal for A26) and visualised them with immunofluorescence using anti-HA primary antibody. I utilised SIM (Gustafsson, 2000) and single-particle averaging using the Fiji plugin VirusMapper (Gray et al., 2016, 2019) to generate models of the protein distribution (Figure. 4.4A). This revealed that both proteins are largely localised to the sides of the virus, like the previously described localisation of D8 and A27 (Gray et al., 2019).

Although the SIM and VirusMapper methodology led to high precision and signal-to-noise ratio models of average membrane protein localisation, the resolu-

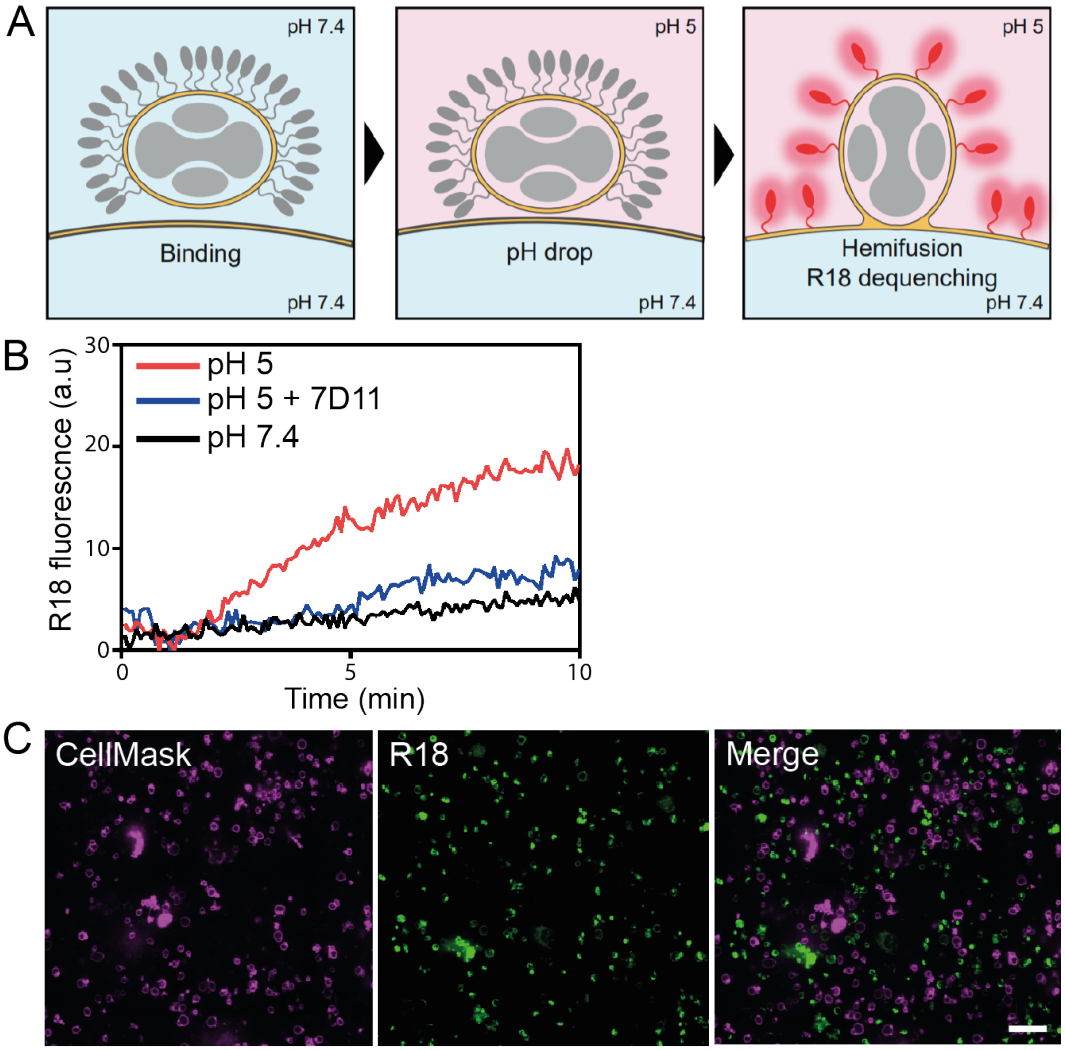

Figure 4.3: VACV can fuse with blebs. A) Virus is loaded with self-quenching quantities of R18 dye, bound to blebs and the pH is lowered. When hemifusion is induced, the R18 dye diffuses into the bleb membrane and an increase in fluorescence is achieved. B) Blebs from HeLa cells were incubated with R18 loaded WT virus for 1 hr at 4°C. In one sample virus was preincubated with fusion inhibiting antibody 7D11 for 1 hr. The pH was lowered or kept at pH 7.4 after 1 min of recording. Fluorescence is normalised to the initial value and the final fully dequenched value after TX-100 addition. C) Blebs were loaded with CellMask plasma membrane stain or R18 lipid dye, mixed for 1 hr at pH 5.0 and imaged. Scale bar, 20 µm.

tion remained at roughly 120 nm. Therefore, I extended the investigation to single virions using (direct) stochastic optical reconstruction microscopy (dSTORM) (Hagen et al., 2014), which has the potential to elucidate further details on the protein organisation. While this revealed the same overall localisation of H3 and A26 as the SIM data, dSTORM imaging revealed that the binding proteins form clusters rather than exhibiting a homogenous distribution within their polarised domain. To quantify the extent of and the differences between the clustering of the binding proteins, a tessellation based cluster analysis method using the SR-Tesseler software (Levet et al., 2015) was employed. Using this software, dSTORM images were subject to Voronoi tessellation, segmentation and cluster identification. A13-EGFP was used to set a baseline for clustering as it appears minimally clustered when labelled with an EGFP nanobody (Figure. 4.4B). The density factor is the relative threshold over which the average localisation density is designated as 'clustered'. Based on the A13-EGFP dSTORM data, the density factor was set to 3 - the lowest value that gave very little clustering.

When subjected to localization, segmentation and cluster identification using SR-Tesseler (Levet et al., 2015), both A26 and H3 appeared to reside in clusters on the virion membrane similar to what is seen with D8 (Figure. 4.4B, (Gray et al., 2019)).

4.3.2 Binding orientation quantification

Blebs were then used to assess the binding orientation of VACV. I hypothesised that the virus may bind on its side and reorient in response to low-pH to allow fusion at the tips. To evaluate this, I developed a binding orientation assay using recombinant virus with an mCherry tagged core and EGFP tagged F17 (found in the lateral bodies (Schmidt et al., 2013a)) in combination with the higher resolution of SIM. I could use core elongation and LB separation as indicators of virion orientation (Figure. 4.5A). mCherry-A4, EGFP-F17 tagged virus was R18 labelled and the side/tip ratio of bound virus compared between pH 7.4 and pH 5.0. The R18 labelling allowed us to elucidate the orientation of fused and non-fused virions when blebs with only one bound particle were analysed. The side/tip ratio of VACV binding did not

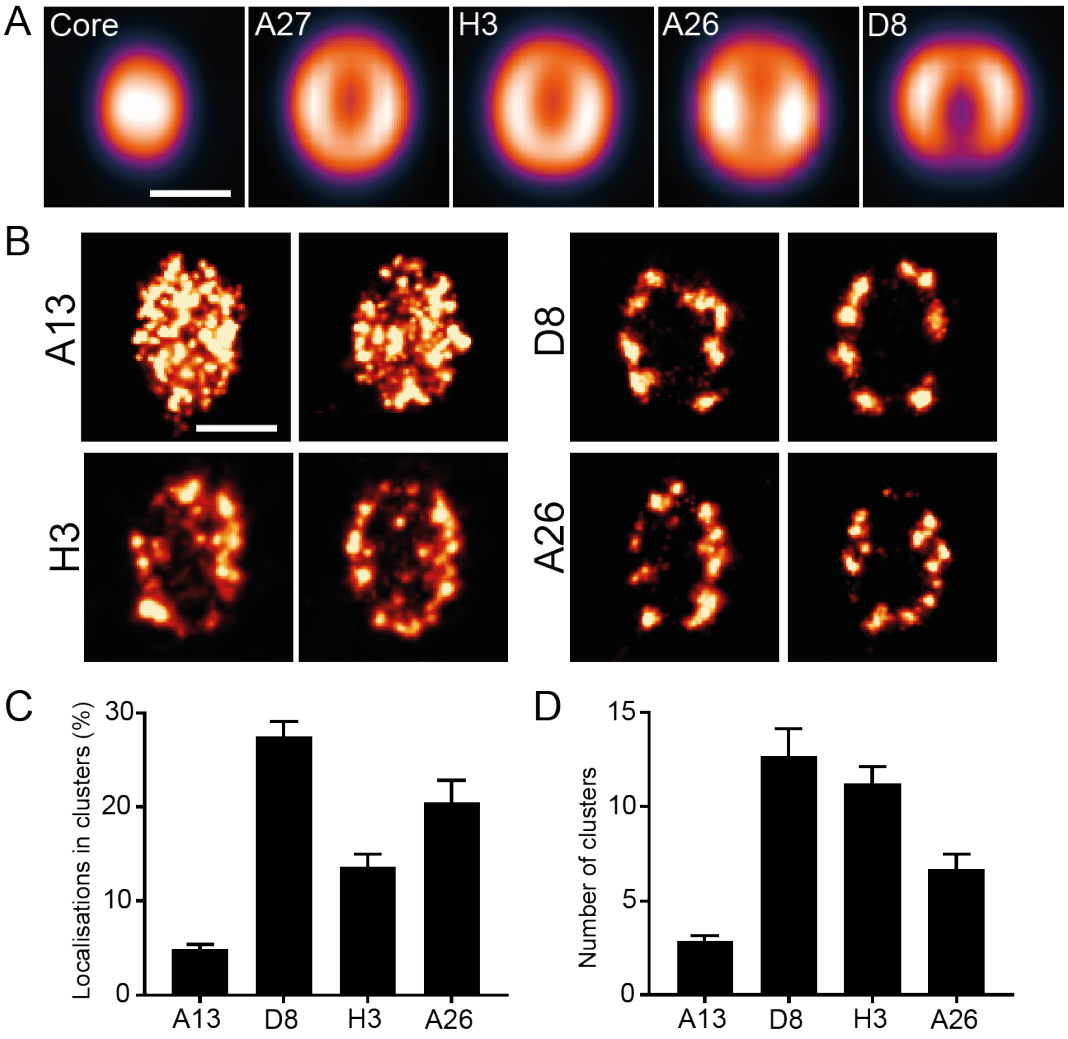

Figure 4.4: VACV binding protein distribution. A) The localisation of the VACV binding proteins were analysed using SIM and VirusMapper (Gray et al., 2016). The core was visualised using recombinant EFGP-A4 or mCherry-A4 virus and used for alignment. A27 and D8 were imaged as in (Gray et al., 2019). H3 and A26 were imaged using recombinant HA-H3 EFGP-A4 or A26-HA mCherry-A4 virus with primary anti-HA antibody and AlexaFluor488 or 594 secondary. Models are representative of $n<200$ virions. B) dSTORM imaging of the distribution of A13, D8, H3 and A26. Two representative virions are shown for each protein. Scale bars, 200 nm. C) Analysis of the percentage of localisations in clusters using SR-Tesseler (Levet et al., 2015). D) Average number of clusters for each protein. Bars represent means $\pm$ SEM of n=10 virions.

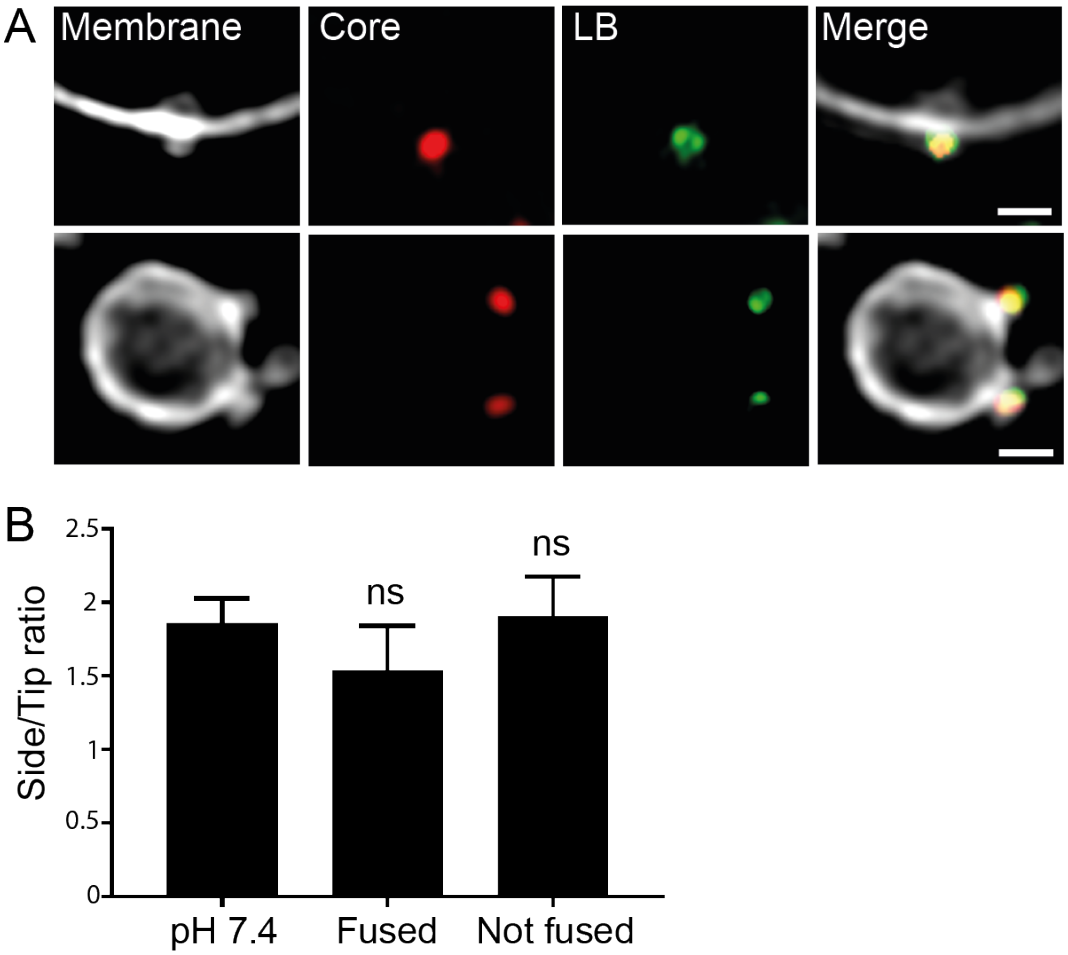

Figure 4.5: VACV binding orientation at pH 7.4 and pH 5.0. A) VACV orientation was assessed using mCherry-A4, EGFP-F17 tagged virus. R18 labelled virus was bound to HeLa blebs at 4°C for 1 hr, washed and the pH adjusted to 7.4 or 5.0. Samples were incubated at 37°C for 10 min. Samples were fixed and imaged using SIM. Examples for tip (top) and side (bottom) binding virions are shown. Scale bar, 1 μm. B) Blebs were purified from HeLa cells. Orientation was quantified at pH 7.4 and pH 5.0, with the subsets of fused or non-fused virions quantified separately in the pH 5.0 case. The side/tip ratio was plotted. Data are means ± standard deviation of three experiments.

change significantly between pH 7.4, pH 5.0 fused and pH 5.0 non-fused virions. This suggests that VACV binding is a static process and the virus does not reorient in response to low-pH. This data also suggested to me that the virus does not need to be bound on its tip to fuse with blebs.

Having quantified the pH dependence of WT orientation and determined that the binding proteins reside largely at the sides of the virus, I looked to elucidate the function of each binding protein in orientation. To do this I utilised recombinant

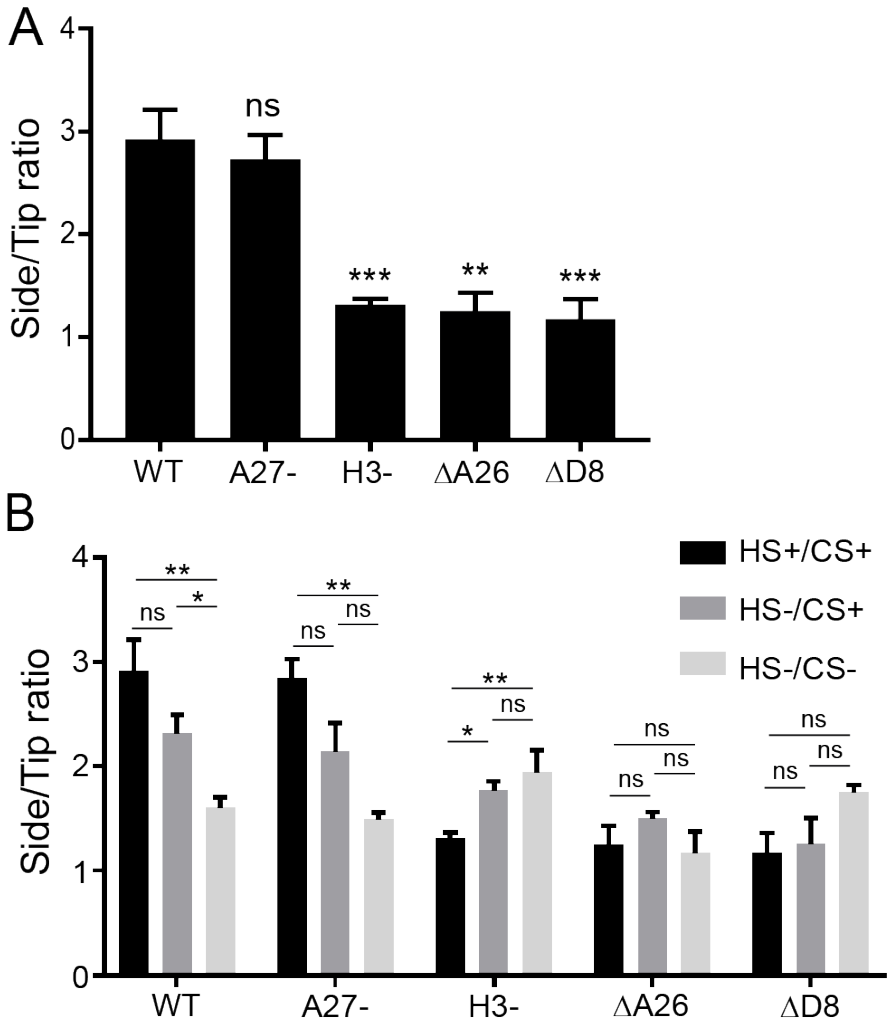

Figure 4.6: Binding orientation of binding protein knockout virions. A) Side/tip ratio was calculated for binding protein knockout mutants on blebs derived from HS+/CS+ cells utilising binding protein knockout viruses with EGFP-A4 tags. Two-tailed unpaired t-test was used for statistical comparison. B) Side/tip ratio was calculated for binding protein knockout mutants on blebs derived from HS+/CS+, HS-/CS+ and HS-/CS- cells. Data from HS+/CS+ is the same as in A. One-way *ANOVA* and Tukey's post-hoc test was used for statistical comparison between cell types for each mutant. Adjusted p-value reported. Data are means ± SD of at least two experiments. *P<0.05, **P<0.01, ***P<0.001, ns P>0.05

virions, deleted for one of the four known binding proteins. Figure. 4.6A shows the side/tip ratio of the binding protein knockout viruses on HS+/CS+ cells. Significant reorientation toward tip binding was seen for the H3-, ΔA26 and ΔD8 viruses. This result suggests that, in line with their side localised distribution on the virus, H3, A26 and D8 are all important for the orientation of viral binding.

H3 and A27 are reported to bind HSPG (Vázquez et al., 1999; Lin et al., 2000) and D8 reported to bind CSPG (Hsiao et al., 1999). To asses the role of GAGs in influencing binding orientation, I utilised the HS+/CS+ derived cell lines, HS-/CS+ and HS-/CS-. Comparing the binding orientation on these cell lines allows for further understanding of the effect of each binding protein in binding orientation. Figure. 4.6B further confirmed the importance of HSPG and CSPG binding proteins H3 and D8 in the side-binding orientation of VACV on the membrane, with WT virus displaying more tip binding when HS and CS were removed. Interestingly, the H3- and ΔD8 displayed more side binding when both HS and CS were removed. This may reflect the activity of A26, which is heavily involved in maintaining a side-binding orientation (Figure. 4.6A).

Figure. 4.7 shows a simplified schematic of the binding orientation data in Figure. 4.6. Overall, the data shows a trend toward more tip binding on HS+/CS+ cells when H3, D8 or A26 are deleted. This trend is continued for ΔD8 and ΔA26 viruses, as well as WT and A27- virus, on HS-/CS+ and HS-/CS- cells. Moreover, this diagram clearly demonstrates that non-GAG and non-laminin interactions of VACV in binding should be explored.

4.4 VACV induces cell-membrane invagination

4.4.1 VACV induced cellular membrane remodelling

I next investigated why WT virions still bind significantly more on their side than tip even when fused (Figure. 4.5B). This result is counter-intuitive as the fusion proteins are polarised to the tips of the virion (Gray et al., 2019). Therefore, the question arises as to how the fusion machinery can engage productively with the cellular membrane when the virus is bound on its side. To answer this, a higher resolution view of the virus-bleb interaction was needed. WT virus was bound to blebs at 4°C for 1 hr, incubated at pH 7.4 or 5.0 for 15 min at 37°C, fixed and imaged with TEM.

This revealed that WT virus can induce dramatic membrane invagination in the bleb membrane at pH 5.0, but not at pH 7.4 (Figure. 4.8A,B). This invagination

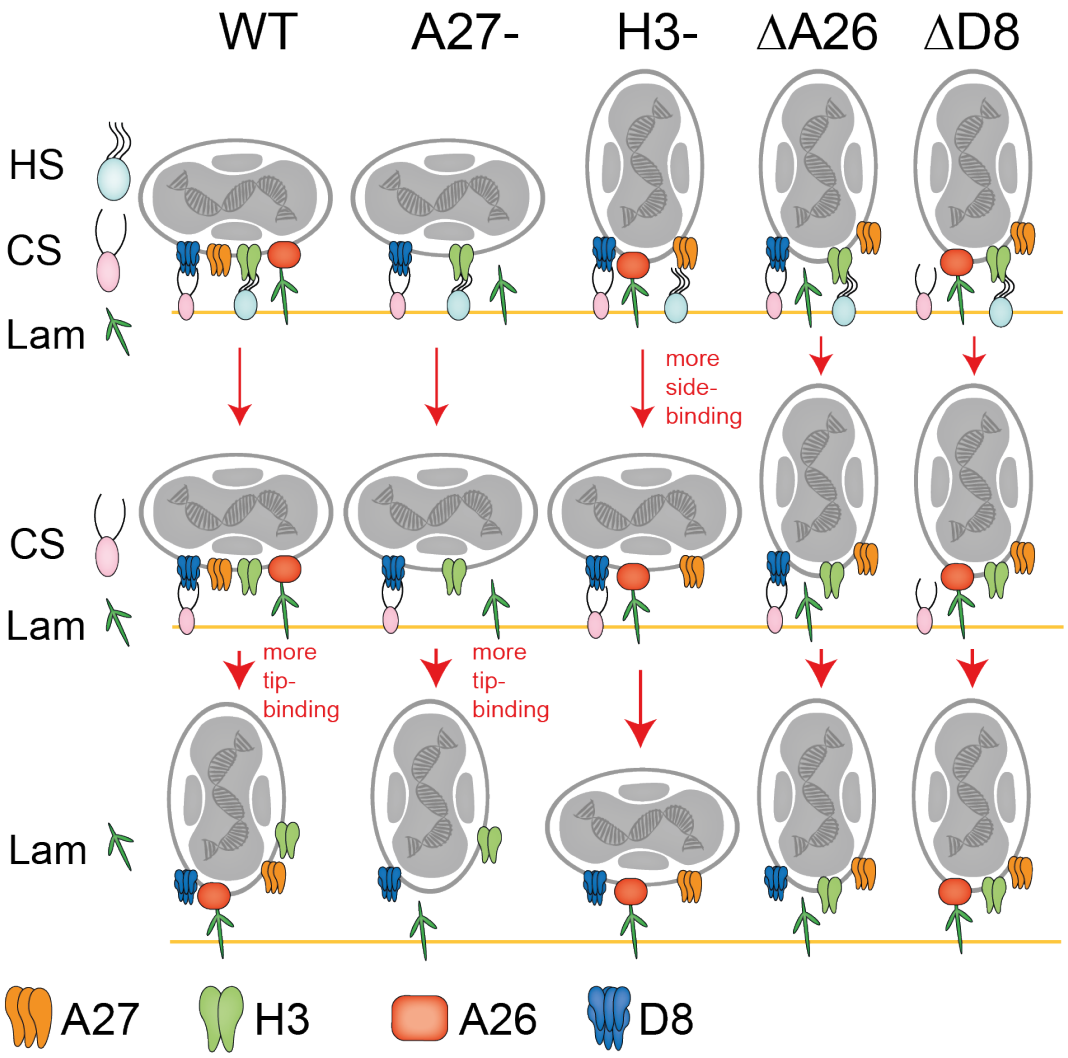

Figure 4.7: Diagrammatic representation of binding orientation data. A simplified diagram representing the binding orientation data in Figure. 4.6 of mutant viruses on parental and GAG deficient cell lines.

was significantly more likely to be induced when the virus was bound on its side as compared to its tip (Figure. 4.8C). I hypothesised that this invagination allows the fusion proteins to contact the cellular membrane at pH 5.0, facilitating productive fusion.

I then sought to ascertain which viral protein(s) are involved in the curvature induction. For this, I again utilised our library of VACV binding and fusion mutants. Due to the side binding bias for invagination induction (Figure. 4.8C), all binding protein mutants were investigated. Under pH 5.0 conditions, all mutants were able to induce invagination in the bleb membrane, except for the ΔD8 virus which in-

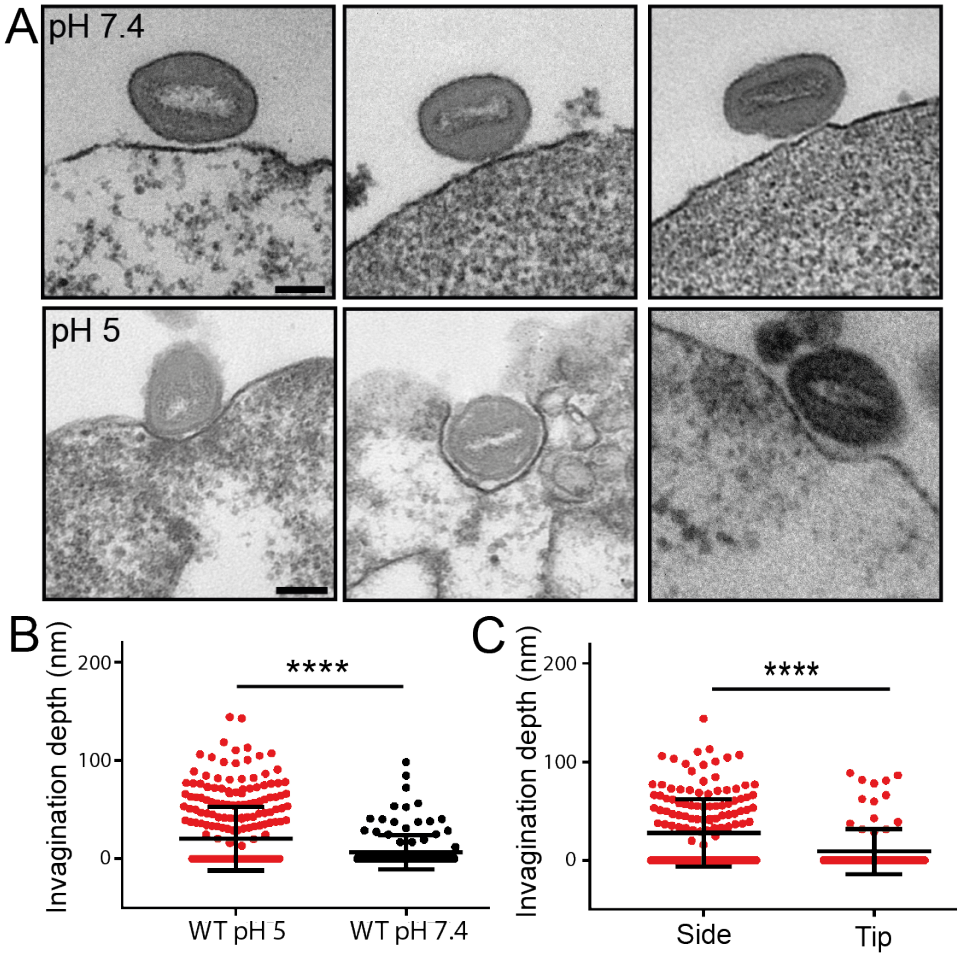

Figure 4.8: VACV induces pH dependent invagination into the bleb membrane. WT virus was bound to HeLa blebs at 4°C for 1 hr, incubated at pH 7.4 or 5.0 for 15 min at 37 °C and fixed. A) Representative bleb-bound virions at pH 7.4 and pH 5.0. Scale bars, 100 nm. B) Invagination depth was quantified and compared between pH 5.0 and pH 7.4 samples. C) Invagination depth was quantified and compared between side and tip bound virions at pH 5.0. Data are means ± SD. Two-tailed unpaired t-test was used for statistical comparison ****P<0.0001.

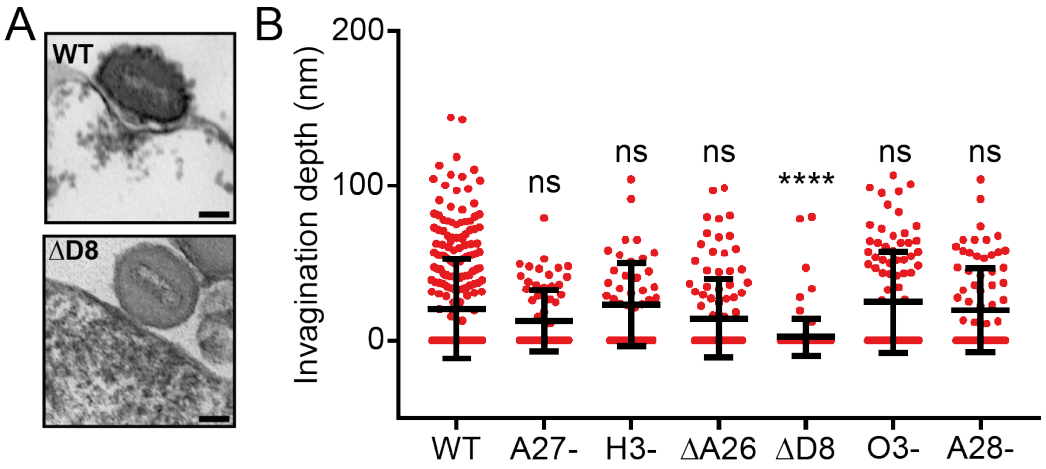

Figure 4.9: ΔD8 virus cannot induce invagination in the bleb membrane at pH 5.0. Virus was bound to HeLa blebs at 4 °C for 1 hr, incubated at pH 5.0 for 10 min at 37 °C and fixed. A) Representative bleb-bound WT or ΔD8 virions. Scale bars, 100 nm. B) Invagination depth was quantified and compared between VACV mutants. Data are means ± SD. Two-tailed unpaired t-test was used for statistical comparison ****P<0.0001, ns P>0.05.

duced significantly less invagination than WT (Figure. 4.9A,B). This suggests that D8 is involved in membrane invagination induction. It is important to note that the the fusion protein mutants, O3- and A28- viruses, could induce invagination at pH 5.0. The A28- virus is able to induce hemifusion but not full fusion, and O3- is not able to induce either (Laliberte et al., 2011). This shows that the invagination under pH 5.0 conditions is not induced by the activation and insertion of the fusion machinery to the membrane.

To further confirm that D8 is involved in bleb membrane invagination induction, we compared invagination induction at pH 5.0 with WT virus on HS+/CS+ and the daughter cell line HS-/CS- cells. As expected, there was significantly less invagination induced on HS-/CS- cells as compared to HS+/CS+ (Figure. 4.10A,B), confirming that D8-CS binding is vital for this process.

4.4.2 pH dependent conformational change of D8

Having found D8 as a key protein involved in the pH dependent membrane curvature induction, I next investigated whether D8 undergoes a conformational change at low-pH to facilitate this. For this, I adapted the papain cleavage protocol from

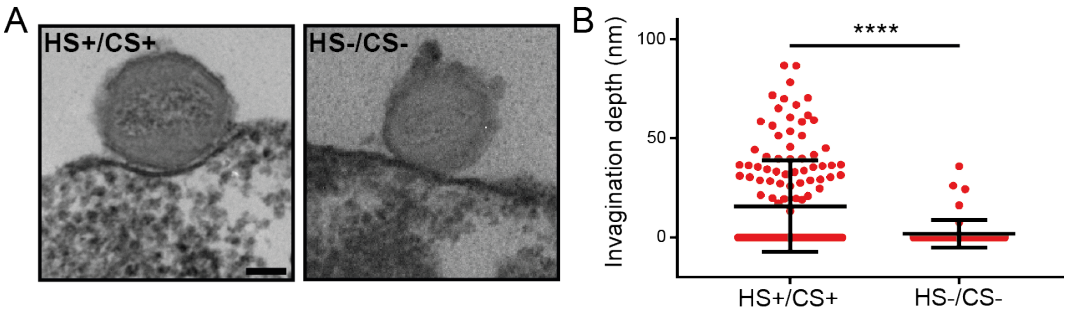

Figure 4.10: Invagination induction on HS-/CS- cells. Virus was bound to HeLa blebs at 4 °C for 1 hr, incubated at pH 5.0 for 10 min at 37 °C and fixed. A) Representative bleb-bound WT virions on HS+/CS+ and HS-/CS- cells. Scale bars, 100 nm. B) Invagination depth was quantified and compared between the two cell types. Data are means ± SD. Two-tailed unpaired t-test was used for statistical comparison ****P<0.0001, ns P>0.05.

Townsley *et al.* (2007). The authors showed that D8 was highly sensitive to the protease papain. I extended this investigation to ask whether the cleavage of D8 differed at pH 7.4 and pH 5.0. WT virions were incubated for 1 hr at 37°C with increasing concentrations of papain at pH 7.4 or pH 5.0, papain was then inactivated, the virions separated by SDS page and D8 blotted for (Figure. 4.11A). Indeed, there was a dramatic difference in the sensitivity of D8 to papain between the two pH points, suggesting that D8 may adopt two different conformations on the viral membrane.

To further investigate the hypothesis that D8 undergoes a conformational change at low-pH, immunoprecipitation (IP) experiments were carried out. First, to confirm that CS-E is the specific CS ligand for D8 (Matho et al., 2014), 0.5 µM soluble D8 was incubated with 0.5 µM or 5 µM biotinylated CS-E or CS-A for 1 hr at RT. CS was then captured by streptavidin coated beads and analysed by western blot for D8. Consistent with the results of Matho *et al.* (2014), significantly more D8 bound to CS-E as compared to the trace amounts that bound CS-A (Figure. 4.11B). Therefore, biotinylated CS-E was used for subsequent experiments. To test whether there is a difference in the binding efficiency of D8 to CS-E at pH 7.4 compared to pH 5.0, soluble D8 was incubated with CS-E at either pH 7.4 or 5. More D8 was detected at pH 5.0 as compared to pH 7.4 (Figure. 4.11C), suggesting that at low-pH D8 adopts a conformation that allows more efficient binding. A 5%

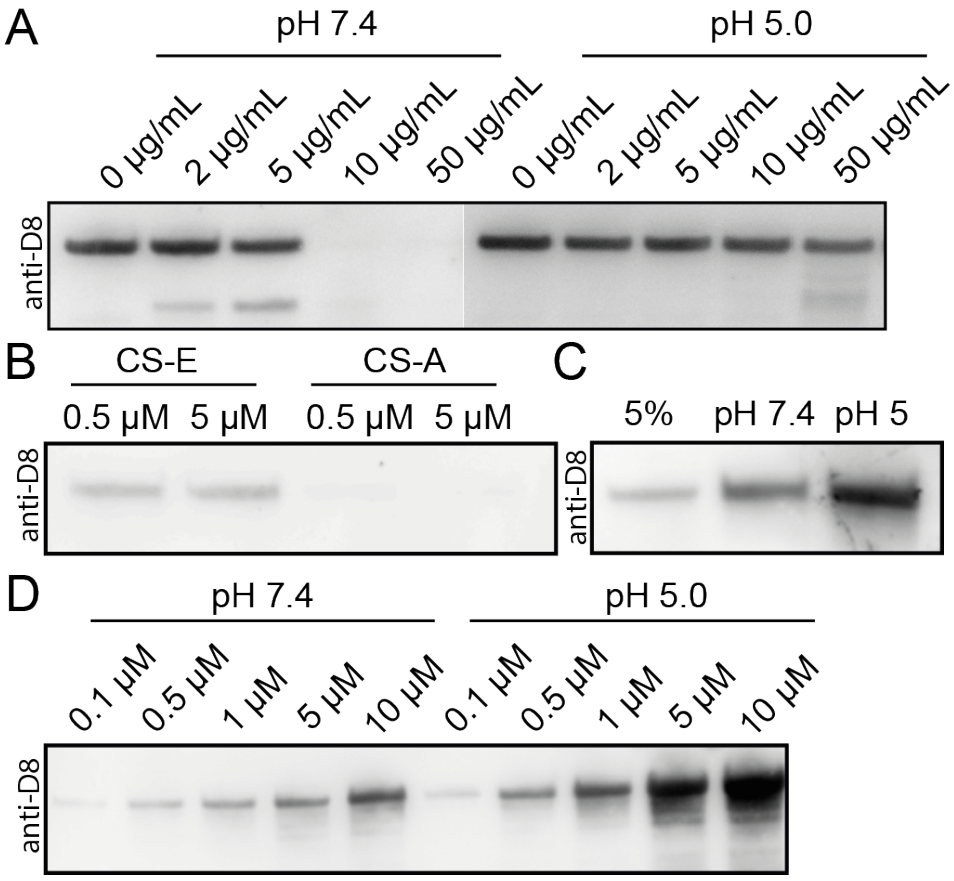

Figure 4.11: D8 may undergo a conformational change at low-pH. A) WT virions were incbuated at 37°C for 30 min with increasing concentrations of papain. After 30 min, papain was inactivated with 40 mM NEM, virions pelleted and analysed by western blot. B) Soluble D8 was incubated with biotinylated CS-E or CS-A for 1 hrs RT and immunoprecipitated with streptavidin beads. C) 0.5 µM biotinylated CS-E and 5 µM D8 were incubated at RT for 1 hr at pH 7.4 or pH 5.0, immunoprecipitated with streptavidin beads and analysed by western blot. 5% input of soluble D8 is seen. D) Experimental protocol as in C but with increasing concentrations of soluble D8. All blots probed with anti-D8 polyclonal rabbit antibody.

input was ran alongside showing that approximately 16% of D8 bound at pH 7.4 compared to 42% at pH 5.0 (Figure. 4.11C). This result was further confirmed by an IP of 0.5 µM biotinylated CS-E with increasing concentrations of D8 (Figure. 4.11D).

Based on the idea that D8 undergoes a pH dependent conformational change at low-pH, I asked whether this was reversible. For this, papain cleavage was used again. WT virus was incubated for 30 min at 37°C at either pH 7.4 or pH 5.0, pelleted and incubated for a further 30 min with papain treatment at the other pH.

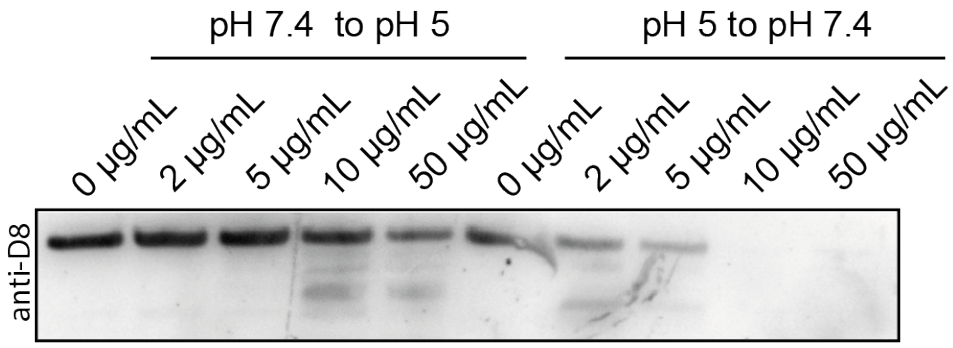

Figure 4.12: The low-pH induced conformational change of D8 appears to be reversible. WT virions were incubated at 37°C for 30 min at pH 7.4 or pH 5.0. After 30 min, virus was pelleted and incubated with increasing concentrations of papain at the other pH. Papain was then inactivated with 40 mM NEM, virions pelleted and analysed for D8 expression by western blot.

As can be seen in Figure. 4.12, the conformational change appeared to be reversible.

Taken together, the data presented in Figure 4.11 strongly suggests that D8 undergoes a reversible conformational change at low-pH to allow more efficient binding to its cellular binding partner, CS-E. This indicates that increased binding of D8 may function to bring the celluar membrane in around the virion, inducing curvature.

The data presented thus far demonstrates that VACV can induce membrane curvature at low-pH which may be mediated by a conformational change in D8. The structure of D8 has been determined by both crystallography and cryo-EM and a positively charged crevice has been identified as the potential D8 binding pocket (Matho et al., 2012, 2014). This contains two highly conserved His residues (Matho et al., 2012). These may be candidates for mediating the conformational change of D8 at low-pH, due to their surface exposure and their ability to be protonated.

Therefore, a mutant virus with His80 to Ala and His176 to Ala mutations was generated and its ability to induce invagination at pH 5.0 investigated (Figure. 4.13A). The histidine mutations appeared not to significantly affect the invagination induction (Figure. 4.13B) and therefore I concluded that these residues are not involved in mediating the hypothetical pH dependent conformational change of D8. The binding efficiency of the point mutant was then compared to WT and ΔD8 using the EGFP core of the viruses as a read-out with flow cytometry (Figure. 4.13C).

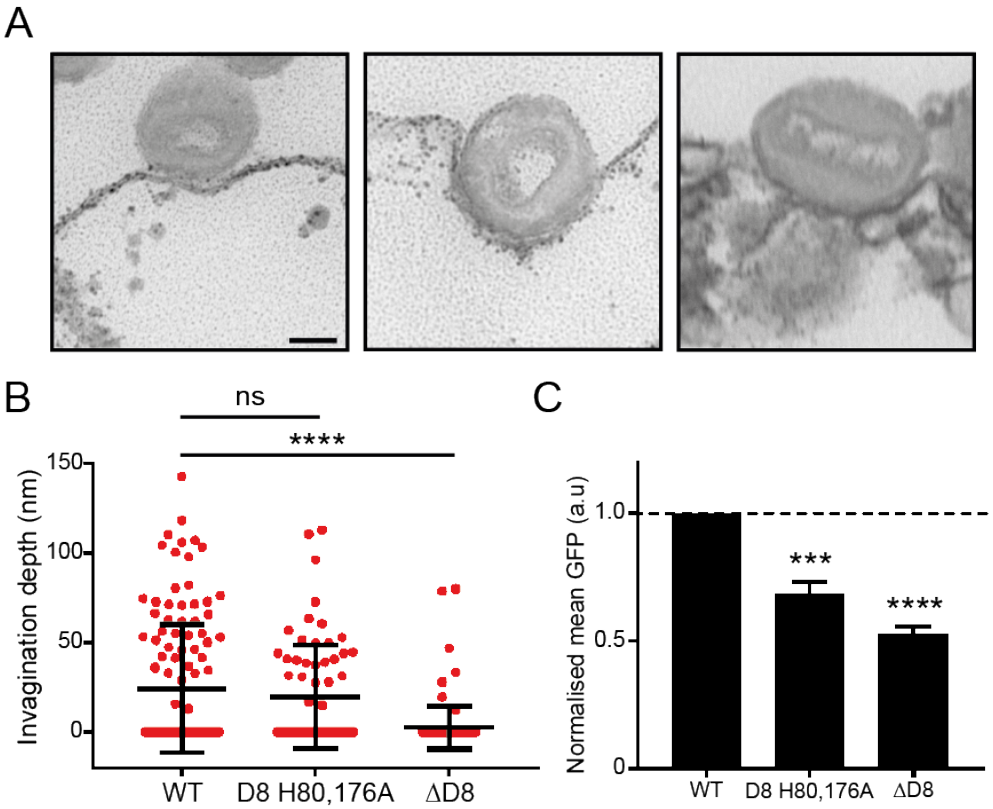

Figure 4.13: Histidines 80 and 176 of D8 are not involved in mediating the low-pH induced cellular curvature. A) D8 H80,176A virus was bound to HeLa cell blebs at 4°C for 1 hr at RT. The pH was then adjusted to pH 5.0 for 10 mins at 37°C. Representative TEM images of D8 H80,176A virus induced curvature are shown. Scale bar, 100 nm. B) Invagination depth was quantified alongside that of WT and ΔD8 virus for comparison. C) EGFP core D8 H80,176A virus, WT virus and ΔD8 virus was bound to L929 cells at 4°C for 1 hr. Cells were fixed and scraped. EGFP mean intensity was analysed by flow cytometry. Data are means ± SD. Two-tailed unpaired t-test was used for statistical comparison ***P<0.001, ****P<0.0001, ns P>0.05.

Binding of the point mutant was significantly lower than WT virus revealing that, although not involved in the membrane invagination mechanism, these two histidine residues are important in the D8-CS interaction. This finding is consistent with these two histidine residues being found within the binding pocket of D8 (Matho et al., 2014).

4.5 A model for VACV induced cellular membrane curvature

The VACV induced membrane curvature has thus far only been visualised on our minimal model system. It is important to now understand this data within the context of cellular infection. The model hypothesised can be seen in Figure 4.14. In this model, WT virus is likely to bind to the plasma membrane on its side, based on the orientation data (Figure. 4.6). Binding induces macropinocytosis (Mercer and Helenius, 2008; Mercer et al., 2010a; Schmidt et al., 2011). It is known that VACV is released from the macropinosome at a late maturation stage (Rizopoulos et al., 2015) when the pH reaches 5.0 or lower within the endosome. I hypothesise that D8 responds to this low-pH environment by undergoing a conformational change resulting in the induction of membrane curvature within the endosome (Figure. 4.8, 4.9, 4.11). This conformational change may increase the ability of D8 to bind CS leading to the membrane being pulled in and around the virus. This envelopment of membrane brings the tips of the virus into intimate contact with the limiting membrane of the macropinosome, resulting in productive fusion and subsequent infection.

4.6 Discussion

In this chapter, blebs were used as a minimal model system to study VACV binding orientation and membrane remodelling. Blebs are a fantastic tool for this due to their smooth surface, small size and lack of the complexity found in living cells. The ability for blebs of different cell types to support VACV binding and fusion was first assessed. VACV could bind and hemifuse with all blebs tested and the kinetics of fusion with HeLa cell-derived blebs was very similar to that seen with cells ((Schmidt et al., 2013b), Figure. 4.3). However, cores were rarely seen within the bleb suggesting that blebs may only support hemifusion and not full fusion. It cannot be ruled out that cores do enter the bleb and are immediately degraded. To test this, it would be useful to carry out the pH 5.0 bleb assay in the presence of cyclohexamide, a drug which prevents core degradation. It is known that increas-

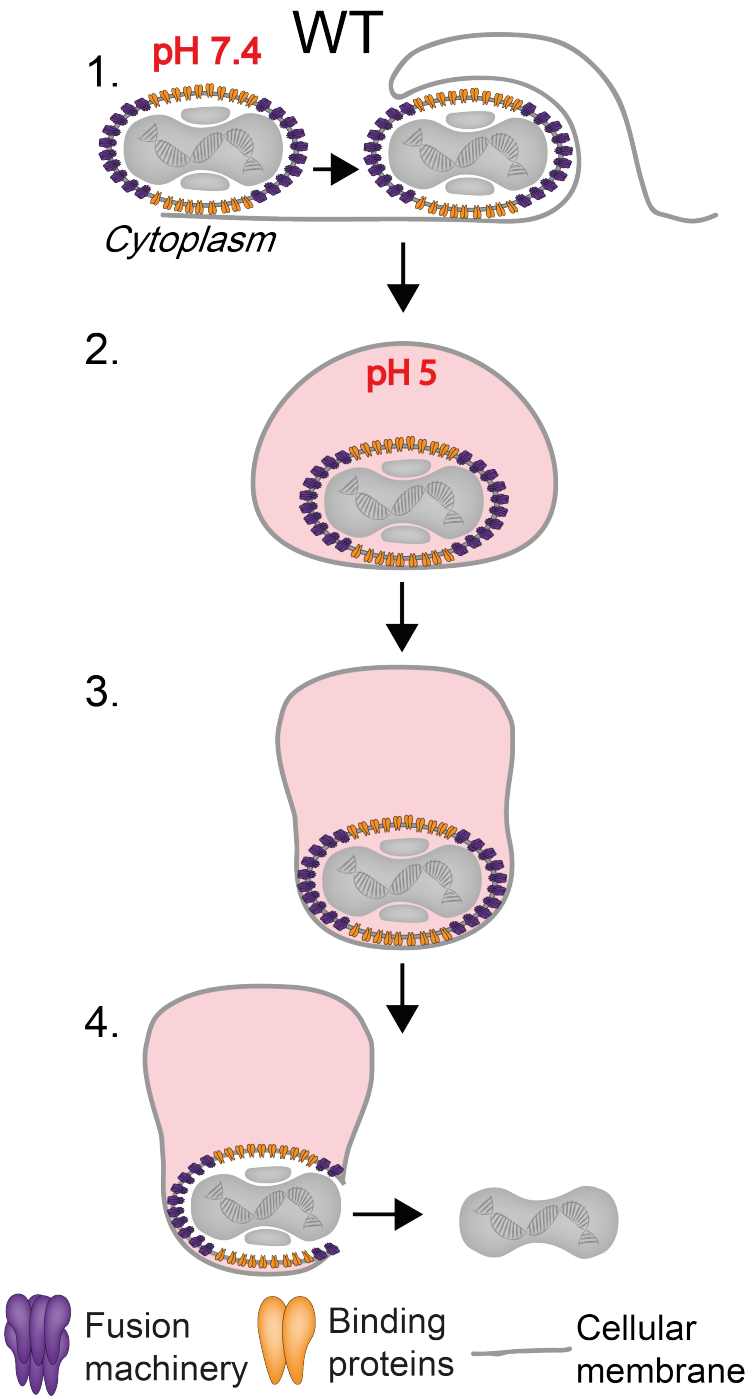

Figure 4.14: A model for VACV induced membrane curvature. (1) WT virus is more likely to bind to the cellular membrane via a side-on orientation. (2) The virus is taken up into the macropinosome. The pH of the macropinosome is lowered to pH 5.0 during macropinosome maturation. (3) WT then can induce curvature in the macropinosome membrane. (4) Virus can fuse with the cellular membrane, leading to core release and productive fusion.

ing positive curvature of the cellular membrane has an inhibitory effect on virus-cell fusion (Tamm et al., 2003; Stiasny and Heinz, 2004; Churchward et al., 2008), therefore it is possible that the high positive curvature of the bleb does not support efficient pore formation and expansion - an energy intensive process (Chernomordik and Kozlov, 2008; Kozlov and Chernomordik, 2015). Overall, our minimal system is amenable to studying the process of binding and hemifusion.

The binding orientation of the virus and the impact of each known binding protein in orientation was then studied. Gray *et al.* (2019) have recently shown that the binding proteins are distributed to the side of the virus, whilst the fusion proteins reside at the tips. To date, the only other virus for which viral protein distribution has been examined is HIV-1. Clustering of Env trimers was shown to correlate with entry competence (Chojnacki et al., 2012), similar to the findings by Gray *et al.* (2019) relating to the VACV EFC. By extending the investigation of protein distribution to H3 and A26, we now have a full picture of VACV binding protein localisation which can be used to understand the binding orientation data (Figure. 4.4).

D8 appeared to be the most side distributed protein, with H3 and A26 appearing more similar to A27 (Figure. 4.4A). dSTORM imaging revealed that both H3 and A26 were clustered similarly to D8 (Figure. 4.4). A26 is known to be a fusion suppressor (Chang et al., 2010, 2012, 2019) which binds to the fusion proteins A16 and G9 (Chang et al., 2012). Therefore, as A16 and G9 are assumed to reside at the tips (Gray et al., 2019), at least some A26 must as well. It would be useful to image both G9 or A16 with A26 using dual-coloured dSTORM and analyse whether and which clusters co-localise. Interestingly, it seems that, from the SIM and dSTORM imaging presented in this thesis, more A26 is found at the sides as compared to the tips (Figure. 4.4A,B). Moreover, A26 is important in maintaining side-on binding (Figure. 4.6). Taken together, this data suggests that A26 may have two distinct functions based on its localisation on the VACV membrane: A26 on the sides of the virus would be involved in binding, whilst A26 localised to the tips of the virus is involved fusion suppression. Additionally, when comparing the clustering of A26's

binding partner, A27 (Gray et al., 2019), A26 clusters are more sparse. This suggests that not all A27 binds A26, a result echoed by Ching *et al.* (2009) and Howard *et al.* (2008) and both who found that A27 migrated alone, as well as in complex with A26 in blots of MVs under non-reducing conditions.

The distribution of H3 on the membrane was interesting. Recently, Mirzakhanyan and Gershon (2019) showed through protein-protein crosslinking and mass spectrometry that H3 is a central hub mediating interactions of A26, A25, D8, A27 and fusion proteins G9, L5, F9, 03 and A28 on the virion membrane (Mirzakhanyan and Gershon, 2019). As the fusion proteins are found at the tips of virions (Gray et al., 2019) and A26, A27 and D8 are found at the sides (Figure. 4.4, (Gray et al., 2019)), it is not surprising that H3 is found at both the tips and sides. In the same way as A26, the involvement of H3 in regulating side-on binding of MVs (Figure. 4.6A,B) can be explained by H3 being more distributed to the sides than the tips.

A27 appeared not to be involved in regulating the binding orientation: the A27(-) and WT viruses were not significantly different in terms of side/tip ratio on all three cell types tested (Figure. 5.2). It is possible, therefore, that A27 is not involved strongly in binding to the cell surface. All evidence to date claiming that A27 is a binding protein has been based on soluble A27 protein or GAG competition assays, and not with A27(-) virus (Chung et al., 1998; Hsiao et al., 1998). The role of each binding protein in virus-cell attachment will be assessed in the next chapter.

Our binding orientation studies were aided by the large size, asymmetry and genetic tractability of VACV, meaning our experimental set-up was simple and easily repeated. Orientation of virus with respect to membrane has been studied for the icosahedral sindbis virus (SINV) (Cao and Zhang, 2013), SFV and poliovirus (Bubeck et al., 2005, 2008). For these studies, liposome-virus complexes were imaged by cryo-EM and post-imaging fiducial markers were added to the point on the target membrane closest to the bound particle. In the icosahedral reconstruction map, the marker introduces a high-density feature if there is a consistent binding orientation. SFV and poliovirus were seen to bind along their 5-fold symmetry axis at neutral and low-pH (Bubeck et al., 2005, 2008), showing similarities to VACV

in that binding is a static and coordinated process, whilst SINV did not bind in a specific orientation (Cao and Zhang, 2013). Although these studies revealed important information on the very first stages of entry and the interplay between binding and fusion for these viruses, they rely on cryo-EM and single-particle averaging methodologies which are time intensive and require rigorous training and expensive equipment. Our set-up is much more simple and faster, requiring less training and specialist equipment, meaning we could easily probe many questions such as the involvement of multiple proteins in binding orientation of VACV.

TEM studies with blebs allowed the discovery of a completely novel function of the protein D8: D8 was able to induce the invagination of the cellular membrane at low-pH (Figure. 4.9). Low-pH conditions mimic the late endosome, the structure that VACV is known to be released from, therefore I hypothesise that the virus can induce this invagination within the macropinosome to aid contact of the fusion machinery at virion tips with the cellular membrane (Figure. 4.14).

It is not surprising that D8 appears to have a role other than that of binding. For example, A26 is both a binding protein and a fusion suppressor (Li et al., 2007; Chang et al., 2010, 2012, 2019), A27 acts in binding, maintaining polarisation of the EFC and in wrapping (Chung et al., 1998; Ward, 2005; Gray et al., 2019) and H3 has a role in both binding and morphogenesis (Lin et al., 2000; da Fonseca et al., 2000b). Multifunctionality of viral glycoproteins is also common throughout the virus genera, especially those with much smaller genomes than VACV. Precedent has indeed been set for viral binding proteins acting to promote fusion, either directly or indirectly. For example, influenza virus HA, dengue virus E protein and rhabdovirus G protein all directly mediate binding and fusion and, as it seems for D8, can undergo pH-dependent conformational changes (Anderson et al., 1992; Chen et al., 1996; Lindenbach and Rice, 2007; Albertini et al., 2012; Edinger et al., 2014). The coronavirus spike protein also mediates both binding and fusion, inducing fusion after proteolytic cleavage within the endosome (Cavanagh, 1995; Belouzard et al., 2012; Heald-Sargent and Gallagher, 2012; Walls et al., 2017). HSV binding protein gD indirectly promotes fusion by undergoing a receptor binding induced conforma-

tional change that leads to activation of gH/gL (Krummenacher et al., 2005; Lazear et al., 2008, 2012; Gallagher et al., 2013; Cairns et al., 2019). gH/gL in turn trigger the fusion protein gB to undergo rearrangements leading to membrane fusion (Heldwein et al., 2006; Atanasiu et al., 2013, 2016).

It makes sense for a virus, with a minimal genome, to utilise its cell surface proteins for multiple roles. This chapter shows that the roles of VACV surface glycoproteins are still being discovered, highlighting just how complex the poxvirus entry mechanism is. As three of the four VACV binding proteins are now known to have a role in promoting virus-cell fusion, it is also becoming clear just how highly regulated this process is.

The invagination induction of VACV on blebs draws parallels with that seen on GUVs with SV40 (Ewers et al., 2010) and human norovirus (Rydell et al., 2013). However, in these cases interaction with lipids were found to be important in inducing the curvature. It was shown for SV40 that curvature induction directly induced uptake (Ewers et al., 2010). VACV induced curvature by D8 differs from this as its pH dependence means it happens post-uptake and instead promotes efficient fusion. It would be interesting to minimise our system even further and to form GUVs with only CSE in the membrane to understand the minimum requirements for invagination and whether other cellular factors are involved. What's more, binding D8 protein to blebs and lowering the pH could show whether other viral factors are involved in mediating this phenotype.

Molecular dynamics (MD) simulations of D8 induced curvature could help us understand more at the atomic level. For SV40 VP1, MD simulations proposed that VP1 adopts a tilted conformation upon binding GM1, causing the protein to push down the lipids underneath leading to induction of negative curvature of the membrane (Kociurzynski et al., 2019). This effect is increased when VP1 molecules cluster, such as on a capsid (Kociurzynski et al., 2019). A very similar mechanism has been proposed for curvature induction by cholera toxin and Shiga toxin B subunits (Pezeshkian et al., 2016, 2017). It would be interesting to use MD simulations to characterise, at the molecular level, the effect of D8-CS interaction on curvature

induction. This would help us understand the minimal number of molecules needed, the architecture of the interaction and the requirements of the cellular membrane.

The actin cortex is known to control cell shape and, along with myosin-II, tension (Vicente-Manzanares et al., 2009; Salbreux et al., 2012; Bergert et al., 2015; Ennomani et al., 2016; Chugh et al., 2017). As the blebs have an actin cortex (Section 3.3.2), the curvature induced by virus on bleb must overcome the mechanical forces presented by the cortex. This force would be less within the low-pH endosome as the actin dissociates during maturation (Schink et al., 2017), again suggesting that the curvature may be even deeper in a real infection setting.

It would be interesting to look for cellular proteins that help to stabilise the membrane invagination and see if these are recruited. Examples of these may be bar-domain proteins (Mim and Unger, 2012). Due to the small size of the blebs, dSTORM would be a way to study this as the resolution would be high enough to quantify if the cellular candidates are enriched only under the virus. If the resolution of SIM is be high enough to resolve candidates, this could be imaged live and the dynamics analysed. In the same way, VACV can be thought of as a tool to study bleb dynamics and ask if cellular processes are activated within blebs. Does actin polymerise under the bleb-bound virus, as it does in macropinocytosis (Swanson, 2008; Mercer et al., 2010a)? Are PAK1 and EGFR, which are essential for MV induced macropinocytosis (Mercer and Helenius, 2008; Mercer et al., 2010a), activated in virus-bound blebs? Understanding this would allow us to map which signaling pathways can be studied in the bleb minimal system. Biochemical experiments suggested that D8 could undergo a pH dependent conformational change on the virus in order to induce the invagination. This was shown to increase the binding of D8 to its binding partner, CSE (Figure. 4.11). In terms of pH-induced conformational changes, this draws parallels with A26 which undergoes a pH dependent conformational change in its role as a fusion suppressor (Chang et al., 2019). This was shown to be mediated by His48 and His53 (Chang et al., 2019). Using a similar logic, I mutated two His residues in the D8 binding pocket to ask whether they mediated the conformational change leading to invagination. It seemed that mu-

tating these did not make a difference in invagination induction on blebs (Figure. 4.13A,B). It is possible that the conformational changed is mediated by other amino acids which can be protonated. It would be advantageous to solve the structure of D8 and pH 7.4 and at pH 5.0 to prove unequivocally that D8 can undergo conformational change.

The pH dependent membrane invagination data is interesting when thought of in the context of the work of Townsley *et al.* (2007). The authors showed that VACV entry involves two independent low-pH steps: exposure to low-pH before cellular attachment stably activated the virus however entry remained sensitive to inhibitors of endosomal pH, whereas treatment of bound virions with low-pH were insensitive to inhibitors of endosomal pH. It is likely that the VACV induced invagination and core activation (Schmidt et al., 2013b) plays a role in one of these pH dependent steps, whilst removal of the fusion suppressor, A26, at low-pH (Chang et al., 2010, 2012, 2019) acts as the other. The interplay between D8 and A26 as regulators of entry is explored further in the following chapter.

Together, the data presented in this chapter shows that blebs can be used as a minimal system to study virus binding, fusion and cellular membrane remodelling. This system can now be used in combination with other viral pathogens to study these activities. Blebs offer a cellular membrane mimic and thus a powerful tool in understanding binding and fusion in a simplified but relevant cellular context. The next chapter will look to understand the results found using our minimal system in the context of cellular infection.

Chapter 5

VACV binding and fusion in a cellular context

5.1 Introduction

As outlined in Section 1.4.1, VACV binding is a highly complex process with an unprecedented number of proteins involved in cell surface attachment (Vázquez et al., 1999; Hsiao et al., 1999; Lin et al., 2000; Li et al., 2007; Foo et al., 2009). Adding to this complexity, the interaction with GAGs appears to vary with cell type, virus strain and experimental condition (Carter et al., 2005; Bengali et al., 2009; Whitbeck et al., 2009). Up until now, almost all of the literature on VACV binding has been carried out with soluble GAG inhibition assays or with soluble VACV protein. Although useful, these are not direct read-outs of the role of each binding protein in infection. It is now important to understand the role of each protein in the context of virion binding.

Therefore, this chapter starts by detailing a flow cytometry based virus binding assay. VACV mutants and GAG-deficient cell lines are utilised with this assay to thoroughly explore binding. This gives a direct read-out of virus binding and, by using both virus and cell line mutants, a full picture of the redundancies and hierarchies between binding proteins is mapped. This information is then corroborated with GAG-inhibition assays to rigorously investigate VACV cell surface interactions.

In Chapter 4, a novel pH dependent step in virus entry was found and a model proposed for the role of this in infection. This chapter aims to understand the invagination data identified with our minimal system in the context of cellular infection. In similar cases, virus-generated cellular invagination has been shown to induce endocytic uptake (Ewers et al., 2010; Rydell et al., 2013). In the case of VACV, as curvature induction is pH dependent, the invagination is thought to happen within endosomes and act to increase the likelihood of productive fusion. This hypothesis is now explored further, utilising the ΔD8 mutant virus and tracking infection in cells.

Lastly, with the data presented in the previous chapter, there are now two pH dependent steps involved in VACV entry. This echoes the findings of Townsley and Moss (2007), where two distinct and separate low-pH steps were found in entry. It is now known that one of these is likely to be the pH dependent removal of the fusion suppressor, A26 (Chang et al., 2010, 2012, 2019). Therefore, this chapter looks to study these two pH dependent processes in relation to each other and ask how they cooperate in entry.

5.2 Redundancies and hierarchies in VACV binding

5.2.1 Directly evaluating VACV binding

As there is a lack of direct binding assays in the literature, I first sought an assay with a direct read-out of virus-cell binding. Flow cytometry was an ideal technique for this, as high numbers of cells could be counted in a short time. EGFP-A4 recombinant viruses were made for each of the 4 binding protein mutants: A27-EGFP-A4, H3- EGFP-A4, ΔD8 EGFP-A4 and ΔA26 EGFP-A4. Virus was bound to HS+/CS+ cells in the cold for 1 hour. Cells were then washed and scraped into 4% PFA, 5% FBS in PBS to avoid removal of bound virus with trypsin.

Figure. 5.1 shows that A26 appeared to be the most important binding protein, as ΔA26 virus bound less than 40% of WT levels. D8 was the next most important followed by H3. Interestingly, deletion of A27 had no significant affect on virion binding.

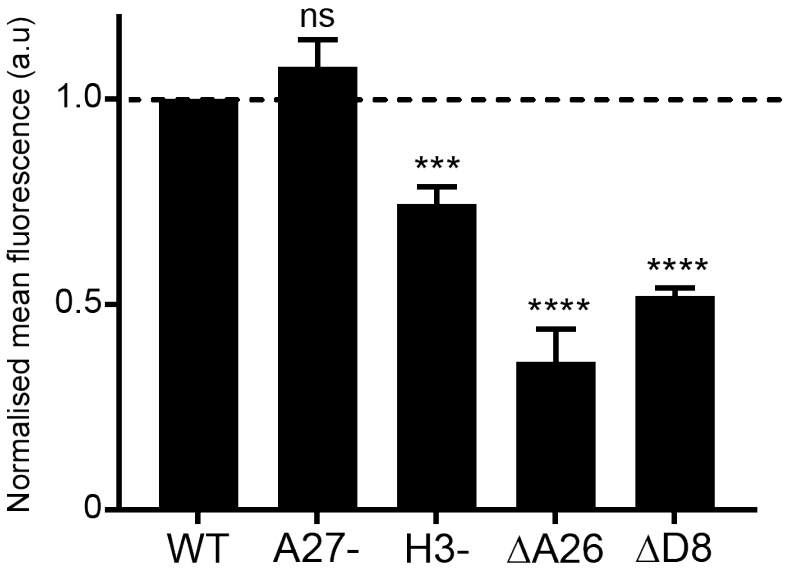

Figure 5.1: VACV binding assay on HS+/CS+ cells. EGFP-A4 binding protein knock-out virus was bound to HS+/CS+ cells for 1 hr, 4°C. Cells were fixed and scraped. EGFP cores were analysed by flow cytometry. Mutant binding data is normalised to WT EGFP-A4 fluorescence. Data are means ± SD of three experiments. Two-tailed unpaired t-test was used for statistical comparison ***P<0.001, ****P<0.0001, ns P>0.05.

Next, to assess the impact of the cellular binding partners, the same assay was carried out on the GAG mutant cell lines. Focusing on WT virus, binding on HS+/CS+ compared to HS-/CS+ cells was not significantly different, but binding to HS-/CS- was approximately 60% of HS+/CS+ (Figure. 5.2). This agrees with a similar experiment by Whitbeck *et al.* (2009) and suggests that CS can compensate for a lack of HS. Taking both this information and the significant decrease in binding of ΔD8 compared to WT on HS+/CS+, the D8-CS interaction appears very important in binding.

There appeared to be no significant difference between H3- binding on HS+/CS+ and HS-/CS+ confirming that H3 does indeed bind HS on cells.

A27- binding follows a similar pattern to WT virus, however binding on HS-/CS- is lower than that of WT. A27- virus lacks A26 (Howard et al., 2008), which most likely accounts for the difference seen here. This result will be explored further in the following experiments. The data with A27- presented in Figure. 5.1 and 5.2

show that A27 does not participate strongly in viral binding.

As the ΔA26 virus can still bind to HS-/CS- cells, this suggests that either L1 (Foo et al., 2009), an unknown binding protein, or a known binding protein with an unknown receptor is able to bind the cell surface in addition to the known interactions. The increase in binding of ΔA26 on HS-/CS+ compared to HS+/CS+ was unexpected and suggests a compensatory mechanism in this situation. This will be explored further in this chapter.

Taken together, the data presented in Figures. 5.1 and 5.2 suggests that CS is more important than HS and that the laminin-A26 interaction dominates in VACV binding. It appears that A26 is the most important binding protein, followed by D8 and then H3. A27 does not have a strong role in cellular binding. It also seems that there are compensatory mechanisms and a hierarchy between the viral binding proteins.

Figure. 5.3 shows a simplified schematic of both the binding affinity and orientation data (Figure. 4.2, 4.6). It is shown clearly in this schematic that reducing the binding affinity of the virus by removing virus-GAG/laminin interaction corresponds with a trend toward more tip binding. Therefore, this correlates with our imaging showing that the binding proteins reside largely at the sides.

5.2.2 Evaluating binding of VACV with soluble GAG and laminin preincubation

Many studies into VACV binding utilise preincubation with soluble GAGs and laminin (Chung et al., 1998; Lin et al., 2000; Carter et al., 2005; Li et al., 2007; Bengali et al., 2009; **?**). As the data presented thus far suggests that there is a hierarchy between the viral binding proteins during cell surface attachment, I further explored this via preincubation studies. This allows the impact of the specific cell surface component to be assessed whilst keeping the availability of all other cell surface factors consistent. WT virus was preincubated with the 100 μg/mL soluble GAG or laminin for 1 hr at 4°C. Virus and GAG/laminin solution was then added to cells for 1 hr at 4°C. Cells were washed to remove unbound virus before fixation. Figure. 5.4A shows that preincubation of virions with CSE or laminin inhibit virus

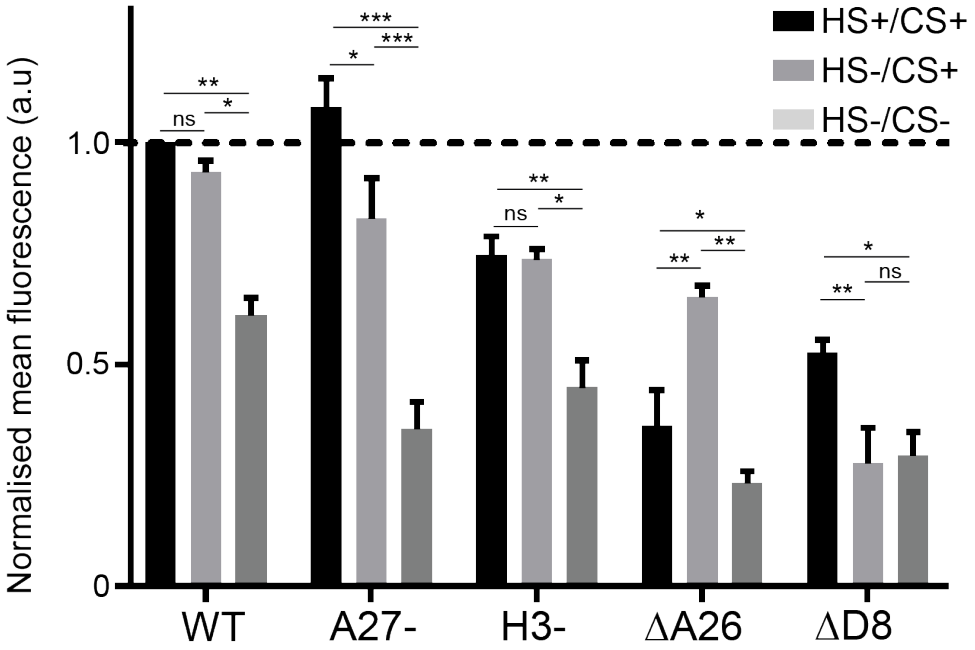

Figure 5.2: VACV binding assay on HS+/CS+, HS-/CS+, HS-/CS- cells. EGFP-A4 binding protein knockout virus was bound to HS+/CS+, HS-/CS+ and HS-/CS- cells for 1 hr, 4°C. Cells were fixed and scraped. EGFP cores analysed by flow cytometry. Data is normalised to HS+/CS+ WT fluorescence. Repeated measures one-way *ANOVA* and Tukey's post hoc test was used for statistical comparison. Adjusted p-value reported. Data are means ± SD of three experiments. *P<0.05, **P<0.01, ***P<0.001, ns P>0.05.

binding the most as compared to no treatment. This indicates that CSE and laminin are the most important cellular factors in binding. As D8 and A26 are their respective viral binding partners, this data is in agreement with what I have shown above (Figure. 5.1). That CSA had no impact agrees with the *in vitro* results from Section 4.4.2. Interestingly, H and HS appeared to have little to no impact on viral binding (Figure. 5.4A). This suggests that these may not be the biologically relevant ligands for H3 on the cell surface of HS+/CS+ cells or that soluble H and HS are unable to bind to the WT virus due to steric effects of the other binding proteins on the membrane.

There appeared to be no additive effect of CSE and laminin together (Figure. 5.4A). The effect of incubating with one first and then adding the other was tested

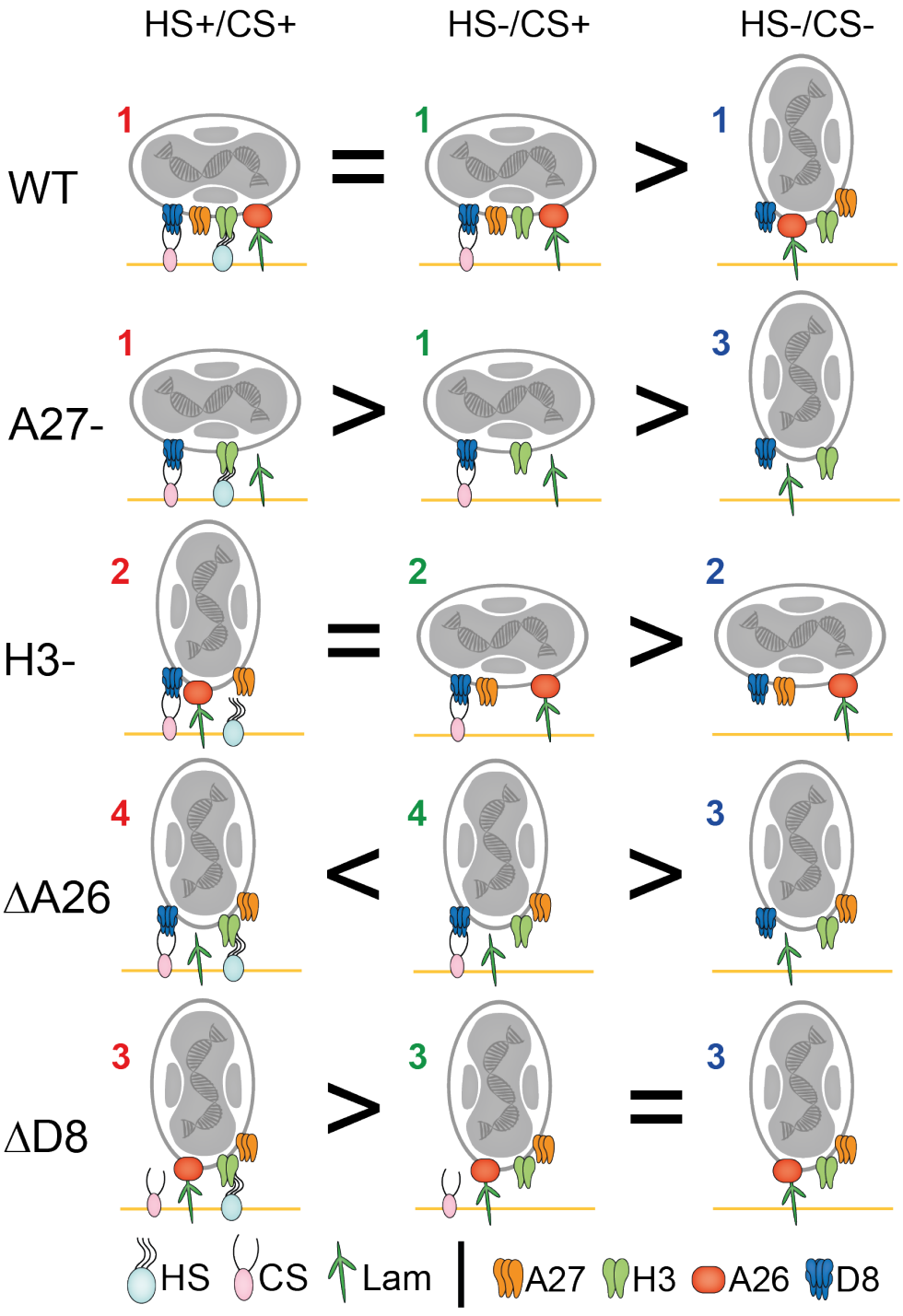

Figure 5.3: Diagrammatic representation of binding affinity and orientation of VACV binding mutants. Schematic of the data in Figure. 5.2 and Figure. 4.6. =, <, >represents comparisons in binding affinity for each virus on the three cell lines. Vertical numbers represents the comparison of binding affinity between mutant viruses on each cell line, with 1 representing highest binding affinity. The trend in binding orientation is also shown.

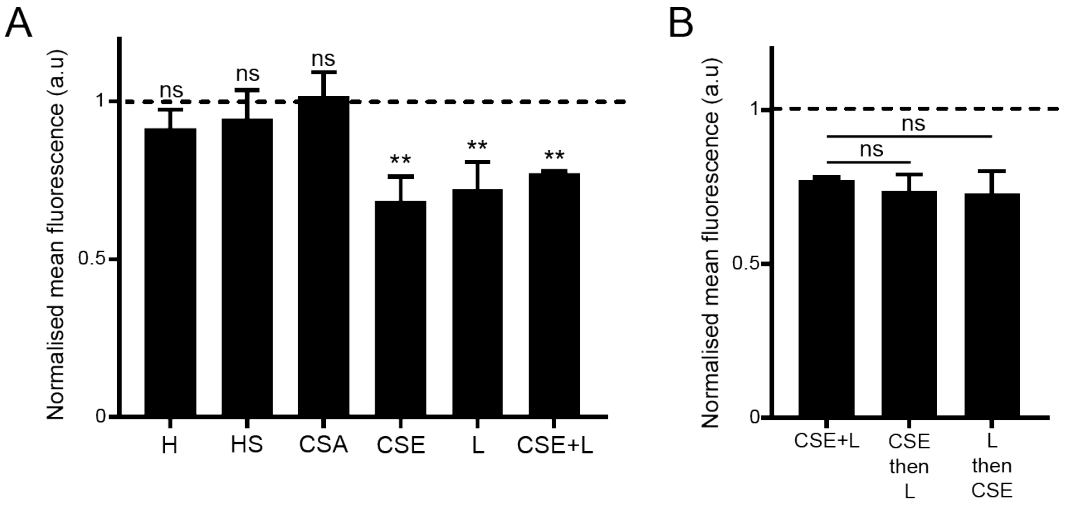

Figure 5.4: VACV binding assay on HS+/CS+ with cellular protein preincubation. A) EGFP-A4 was preincubated with 100 µg/mL heparin (H), heparan sulfate (HS), chondroitin sulfate A (CSA), chondroitin sulfate E (CSE) and laminin (L) for 1 hr at 4°C. B) EGFP-A4 was pre-incubated 100 µg/mL CSE and L together, CSE for 1 hr followed by addition of L for 1 hr or L for 1 hr followed by the addition of CSE for 1 hr at 4°C. Virus and protein solution was then added to HS+/CS+ cells in the cold for 1hr. Cells were fixed and scraped. EGFP cores analysed by flow cytometry. Data is normalised to HS+/CS+ WT fluorescence with no treatment. Data are means ± SD of three experiments. A) Two-tailed unpaired t-test was used for statistical comparison against virus with no treatment. B) One-way *ANOVA* and Tukey's post hoc test was used for statistical comparison between cell types for each mutant. Adjusted p-value reported. **P<0.01, ns P>0.05.

to explore whether there was an impact on the availability for binding of either when added together. There was no significant difference seen between the three conditions (Figure. 5.4B). However, there is still the possibility that steric hindrance prevents efficient binding of both at the same time. Preincubating with CSE and then pelleting virions before incubation with laminin was tried, but a large amount of virus was lost in the pelleting process meaning results were inaccurate.

5.2.3 Binding of A27- virus

Having begun to thoroughly assess the redundancies and hierarchies between binding proteins, I turned back to determining why the A27- virus bound to similar levels as WT to the cell surface despite lacking both A26 (Howard et al., 2008) and A27 (Figure. 5.1). To explore this, the incorporation of the remaining binding proteins

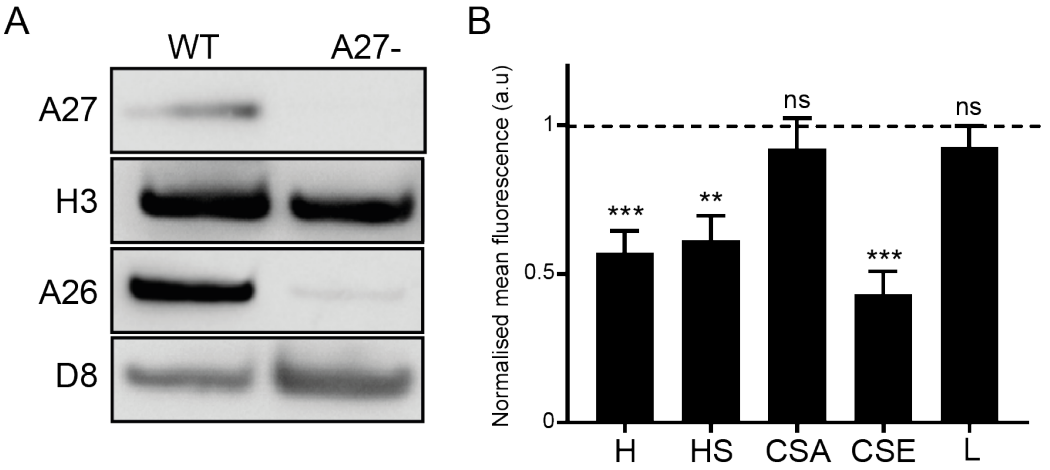

Figure 5.5: Understanding the binding pattern of A27- virus. A) Equal numbers of WT and A27- virions were analysed by western blot. A27, A26, D8 and H3 were blotted for. B) A27- EGFP-A4 was preincubated 100 µg/mL cellular protein for 1 hr, 4°C before incubation with HS+/CS+ cells for 1 hr, 4°C. Data are means ± SD of three experiments. Two-tailed unpaired t-test was used for statistical comparison against virus with no treatment. **P<0.01, ***P<0.001, ns P>0.05.

were first analysed to confirm that deletion of A27 does not alter the packaging of the other binding proteins. A26 and A27 were confirmed to not be incorporated into the virion as expected (Howard et al., 2008) and the amounts of H3 and D8 were comparable to WT virions (Figure. 5.5A).

The cellular protein inhibition assay was then carried out on A27- EGFP-A4 virus to assess the availability and use of each remaining binding protein. Surprisingly, binding of this mutant was significantly inhibited by H, HS and CSE. This inhibition was more than what was seen for the same three GAGs on WT (Figure. 5.4A). This suggests that A27 may shield H3 and D8 somewhat. As the degree of binding with the A27- virus is the same as with WT virus (Figure. 5.1), the data presented here shows that D8 and H3 can compensate for the lack of the strongest binding protein A26, in the A27- virus.

5.2.4 Binding of ΔA26 virus

As it seems that the viral binding proteins show a compensatory mechanism and that there appears to be a hierarchy between them, I wondered if this was the case for the unexpected significant increase in binding on HS-/CS+ cells compared to

HS+/CS+ cells with ΔA26 virus. To explore this idea, ΔA26 binding to HS+/CS+ and HS-/CS+ cells was first visualised by fluorescent microscopy to confirm the increase in binding seen with flow cytometry (Figure. 5.6A). Indeed, ΔA26 bound more to HS-/CS+ cells than HS+/CS+. The amounts of the H3 and D8 incorporated into the ΔA26 virus were then investigated to confirm that these levels were not changed dramatically in the mutant, which could explain differences in binding. A27 was not blotted for as A27 does not participate strongly in binding, based on data presented thus far. Figure 5.6B shows that the incorporation of H3 or D8 was not significantly different to WT.

Next, I asked whether the cellular receptor for the ΔA26 virus on HS-/CS+ cells was proteinaceous. Pronase contains numerous proteases and peptidases and is capable of hydrolysing most peptide bonds (Bermejo-Barrera et al., 1999). Cells were pretreated with or without pronase before incubation with virus. Analysis of bound virions by flow cytometry showed that binding was reduced to very low levels on both HS+/CS+ and HS-/CS+ cells in the presence of pronase, confirming that the prominant receptor(s) on HS-/CS+ is indeed proteinaceous (Figure. 5.6C). Moreover, there was no significant difference in binding between no treatment and pronase treated HS-/CS- cells, showing that the binding of ΔA26 on these cells requires non-protein receptors.

I then carried out the cellular protein preincubation assay on HS+/CS+ cells to discern differences in the protein utilisation of the ΔA26 virus compared to WT. Figure. 5.6D shows that, similar to WT, binding of ΔA26 was not significantly inhibited by H, HS or CSA (compare with Figure. 5.2). The ΔA26 virus was inhibited significantly by CSE, however this inhibition was not as large as with WT (binding normalised to no treatment was 0.81 ± 0.03 with ΔA26 compared to 0.72 ± 0.09 with WT). This shows that, for the ΔA26 virus, the D8-CSE interaction accounts for most of the binding. Additionally, as the cellular protein dependence is similar to WT but the overall binding significantly less, it is clear that the A26-laminin interaction is very important in viral binding.

As CSE was the only GAG that had a significant effect on ΔA26 binding to

HS+/CS+ cells, the cellular protein inhibition assay was then carried out on HS-/CS+ with CSE to test whether interaction with this protein was responsible for the increase in binding. Figure. 5.6E shows the binding on CSE preincubated virus normalised to no treatment on the cell line indicated. Binding was significantly more inhibited by CSE on HS-/CS+ compared to HS+/CS+, showing that in the absence of HS, the D8-CSE interaction becomes much more dominant. When visualised in a different way (and normalised to WT virus), it can be seen clearly that ΔA26 preincubation with CSE reduced binding on HS-/CS+ cells to HS+/CS+ levels, showing that the increase in binding on HS-/CS+ is due completely to CSE binding (Figure. 5.6F).

Taken together, the data presented in Figure. 5.6 shows that VACV can utilise cellular ligands in a cell-type dependent fashion. Moreover, the data suggests that the deletion of one binding protein has an effect on the availability for binding of the other proteins, a result repeated in Figure. 5.5. This demonstrates that there are indeed hierarchies and redundancies between the binding proteins.

5.3 Exploring pH dependence in VACV entry

Thus far, this chapter has shown that the two proteins most important in VACV binding are D8 and A26. Interestingly, both of these may undergo pH dependent conformational changes (Chang et al., 2019). Therefore, we sought to understand the interaction between these proteins in both binding and entry, and how their pH dependent processes impact infection.

5.3.1 The invagination induced by D8 acts to promote entry

Firstly, the role of the invagination produced by D8 at low-pH was investigated in the context of infection. Based on the model hypothesised (Figure. 4.14), there would be less fusion and less productive infection with the ΔD8 virus as compared to WT. To test this hypothesis, the R18 fusion assay was first carried out. Less fusion was induced by ΔD8 compared to WT over the time recorded (Figure. 5.7A).

To investigate whether this delay impacted full fusion or just hemifusion, early gene expression was measured using quantitative reverse transcription-PCR (RT-

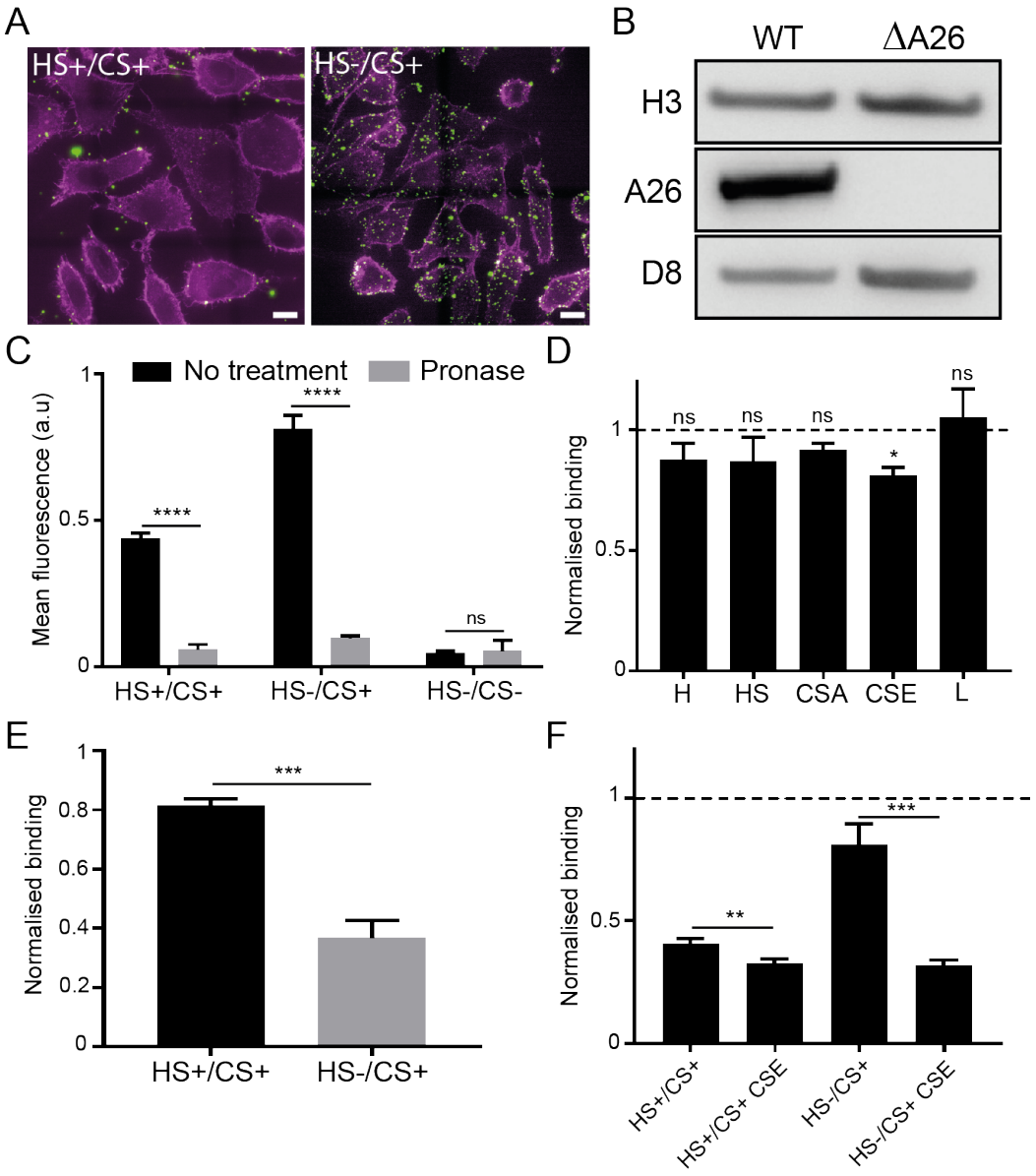

Figure 5.6: Understanding the binding pattern of ΔA26 virus. A) ΔA26 EGFP-A4 virus was bound to HS+/CS+ and HS-/CS+ cells at 4°C for 1 hr. Cells were washed, fixed and stained with phalloidin (magenta). Virus shown in green. Scale bar, 20 µm. B) Equal numbers of WT and ΔA26 virions were analysed by western blot. C) Cells were treated with or without pronase for 1 hr, 37°before incubation with ΔA26 EGFP-A4 for 1 hr, 4°C. Binding analysed by flow cytometry. D) ΔA26 EGFP-A4 was preincubated with 100 µg/mL cellular protein for 1 hr, 4°C before incubation with HS+/CS+ cells for 1 hr, 4°C and analysed by flow cytometry. Data is normalised to ΔA26 no treatment. E) Same experimental protocol as D. Data is shown as the binding normalised to no treatment on the respective cell line. F) The same data as in D. Data is now normalised to WT no treatment. Data are means ± SD of three experiments. Two-tailed unpaired t-test was used for statistical comparison. *P<0.05, ***P<0.001, ****P<0.0001 ns P>0.05.

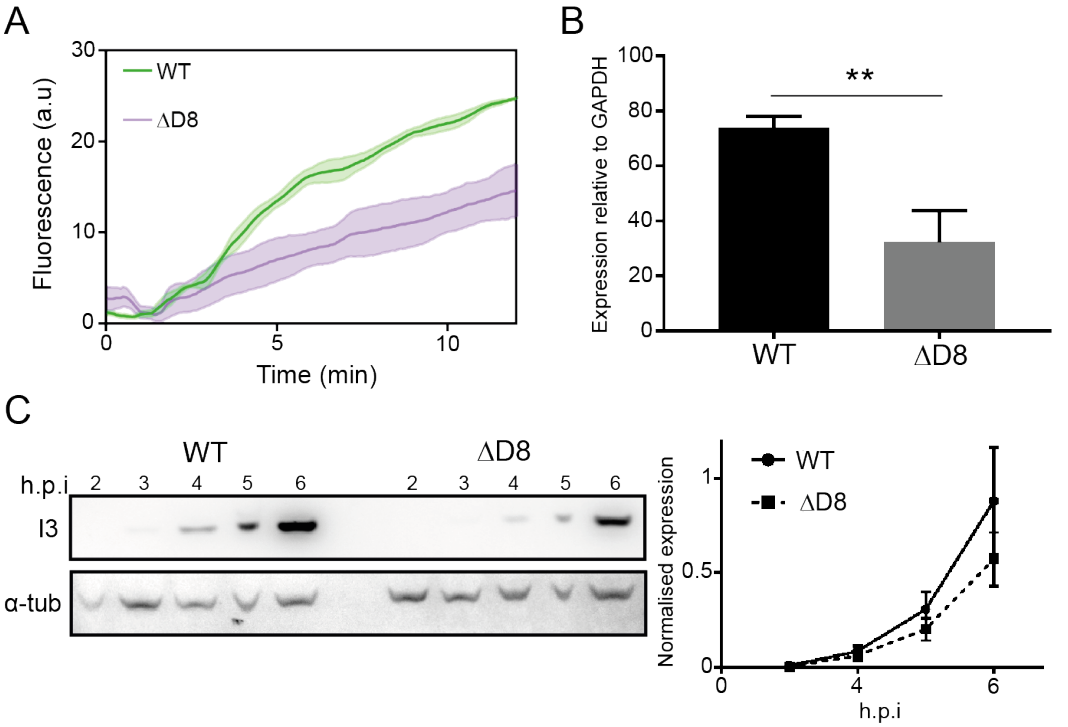

Figure 5.7: ΔD8 virus shows a delay in infection. A) Equal numbers of R18 loaded ΔD8 and WT virions were bound to HeLa cells for 1 hr at 4°C. The pH was lowered after 1 min of recording. Fluorescence is normalised to the initial value and the final fully dequenched value after TX-100 addition. B) ΔD8 and WT at MOI 10 were bound to HeLa cells 1 hr at 4°C for 1 hr, before warming to 37°C for 2 hours. C11 expression was measured by RT-qPCR. C) I3 protein expression was measured by western blot over 6 hours for WT and ΔD8 virus. An example blot is shown, with expression level quantification adjacent of three separate experiments. All data are means ± SD of three experiments. Two-tailed unpaired t-test was used for statistical comparison. **P<0.01.

qPCR). Early genes are expressed immediately after the core enters the cytoplasm (Fields et al., 2007) and are therefore the earliest readout post fusion. The early gene C11 was measured. Figure. 5.7B show significantly less C11 mRNA was produced by the ΔD8 virus as compared to WT at 2 hpi.

This investigation was extended across a 6 hour time-span, and showed that early protein levels produced by ΔD8 were consistently less than WT (Figure. 5.7C). In addition, a different early gene, I3, was used to confirm that C11 expression was an accurate proxy for early gene expression. Together, this data shows that the pH dependent invagination produced by D8 acts to increase the rate of infection, agreeing with the model hypothesised.

5.3.2 VACV can induce D8 mediated curvature within the macropinosome

To validate the hypothesis that VACV can manipulate the curvature of the macropinosome membrane to promote fusion, I aimed to capture images of virus within macropinosomes using TEM. As virus residing in the macropinosome is transient and thus difficult to capture in significant numbers, I utilised the fusion protein deficient virus, A28-. By using a virus which cannot fuse and therefore cannot be released from the macropinosome, I was able to capture more events than with WT. Importantly, A28- virus can induce invagination in the bleb membrane similar to WT (Figure. 4.9B). In addition to this mutant, I also generated an A28-ΔD8 virus to compare curvature induction and validate the model. Figure. 5.8A shows that D8 was indeed knocked out in the double mutant generated. L1 was used as a loading control.

To identify virus within the macropinosome, a TEM workflow was developed which used horseradish peroxidase (HRP) to label endosomes. The peroxidase activity of HRP was used to polymerise 3,3-diaminobenzidine (DAB) monomers within the endosome. This results in an increase in electron density within the endosome making them easily visible in TEM, as well as ensuring only true endosomal events are studied. Equal particle numbers of each virus were bound to HeLa cells at RT for 1 hr. Full media supplemented with 10 mg/mL HRP was added and cells shifted to 37°C for 1 hr before fixation.

With both mutants, many events of virus residing in the macropinosome were captured. To specifically analyse and compare the curvature induced by single virions on the macropinosomal membrane, the Fiji plugin Kappa was used (Mary and Brouhard, 2019). Kappa measures curvature using B-splines (Mary and Brouhard, 2019). Only virions adjacent (assumed to be bound) to the macropinsomal membrane and in a side-on orientation with respect to the membrane were used in the analysis, so as not to skew the data with the high curvature values around the tip of the virus. The macropinosomal membrane contacting the virion membrane was traced, and the curvature values plotted. Figure. 5.8B shows representative images

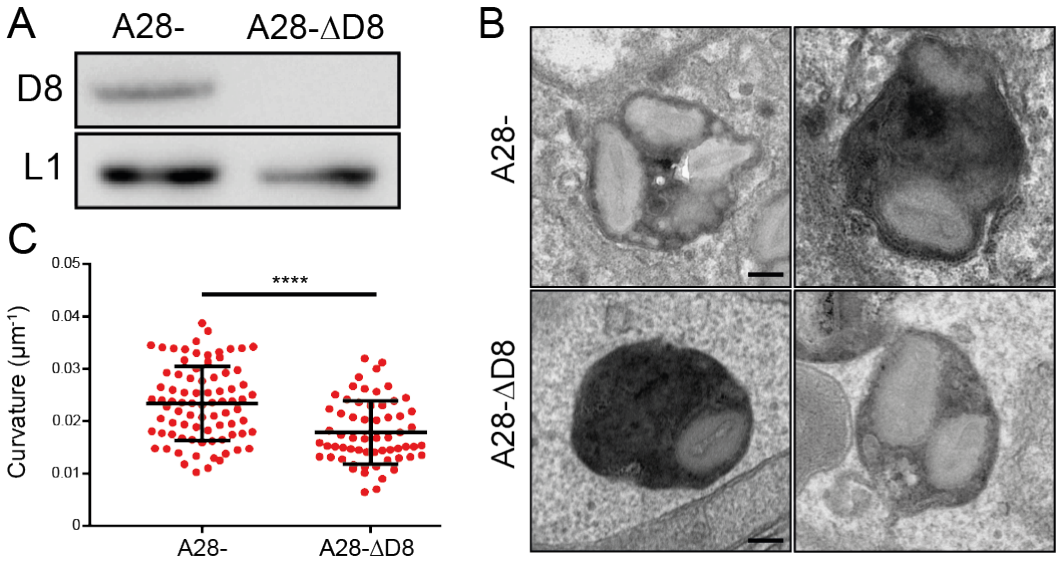

Figure 5.8: VACV is able to induce D8 mediated curvature of the macropinosomal membrane. A28- or A28-ΔD8 virus was bound to HeLa cells for 1 hr at RT. Cells were washed, fresh media supplemented with 10 mg/mL HRP added and samples shifted to 37°C for 1 hr before fixation. A) Western blot analysis of A28- and A28-ΔD8 virions for D8 and L1. B) Representative TEM images of A28- and A28-ΔD8 virus residing within macropinosomes. C) Quantification of curvature of the macropinosome around single virions using the Kappa plugin (Mary and Brouhard, 2019) for Fiji. n=3 separate experiments. ****P<0.0001.

of virus within the macropinosome. When analysed, significantly higher curvature was produced by the A28- virus as compared to the A28-ΔD8 virus, agreeing with the model presented in Chapter 4 (Figure. 4.14).

5.3.3 Increased utilisation of D8-CS interaction correlates to increased entry

Thus far, it has been shown that D8 acts to induce pH dependent invagination within the macropinosome and that this increases the likelihood of productive fusion. It is now important to examine the cellular factors involved in the curvature induction.

Firstly, the role of CS was assessed. As the ΔA26 virus utilised the D8-CSE interaction significantly more for binding on the HS-/CS+ cells compared to the HS+/CS+ cells, I asked whether this was the case for WT VACV and then whether this correlates with increased entry. WT virus was preincubated with CSE and then bound to HS+/CS+ or HS-/CS+ cells for 1 hr at 4°C. Binding was quantified

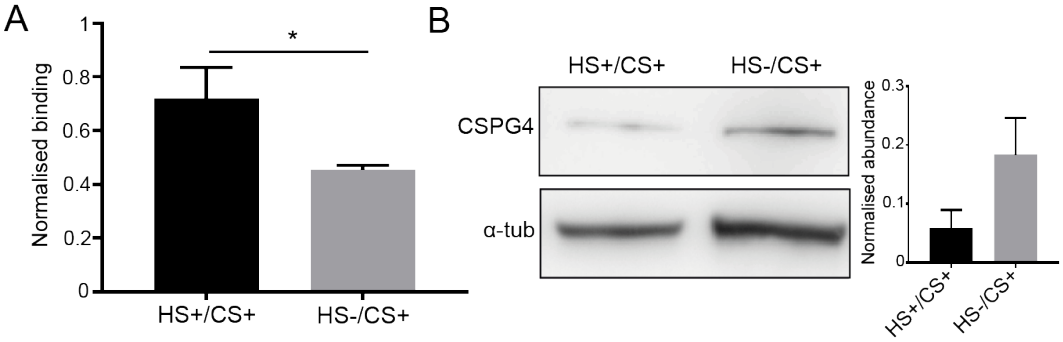

Figure 5.9: HS-/CS+ cells show more CS binding and more CSPG4 A) WT EGFP-A4 was preincubated with 100 µg/mL CSE for 1 hr, 4°C before incubation with HS+/CS+ or HS-/CS+ cells for 1 hr, 4°C and binding analysed by flow cytometry. Data is shown as the binding normalised to no treatment on the respective cell line. B) Representative blot showing HS+/CS+ and HS-/CS+ cells resolved by SDS-PAGE and immunoblotted for CSPG4. α-tubulin was used as the loading control. Data are means $\pm$ SD of three experiments. Two-tailed unpaired t-test was used for statistical comparison. *P$<$0.05.

using flow cytometry (Figure. 5.9A). Indeed, as with the ΔA26 virus, binding was significantly more inhibited on HS-/CS+ cells by CSE preincubation than HS+/CS+ suggesting that the D8-CS interaction compensates for the lack of HS.

Next, I wondered whether HS-/CS+ cells showed up-regulation of any CS containing proteins. Frei *et al.* (2012) showed that CSPG4 was highly important for binding of WT virus to HeLa cells. Therefore, I asked whether more CSPG4 was found on HS-/CS+ compared to HS+/CS+. When CSPG4 protein levels were analysed on both cells types and normalised to α-tubulin levels, more CSPG4 was found on HS-/CS+ cells (Figure. 5.9B). This may account for the increased use of CSE as a ligand on these cells.

Having found the D8-CS interaction was used more on HS-/CS+ than HS+/CS+ cells, I asked what impact this would have on infection. It seemed feasible that the increase in D8-CS interaction may correlate to increased invagination, as D8 has been found to be vital for invagination induction (Figure. 4.9). To this end, blebs were generated from both cells types, WT virus bound and the pH lowered. The invagination was found to be significantly deeper on HS-/CS+ compared to HS+/CS+ cells, suggesting an increased utilisation of D8-mediated binding on this cell type.

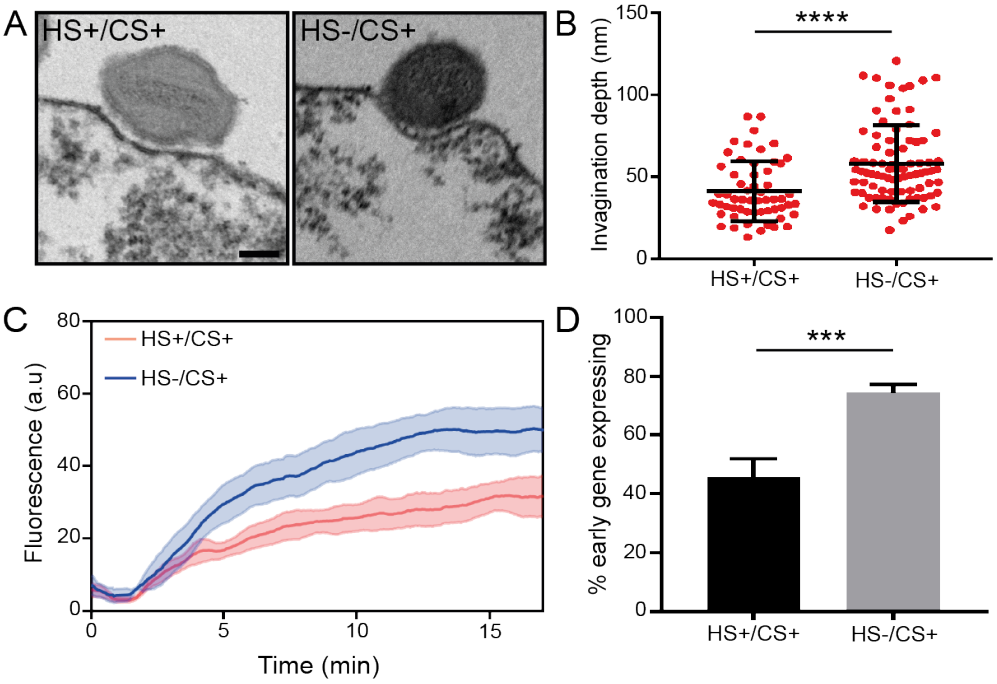

Figure 5.10: Increased CS usage leads to increased entry kinetics. A) Virus was bound to blebs at 4°C for 1 hr, incubated at pH 5.0 for 10 min at 37°C and fixed. Scale bars, 100 nm. B) Invagination depth was quantified for both cell types. Only those inducing invagination are quantified. C) R18 fusion assay was carried out with R18 labelled WT virus on HS+/CS+ cells and HS-/CS+ cells. D) WT virus expressing EGFP under an early gene promoter was bound to HS+/CS+ cells or HS-/CS+ cells for 1 hr at RT. Samples were then washed and shifted to 37°C for 4 hours before fixation and analysis by flow cytometry. Percentage of EGFP expressing cells is shown. Two-tailed unpaired t-test was used for statistical comparison ***P<0.001, ****P<0.0001.

As invagination induction on HeLa blebs correlated to increased fusion and infection, I then asked whether the increased invagination depth on HS-/CS+ cells would lead to more fusion and infection. Hemifusion was first assessed using the R18 fusion assay. Indeed, at MOI 10, the rate of hemifusion was increased on HS-/CS+ cells as compared to HS+/CS+ cells.

I then extended this investigation to virus entry. Early gene expression was used as a read-out for the earliest point post-fusion. A WT virus which encodes EGFP under an early promoter was generated. Cells were infected, fixed after 4 hours at 37°C and EGFP expression determined by flow cytometry. Figure. 5.10D shows that significantly more HS-/CS+ cells expressed early genes at 4 hours post infection.

Taken together, the data in Figures. 5.7, 5.8, 5.9 and 5.10 show that VACV uses the D8-CS interaction to induce curvature of the macropinosomal membrane which acts to increase the likelihood of productive fusion and thus speeds the kinetics of entry and the establishment of VACV infection.

5.3.4 Evaluating the two pH dependent processes of VACV entry

Having correlated the invagination data in Chapter 4 with infection, I now sought to understand how the pH dependent proteins D8 and A26 acted together during entry. It seems that deleting the fusion suppressor A26 increases the rate of infection (Chang et al., 2010, 2012, 2019) while deleting the pH dependent invagination inducer, D8, decreases the rate of infection (Figure. 5.7). In an attempt to tease out an interplay between these two, a double knock-out ΔA26ΔD8 was generated. This mutant allowed me to study how the two pH dependent processes independently influence fusion, as well as how both proteins together cooperate during virus binding.

The ΔA26ΔD8 virus was first characterised for binding and infection. When compared to WT and the single knockouts, the binding of ΔA26ΔD8 was significantly less than WT and ΔD8, and was less but not significantly so than ΔA26 on HS+/CS+ (Figure. 5.11A). This implies a strong compensatory effect from the remaining binding proteins. No significant difference was seen between the HS-/CS+ and HS-/CS- cells as expected due to the lack of D8 and thus the lack of CS binding ability of the virus. Moreover, the increase in binding seen on HS-/CS+ with the ΔA26 virus was abolished with the double knockout, confirming that the increase in binding observed was due to an increased reliance for D8-CS binding (Figure. 5.11B).

Next, the comparative ability of the ΔA26ΔD8 virus to produce infectious particles was determined. BSC40 cells were infected with an MOI 1 and the number of particles produced after 24 hrs was measured by plaque assay. The yield after 24 hrs was significantly reduced compared to WT. This agrees with studies showing that the 24 hour yield of ΔA26 virus is equal to WT (Chang et al., 2010) and that of the ΔD8 virus is a log lower than WT (Hsiao et al., 1999).

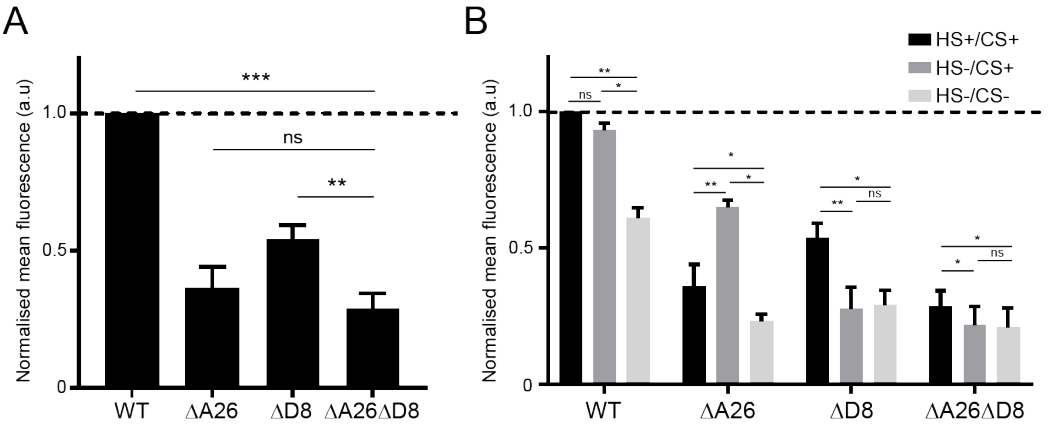

Figure 5.11: Quantification of binding of the ΔA26ΔD8 virus. EGFP-A4 WT or binding protein knockout virus were bound to A) HS+/CS+ or B) HS+/CS+, HS-/CS+ and HS-/CS- cells for 1 hr, 4°C. EGFP fluorescence analysed by flow cytometry. Data are means ± SD of three experiments. A) Two-tailed unpaired t-test was used for statistical comparison. B) Repeated measuresonewayANOVAand Tukey's post hoc test was used for statistical comparison. Adjusted p-value reported. ***P<0.001, **P<0.01, *P<0.05, ns P>0.05.

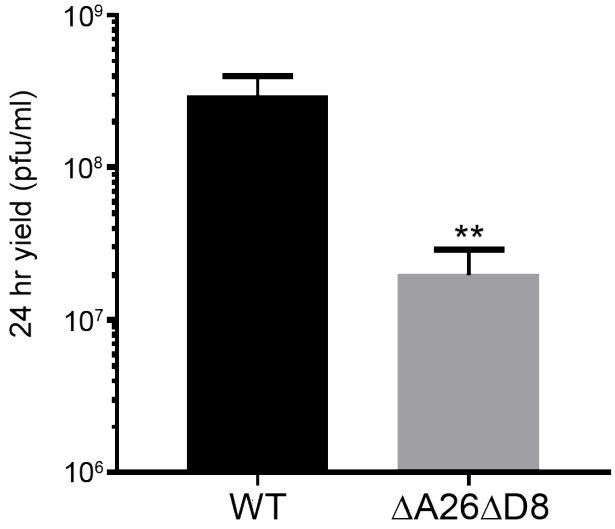

Figure 5.12: Growth of ΔA26ΔD8 virus compared to WT. BSC40 cells were infected with WT or ΔA26ΔD8 and harvested 24 hours post infection (hpi). Infectious virus produced was titred by plaque assay on 6-well plates. Data are means ± SD of three experiments. Two-tailed unpaired t-test was used for statistical comparison. **P<0.01.

Having generated a virus lacking the two known pH dependent steps in entry, the role of each was evaluated by comparing the ΔA26ΔD8 virus to the single knockouts and WT. Firstly, the R18 fusion assay was carried out to compare the ki-

netics of hemifusion (Figure. 5.13). As expected, the rate of fusion of the ΔA26 was faster than WT due to the lack of the fusion suppression (Chang et al., 2010, 2012, 2019). The ΔD8 virus acted in the opposite manner, showing less hemifusion than WT in the given time frame. When both pH dependent steps were removed, the opposite effects of the single deletions balanced out resulting in hemifusion rates similar to WT (Figure. 5.13).

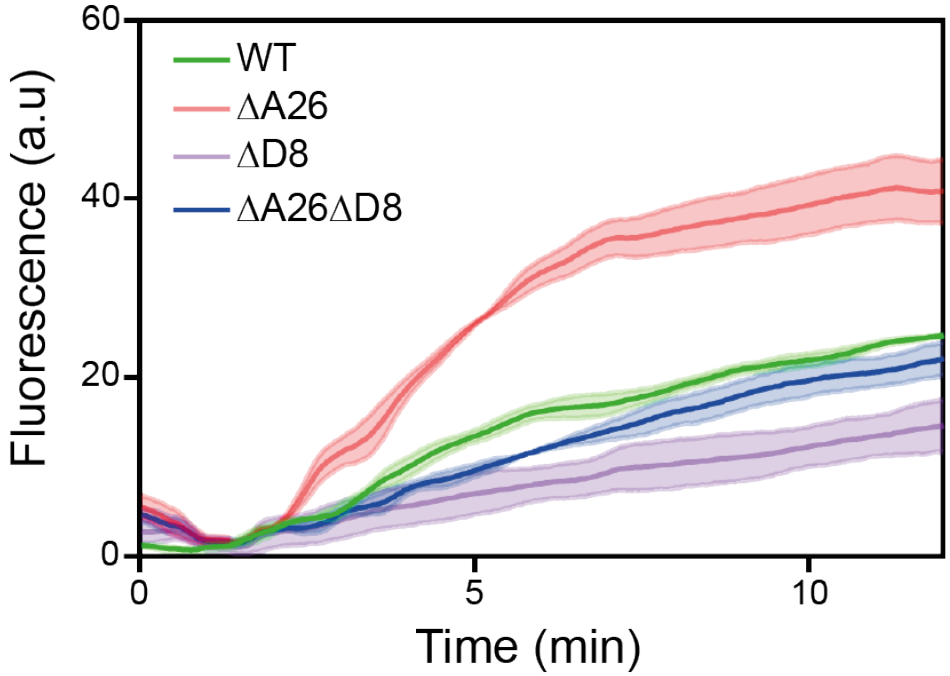

Figure 5.13: Comparative rates of R18 dequenching. Equal numbers of R18 loaded WT, ΔA26, ΔD8 and ΔA26ΔD8 virions were bound to HeLa cells for 1 hr, 4°C. The pH was lowered after 1 min. Fluorescence is normalised to the initial value and the final fully dequenched value after addition of TX-100. Data for WT and ΔD8 are the same as shown in Figure. 5.7. Data are means ± SD of at least two experiments.

Fusion was then alternatively assessed via fusion from without (FFWO), an indirect assay to measure full fusion. In this assay, virus is bound at high MOI to monolayers of BSC40 cells, the pH shifted to 7.4 or 5.0 for 5 min at 37°C, before being returned to neutral pH and incubated at 37°C for 2 hr. If the virus is capable of full fusion, the cells are 'stapled' together forming large multi-nucleated cells termed syncytia. The extent of syncitya formation can be quantified by calculating the fusion index (White et al., 1981; Mercer et al., 2010b) which is given by the

equation:

$$f = [1 - (\frac{C}{N})]$$

where f is the fusion index, C is the number of cells and N is the number of nuclei.

To corroborate the hemifusion rates seen in Figure. 5.13, FFWO experiments were carried out with WT, ΔA26 and ΔA26ΔD8 virus. WT was bound at either MOI 25 (Figure. 5.14A,B) or 100 (Figure. 5.14C,D). The mutants were then added at equal particle count to WT. The apparently lower density of the cells in the pH 7.4 case is due to virus-induced cell rounding or retraction: cell densities were equivalent upon infection.

At MOI 25, the ΔA26 virus did not show a large increase in FFWO at pH 7.4 compared to WT (Figure. 5.14A,B), although this has been reported previously (Chang et al., 2010, 2012; **?**, 2019). This is likely due to differences in cell type, as BSC40s are used here and HeLas used in the referenced publications (Chang et al., 2010; **?**). However, an increased fusion index for ΔA26 compared to WT was seen when more virus was added (Figure. 5.14C, D). As the system was not saturated at MOI 25 pH 5.0, differences in viral fusion between mutants could be determined. Similar to the R18 assay (Figure. 5.13), the increased fusion index seen with the ΔA26 was normalised toward WT levels in the ΔA26ΔD8 (Figure. 5.14B).

Taken together, Figures 5.13 and 5.14 show that D8 acts in combination with A26 to regulate the kinetics of fusion. These results indicate that the two pH dependent steps in VACV entry act opposingly to regulate VACV fusion. This would presumably allow for very precise control of the location and timing of VACV fusion.

5.4 Discussion

In this chapter, VACV binding and the interplay between the four known binding proteins was explored in unprecedented detail. Moreover, a novel invagination phenotype was found using the bleb system and found to be relevant to VACV fusion in the context of infection. Using EGFP-A4 binding protein knockout viruses, GAG knockout cell lines and flow cytometry, the hierarchies and redundancies between

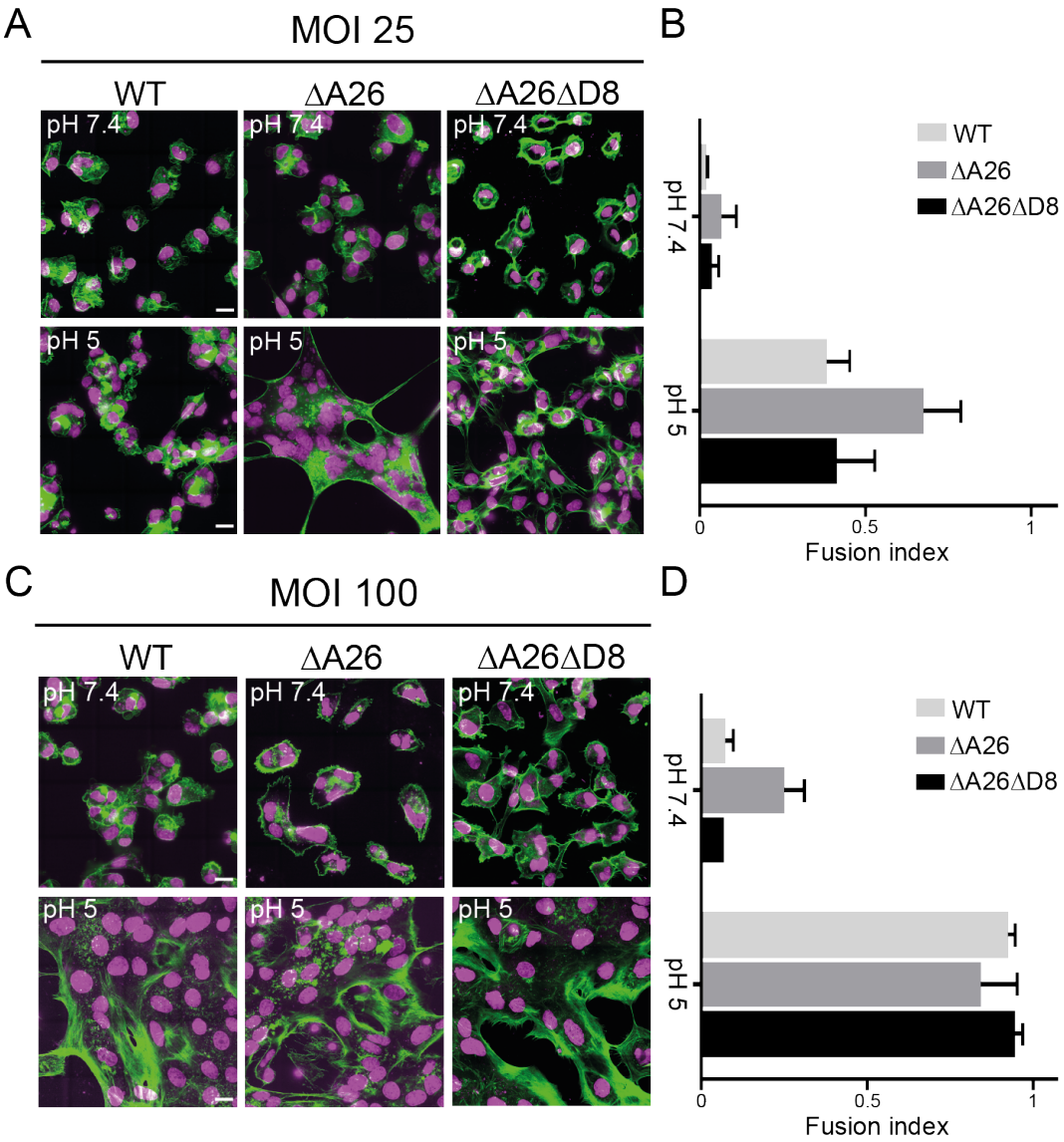

Figure 5.14: WT, ΔA26 and ΔA26ΔD8 fusion from without. Equal particle numbers of WT, ΔA26 and ΔA26ΔD8 virus was bound to BSC40 cells in the cold for 1 hr, shifted to the indicated pH for 5.0 min at 37°C and returned to neutral pH and incubated at 37°C for 2 hr. Confocal images of fusion from without experiments with WT, ΔA26 and ΔA26ΔD8 virus at A) MOI 25 or B) MOI 100. Scale bars, 20 μm. Nuclei shown in magenta and actin in green. B and D) Quantification of the fusion index for A and C respectively. Data are means ± SD of three experiments.

the viral binding proteins were investigated. A26 was found to be the most important viral protein involved in VACV binding, followed by D8 and H3. Contrary to published literature (Chung et al., 1998), very little role for A27 was found in WT virus binding. In agreement with my results, CSE and laminin were found to inhibit binding most strongly, with H and HS showing little effect. This data is strongly supported by Frei *et al.* (2012), who showed A26, CSPG4 and laminin binding protein DAG1 to be major players in VACV binding to HeLa cells.

The sub-type of CS was found to be very important. When comparing the binding efficiency of CSA, C, D, E, H, HS and dermatan sulphate to soluble D8 protein, Matho *et al.* (2014) found that CSE was the only one to bind efficiently. I extended this to show that CSE is more important than CSA for viral binding (Figure. 5.4). CSA is the most commercially available sub-type of CS and therefore the one used in most of the literature, which may explain why CS has never been shown to have a strong effect on virion binding (Chung et al., 1998; Carter et al., 2005; Li et al., 2007; Bengali et al., 2009; **?**).

CSE and CSD are both highly sulfated, whilst CSA and CSC are monosulfated. CSA and CSC have been shown to have no inhibitory effect on VACV binding (Carter et al., 2005) and CSD has been shown not to bind D8, even though CSE can bind strongly (Matho et al., 2012). Therefore, it seems that both the degree and position of sulfate groups is important. CSE has been shown to be the specific CS sub-type used for HSV (Bergefall et al., 2005), dengue virus (Avirutnan et al., 2007; Kato et al., 2010) and HTLV-1 (Sugiura et al., 2013) binding, all of which also bind heparin sulfate (WuDunn and Spear, 1989; Yaping et al., 1997; Marks et al., 2001; Lin et al., 2002; Pinon et al., 2003; Jones et al., 2005). Therefore, as CSE and HS share some common carbohydrate structures - 4,6-bis-O-sulfated GalNAc and 2,3,6-tri-O-sulfated GlcNAc - it may be possible that HS-binding viral proteins can bind CSE somewhat, adding to the degree of inhibition seen by CSE and to the efficiency of viral binding. To this end, the CS-binding domain of HSV-1 gC has been shown to overlap with the HS binding site of this protein (Mårdberg et al., 2002). Moreover, CSE has been seen to bind to heparin-binding growth fac-

tors such as midkine (Ueoka et al., 2000), pleiotrophin, heparin-binding epidermal like growth factor, fibroblast growth factor (FGF)-2, FGF-10, FGF-16 and FGF-18 (Deepa et al., 2002). It would therefore be interesting to test whether H3 and A27 are able to bind CSE *in vitro*, as perhaps they can compensate when there is a lack of HS. This idea is supported by VACV binding being more sensitive to CSE preincubation on HS-/CS+ cells than on HS+/CS+ cells (Figure. 5.9A). Moreover, there is less binding on HS-/CS+ cells with H3- virus than WT (Figure. 5.2). Perhaps H3 can bind CSE or, alternatively, another cellular receptor in addition to HS.

Promiscuity in binding factor utilisation would be highly advantageous to the virus, allowing it to bind many different cells types and adapt quickly to different or changing conditions.

CSE has been shown to be critical for brain development and for the central nervous system (Deepa et al., 2002; Purushothaman et al., 2007). The VACV WR strain is known to be neuroinvasive (Garcel et al., 2012) and a VACV D8 knockout showed decreased ability to infect the rat brain (Chermos et al., 1993). Thus it would reason that the ability of VACV to bind CSE may aid its broad tropism and ability to cross the blood brain barrier (BBB). In addition to this, the specific VACV receptor CSPG4 (Frei et al., 2012) is a marker of oligodendrocyte precursor cells and found in high concentrations in the CNS (Sakry and Trotter, 2016; Schiffer et al., 2018). Taking into account the data shown in this chapter that CSPG4 is upregulated on HS-/CS+ cells and that VACV utilises CSE much more in its binding to these cells compared to HS+/CS+ (Figure. 5.9), it would be interesting to find out whether CSE specifically is found on CSPG4. VACV may be able to strategically utilise different ligands on different cell types to aid selective infectious routes, perhaps in this case to efficiently cross the BBB. Moreover, perhaps CSE utilisation is a strategy to allow orthopoxviruses to travel long distances within axons of neuronal cells.

Some investigators have shown H and HS to display a more inhibitory effect than found here. There are many possible reasons for this: firstly, the usage of heparin in viral entry varies hugely with cell-type - a large inhibitory effect on binding

and entry of heparin preincubation is seen on some cell types, and a small effect on others (Carter et al., 2005; Whitbeck et al., 2009). It is also possible that differences in the preparation of the compounds may give different results. Indeed, Carter *et al.* (2005) showed that over-sulfated heparin displayed a greater inhibitory effect than heparin on MV infectivity. Moreover, very few studies directly measure viral binding and instead utilise read-outs such as early gene expression and plaque neutralisation assays. To this end, a relationship between heparin usage and entry pathway was shown - WR low-pH induced fusion at the plasma membrane and IHD-J pH independent macropinocytosis appears to rely more heavily on heparin binding than WR entry by pH dependent macropinocytosis (Bengali et al., 2009; **?**). Perhaps binding to heparin aids fusion more strongly than cell attachment.

In this thesis, I show that VACV binding has built in redundancy and this likely accounts, in part, for the broad host range of the virus. VACV could compensate for lack of HS by relying more strongly on CS (Figure. 5.9A). Moreover, when the viral protein distribution was altered by the deletion of A27 (Gray et al., 2019), the utilisation of cellular binding partners changed (Figure. 5.5B). This may be due to the altered protein architecture of the A27 deletion virus (Gray et al., 2019). It also suggests that A27 may act almost as a cap on the membrane, shielding H3 and D8 somewhat. This is in accordance with the localisation of A27, which seems highly abundant and with a similar distribution to H3 and D8 around the membrane (Figure. 4.4) (Gray et al., 2019). Moreover, a strong link between A27 an H3 was seen in protein-protein XL-MS (Mirzakhanyan and Gershon, 2019) (Figure. 1.7) showing that these proteins are closely apposed on the membrane.

I also see redundancy when cellular proteins are deleted. The minimal decrease of WT binding on HS-/CS+ compared to HS+/CS+ cells (Figure. 5.2) shows that D8-CS and A26-laminin can compensate for a total lack of HS. This implies that VACV can adapt not only when binding proteins are deleted but also when the binding environment is changed. Moreover, the increase in binding on HS-/CS+ compared to HS+/CS+ when the strongest binding protein, A26, is deleted (Figure. 5.2) again shows that D8-CS interaction can be highly compensatory. A strong

precedent for binding protein hierarchy (A26 >D8 >H3) has therefore been established.

I then related the invagination data seen on our minimal model system to cellular entry. By comparing the entry of WT and ΔD8 virus (Figure. 5.7), I showed that D8 acts to increase the rate of fusion and thus entry of cores into the cytoplasm. TEM data of virus in macropinosomes (Figure. 5.8) shows that D8 induced curvature happens within macropinosomes, making it more likely that the cellular membrane contacts the fusion tips. This demonstrates a novel mechanism in VACV entry. To our knowledge, viral induced remodelling of the endosomal membrane has not been seen before. Of course, structural analysis via NMR or crystallography at pH 7.4 and pH 5.0 would be advantageous to confirm whether D8 undergoes a conformational change in order to mediate this.

As D8 and A26 were shown to be the strongest binding proteins and that they both are involved in pH dependent entry, a double knockout virus was generated. When analysing the binding of this mutant, there was not a strong additive effect on HS+/CS+ cells compared to the single ΔA26 knockout (Figure. 5.11). This agrees with the data that CSE and laminin did not have an additive effect on WT binding, however this could also be due to a steric effect when adding both CSE and laminin the same time. The binding assay results with the ΔA26ΔD8 again shows that VACV has effectively built in binding redundancy, and that there is indeed non-GAG and non-laminin receptors for VACV binding. Comparing the binding of the inducible L1 virus on HS-/CS- to WT and ΔA26 would be beneficial in confirming the effect of L1 on VACV binding (Foo et al., 2009).

In the introduction to this chapter, I introduced the idea of two pH dependent steps in entry: VACV entry was increased upon exposure of unattached virions to low-pH at 37°C and was not increased further by a second low-pH treatment following absorption to the plasma membrane, however entry of low-pH treated virions prior to absorption was still sensitive to inhibitors of endosomal acidification (Townsley and Moss, 2007). Thus, virions were still entering though an endosomal route (Townsley and Moss, 2007). Since the publication of that paper, A26 was

shown to be an acid-sensitive fusion inhibitor which dissociated from the MV at low-pH (Chang et al., 2010, 2012, 2019). However, this fusion suppression mechanism seems to be cell type dependent (Chang et al., 2010; **?**) and therefore cell specific factors must also be involved. Bengali *et al.* (2012) also showed that the fusion suppressors A26 and A25 are highly conserved in the bafilomycin insensitive VACV strains IHD-J and Elstree and sensitive strains WR and Wyeth. Moreover, swapping the A26 ORFs between WR and IHD-J did not alter their relative bafilomycin sensitivity, but deleting A26 from IHD-J did increase its ability to undergo FFWO at neutral pH (**?**). Therefore, there are many steps involved in fusion and the removal of A26 is only one part of this. Moreover, it was shown that protons can access the core, possibly through a proton channel, suggesting that low-pH may be important in core activation (Schmidt et al., 2013b).

To better understand the regulatory mechanisms of fusion and entry, entry of the ΔA26ΔD8 virus was compared to WT and the single knockouts. Deleting D8 from the ΔA26 reduced the rate of fusion and reduced FFWO at pH 5.0 compared to the ΔA26 (Figure. 5.13, 5.14) showing that A26 and D8 act cooperatively to regulate fusion. Their pH dependence acts to regulate fusion within the low-pH endosomal compartment. Furthermore, although some FFWO was seen with the ΔA26 virus at neutral pH, a marked increase in fusion index was seen at low-pH, showing that, in agreement with the work of Townsley *et al.* (2007), de-repression by A26 is only part of the low-pH dependent mechanism involved in VACV entry.

Moreover, the fusion peptide remains to be found. This may also undergo a conformational change at low-pH. If this change is reversible and/or needs insertion into the membrane to induce hemifusion, this could also account for a different pH dependent step, as the second step of the two step process toward entry is likely to include an essential interaction with cellular membrane. It is likely that a combination of the pH dependent entry steps involving A26, D8, the fusion peptide(s) and core activation (Schmidt et al., 2013b) are needed, and the accumulation of all of these steps would lead to the results in Townsley *et al.* (2007).

Regulation of viral fusion via conformational changes of viral membrane pro-

teins, other than the fusion protein, is emerging as an important mechanism. This has recently been shown with VACV A26 (Chang et al., 2019). A26 undergoes a conformational change at low-pH resulting in de-repression of the viral fusion machinery (Chang et al., 2019). Moreover, Rift Valley Fever Virus (RVFV) envelope protein Gn shields the hydrophobic loop of the fusion protein Gc at neutral pH, to prevent premature fusion (Halldorsson et al., 2018). At low-pH, the Gn-Gc complex rearranges, allowing insertion of the fusion loop into the cellular membrane (Halldorsson et al., 2018). Similarly, the glycoprotein E2 of the alphaviruses SFV and chickungunya shields the E1 fusion protein at neutral pH and undergoes a conformational change at low-pH revealing the fusion loop of E1 (Julien Lescar, Roussel et al., 2001; Li et al., 2010; Voss et al., 2010; Cao and Zhang, 2013). Although the low-pH induced conformational change of D8 does not reveal the fusion protein directly, it acts similarly to the proteins outlined here in that an additional surface protein acts to promote fusion. Cellular remodelling via viral envelope proteins should be studied in more depth, as we have shown important roles of viral proteins may have been missed.

In conclusion, I have shown that there is both redundancy and a hierarchy between the four known VACV binding proteins. I have also shown that the invagination produced by D8 acts to induce curvature in the macropinosome, making EFC-cellular membrane contact more likely. During infection, removal of the fusion suppressor, A26, acts concurrently with macropinosomal curvature induction by D8 to accelerate fusion kinetics. In addition, there appears to be further unaccounted for pH dependent steps involved as A26 removal and D8 curvature induction do not fully explain the two separate pH dependent steps described by Townsley *et al.* (2007). Having many pH dependent entry steps is advantageous for the virus as it allows strong regulation over when and where VACV enters host cells.

Chapter 6

General conclusions and open questions

In this thesis, a novel minimal model system has been used to evaluate the very first steps in VACV entry. This original way of probing binding and fusion allowed for the discovery of a previously unknown mechanism in VACV entry. In addition to this, the binding of the virus was completely examined and a thorough understanding of the redundancies and hierarchies at play was achieved.

Understanding poxvirus entry is of paramount importance. The causative agent of smallpox, variola virus, remains the deadliest disease in human history and accounts for over 500 million deaths. The cessation of the smallpox vaccination campaign means the world is now largely unvaccinated and hence susceptible to disease. The growing threat of zoonotic infections such as monkeypox or cowpox, or the re-emergence of smallpox by bioterrorism leaves the population distinctly at threat. In addition to this, VACV is an exciting and emerging tool in cancer virotherapies and is used widely in vaccine design.

The virus-cell binding interaction is a key target for antivirals. Inhibitors of entry can be less toxic as they do not have to be membrane permeable and they provide a rational basis for prophylactic therapy. Indeed, two of the approved drugs for HIV treatment, enfuvirtide and maraviroc, are entry inhibitors.

This chapter aims draw some concluding remarks about the data presented in this thesis and seeks to pick out the most interesting questions raised and how these

could be studied in the future.

6.1 Cell-derived membrane blebs

I have shown here that blebs can be generated from many different cell types, and that they maintain an intact actin cortex for at least 5 hrs without the need for exogenous ATP. This made them highly amenable to the study of VACV binding and fusion. When characterising the bleb system, blebs appeared not to support canonical macropinocytic uptake. However, a subset did appear to take up 100 kDa dextran (Figure. 3.7). This was unchanged in response to the macropinocytic inhibitor EIPA or to stimulation by the addition of VACV (Figure. 3.7C, 3.8), therefore the entry of dextran into blebs did not appear to occur through macropinocytosis. It is possible that blebs may be able to undergo more active processes when they are reconstituted with ATP and this could be investigated. Indeed, blebs reconstituted with ATP were reported to display active actin turnover and dynamic shape changes (Biro et al., 2013), however these shape changes were not seen in our experiments. This raises questions on how the dextran entered the bleb and, more widely, what active processes are available in blebs. Can blebs undergo any forms of endocytosis? Which, if any, signalling factors are recruited in response to endocytic stimuli (eg. EGF, vaccinia)? Can blebs support any of the primary steps in endocytosis? Staining for signalling factors such as PI3K, SNX proteins and actin would help address these questions. I would hypothesise that any signalling cascades available within blebs would not be homogeneous across the whole bleb population, as each are a random 'gulp' of plasma membrane and cytoplasm. The ability to image so many blebs in a single frame may allow questions regarding the heterogeneity within the system to be answered more easily.

In this way, blebs could be used as a tool to study membrane remodelling activities in response to stimuli such as pathogens or growth factors. Indeed, they have already been used to study the assembly of the actin cortex (Charras et al., 2006; Biro et al., 2013). If the first steps of membrane remodelling pathways are captured in blebs, they would serve as a minimal system for the study of the pathway. This

would be highly useful as it would allow for these processes to be studied in a more controlled environment than within a cell. Blebs do not have many of the redundancies of cells, as they are not living. They lack a nucleus, and most organelles. Also, blebs are more easily perturbed than cells and would be able to withstand higher concentrations of drugs and inhibitors, as well as undergoing fluorescence imaging for longer time periods and at higher laser powers.

6.1.1 Utilising cell-derived membrane blebs further with different pathogens

In this thesis, I have shown that blebs are highly amenable to the study of VACV binding and fusion. An aim of this project was to create a minimal model system that could be used for the study of many different pathogens. I have shown that blebs can be made from at least four separate cell types, and there is no reason why this would be limited to these four. Therefore, the system could theoretically be used to study binding of any virus if the permissive cell type is used in the bleb generation.

Blebs can be used in the place of, or alongside, GUVs to offer a more biologically relevant minimal system for host-pathogen interaction analysis. Many viruses have complex cellular membrane requirements for binding and fusion. For example, HSV (Shieh et al., 1992), human papillomavirus (HPV) (Giroglou et al., 2001), hepatitis C virus (Barth et al., 2003), HIV (Patel et al., 1993) and dengue virus (Yaping et al., 1997) all utilise GAGs in their binding and fusion. Therefore, for these viruses, maintaining the original plasma membrane is highly advantageous. Studying viral binding and fusion on these cell mimics allowed us to discover a novel membrane remodelling capacity of VACV, one which would have been easily missed on cells. This could be the case for many more viruses. This novel system offers a way to simplify the study of the very first pathogen-host interaction under biologically relevant conditions.

So far, HIV-1 is the only other viral pathogen where clustering a viral membrane component, Env, has been correlated to entry efficiency (Chojnacki et al., 2012). It therefore seems that membrane protein polarisation may be common for

many viruses and studying it on other viruses could be highly informative in understanding the steps leading to fusion. Thereafter, blebs can serve as a minimal system, as in this thesis, to study polarisation in relation to the cell surface.

6.1.2 Additional VACV bleb studies

The recently published work from our laboratory on the polarisation of the binding and fusion proteins on the virion membrane (Gray et al., 2019) has opened questions about the impact of this polarisation on cellular interaction. Blebs serve as an ideal system to study the orientation of the virus due to their small size and smooth surface. I was able to begin to address the functionality behind the polarisation of the binding proteins.

I saw that the virus did not re-orient on the membrane in response to low-pH and was more likely to bind on its side that its tip (Figure. 4.5). I found that the four main binding proteins were polarised largely to the sides of the virus (Figure. 4.4). With the sides having a larger surface area than the tips, it makes sense to have the majority of binding proteins here. This would enable the highest possible likelihood of binding and remaining attached to the membrane. Moreover, having the fusion proteins at the tips of the virion (Gray et al., 2019) means that the least possible energy is required in opening the fusion pore, as this would be the most narrow orientation for core release. A conundrum then is raised on how the virus is able to bind on the side and fuse at the tip. I have shown in this work that VACV is able to induce invagination, using the binding protein D8, in the macropinosome membrane, increasing the possibility that the tip-concentrated fusion machinery comes in contact with the cell membrane (Figure. 6.1).

It should be noted that the polarisation of the EFC was not studied on bleb bound virions here. It has been shown that the viral core and DNA de-condense upon cell contact, becoming less elongated (Cyrklaff et al., 2007; Gray et al., 2016) showing that the virus does undergo nanoscale structural changes in response to host membrane interaction. Therefore, it would be interesting to map the EFC upon cell contact as well, and blebs would allow us to do this whilst taking into account the orientation of the bound virion. However, as it is known that the clustering

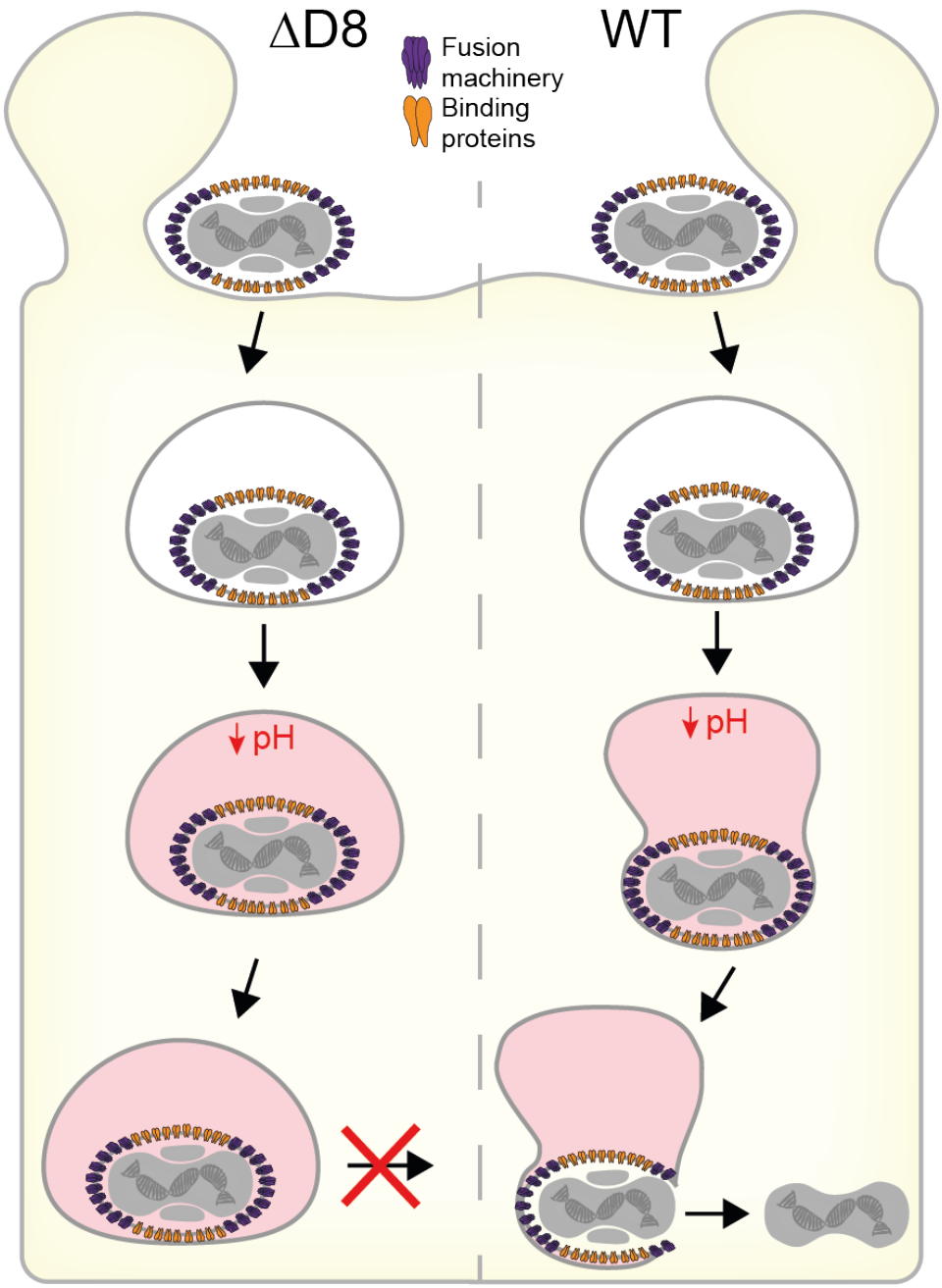

Figure 6.1: Model for VACV induced macropinosome invagination. WT VACV is more likely to bind to the cellular membrane in a side-on orientation. When taken up into the macropinosome, the pH within is lowered which causes the viral protein D8 to induce invagination in the macropinosome membrane. This increases the possibility that the fusion machinery comes into contact with the cellular membrane. In the case of the ΔD8 virus, when taken up into the macropinosome in a side-on orientation, it is unable to induce invagination. This results in less productive fusion. That the ΔD8 virus is more likely than WT to bind the membrane tip-on may be a mechanism to increase its likelihood of productive fusion.

and polarisation of the EFC is needed for productive fusion (Gray et al., 2019), it seems unlikely that polarisation would be lost upon host cell binding. Nonetheless, questions remain: does the EFC rearrange to one pole of the virion during binding or fusion? Does the de-condensation of the core mean that the polarisation becomes more spread but not altogether lost, allowing polarisation and side-bound induced invagination to work more efficiently together? Moreover, it would be intriguing to quantify the polarisation of A26 upon low-pH conditions. If, as suggested in Chapter 4, there exists two distinct pools of A26 - one for fusion suppression and one for binding - is only the A26 found at the tips lost when treated with low-pH? It has, indeed, been shown that some A26 is lost to the supernatant under low-pH conditions (Chang et al., 2012).

Furthermore, the real time dynamics of viral movement on the bleb was not studied here. The smooth surface of the bleb would allow changes in orientation to be studied during primary attachment. Does the virus show tumbling activity before settling on its bound orientation? Very few studies have tracked VACV particles on the plasma membrane. VACV is known to attach to filopodia and move toward the cell body using actin retrograde flow, where the cells are induced to bleb (Mercer and Helenius, 2009; Huang et al., 2008). Recently, Huang *et al.* (2017) used the scattering-based technique coherent brightfield (COBRI) microscopy to track label-free VACV particles on the HeLa cell membrane. The lack of fluorescent tag needed means that the particle can be followed for long periods of time as bleaching and photo-damage are not a problem. Moreover, scattering-based techniques allow extremely high spatial and temporal resolution (Jacobsen et al., 2006; Cheng et al., 2019). The authors showed that immediately after landing, the virus diffused laterally with a very high diffusion coefficient for seconds before confinement (Huang et al., 2017). However, this study does not take into account the elongated shape of the virion and therefore some of the diffusion activity of the virus shown may actually be tumbling activity.

It would be interesting to track the particle whilst also taking into account orientation changes. Due to their smooth surface, blebs would act as a system to

accurately visualise and quantify real-time orientation changes of the virus and, subsequently, differences with the binding mutants. This could, alongside the data presented in this thesis, add novel functional information for the polarisation and clustering of the binding proteins.

In this way, (Kukura et al., 2009) showed iSCAT to be highly effective at tracking SV40 particles at high temporal and spatial resolution on a lipid bilayer. In addition, virions were labelled with a single quantum dot and orientation changes could be simultaneously followed using single-molecule fluorescence microscopy (Kukura et al., 2009). In this, the photo-damaging effect of the laser power used in the fluorescence microscopy limited acquisition times. Theoretically, as the size of VACV is above the diffraction limit, the orientation could be determined without a fluorescent marker. This would mean that the orientation changes, alongside tracking the movement of the virus, could be taken for long periods of time.

Leading on from studying the live dynamics of orientation changes of the virus and using the findings of Huang *et al.* (2017), many questions remain to be answered. What receptors are involved in confinement? How does receptor concentration affect motion? Does the particle motion change significantly on different cell types? Does the onset of cellular blebbing slow down lateral movement on the plasma membrane?

Scattering-based imaging is easily compatible with super-resolution microscopy (Ortega Arroyo et al., 2016). Therefore, it would be interesting to fluorescently label certain cellular components and track the interaction between virus and component. For example, as actin-retrograde flow is important in VACV entry (Mercer et al., 2010a), actin could be labelled and the dynamics followed alongside the virus. In this way, Ashdown and colleagues have shown that cortical actin flow can be imaged and flow velocities quantified with high spatio and temporal resolution using TIRF-SIM and spatio-temporal image correlation spectroscopy (Ashdown et al., 2014, 2017). Additionally, certain specific viral receptors could be tagged and followed in relation to viral particles. Utilising live-cell super-resolution microscopy (methods such as STED), the cellular component can be tracked on the

nanometer scale. This would be useful in understanding the role of lipid rafts in viral entry which has, to date, only been shown biochemically or indirectly (Chung et al., 2005; Schroeder et al., 2012). What's more, if it is confirmed that rafts form on blebs in a similar manner to cells, the dynamics could be imaged over longer periods time. Blebs should be less sensitive to the phototoxic effects of the high laser powers used in super-resolution microscopy.

Altogether, the data presented in this thesis on understanding the functionality behind VACV membrane protein polarisation could, in future work, be expanded further. By using state-of-the-art imaging techniques the virus could be tracked across the bleb membrane over long periods of time, the orientation changes taken into account alongside and the cellular membrane imaged at the same time. This would provide highly important novel information on how exactly the virus infects cells, how it may spread between cells and how the cellular membrane responds to the virus.

Lastly, blebs of diameters up to 2 μm are amenable to cryo-electron tomography (cryo-ET; Paluch lab, personal correspondence). Therefore, this could be harnessed to gain a high-resolution, cryo-ET model of the virus during fusion using single-particle averaging. Ambitiously, it then may even then be possible to map the EFC proteins with known atomic models onto this and gain an idea on their organisation and their conformational changes during the fusion process. Similar studies have been done with avian sarcoma/leukosis virus (ASLV) (Cardone et al., 2012), influenza virus (Lee, 2010; Chlanda et al., 2016) and SINV (Cao and Zhang, 2013) using liposomes as target membranes, gaining information on the structural changes in the fusion proteins during membrane insertion. It was also shown with ASLV that viral Env glycoproteins are enriched at the virus/liposome binding site (Cardone et al., 2012). By gaining a high-resolution tomographic reconstruction of VACV bound to blebs at both pH 7.4 and pH 5.0, we might learn whether there is enrichment of the fusion proteins to one pole during fusion. VACV hemifusion and full fusion can be separated by the deletion of any of three EFC proteins - A28, L1 or L5 (Laliberte et al., 2011). Virus lacking any of these can hemifuse but not

infect cells, suggesting that these proteins function in pore formation. It is therefore tempting to utilise these mutants fused to blebs, in combination with cryo-ET, to more easily capture a hemifusion intermediate.

6.2 VACV interaction with cells

Using recombinant viruses and mutant cell lines, I have shown that there is a hierarchy and redundancy between the four known binding proteins. A26 appears to be the most important protein in binding followed by D8 and then H3. It seems that A27 is not involved in cell surface interaction. In a similar manner, H and HS were weakly inhibitory during binding, whilst CSE and laminin were more strongly inhibitory. It should be noted that differently sulfated levels of H or HS were not tested in this work. This could reveal more highly inhibiting forms, as has been shown with dengue and VACV and highly sulfated HS (Yaping et al., 1997; Carter et al., 2005; Khanna et al., 2017). In a similar manner, I found different CS subtypes displayed different levels of inhibition. As CSE has never been used in the literature for VACV binding studies, the data presented here showing CSE but not CSA has an inhibitory effect on binding (Figure. 5.4A) explains why soluble CS has rarely been shown to have inhibitory activity (Chung et al., 1998; Carter et al., 2005; Li et al., 2007; Bengali et al., 2009; **?**). Moreover, in the absence of HS, CS could be utilised more strongly. This shows that VACV can adapt quickly to the environment to enhance binding to many different cell types. This goes some way in explaining the broad cell and host tropism of VACV.

Some specific receptors have been found to be used by the virus: integrin $\beta 1$ (Izmailyan et al., 2012; Schroeder et al., 2012), MARCO (Macleod et al., 2015), AXL, M6PR, DAG1, CSPG4 and CDH13 (Frei et al., 2012). Here, I presented added evidence indicating that CSE is very important for infection: CS is inhibitory for binding (Figure. 5.4A), sensitivity to CS increases in the absence of HS (Figure. 5.9A), HS-/CS+ cells express more CSPG4 than HS+/CS+ cells (Figure. 5.9B) and an increase in D8 mediated pH dependent invagination depth was seen on HS-/CS+ cells which results in increased fusion and entry kinetics (Figure. 5.10). Altogether,

this shows that CS binding is highly important for not just binding, but cellular entry as well. CSPG4 may be the specific receptor which mediates this, however knockdown of CSPG4 in both HS+/CS+ and HS-/CS+ cells would be needed to confirm this.

Chahroudi *et al.* (2005) found that VACV could bind and infect activated T cells but not resting T cells. This could be largely due to the upregulation of HSPG on the cell surface during activation (Ibrahim et al., 1999; Jones et al., 2005) implying just how reliant on GAGs VACV binding is. It also suggests that there could be cell specific VACV receptors on activated T cells. That not all cell types encountered by the virus *in vivo* are infected shows that more binding studies should be done with primary cell types for more biologically relevant data. Along the same idea, the *in vitro* and *in vivo* permissiveness of some poxviruses can differ markedly (McFadden, 2005). For example, myxoma virus, a rabbit-specific poxvirus, can replicate productively in selected transformed human cell lines (Sypula et al., 2004). What's more, the extent of the utilisation of GAGs does seem to differ somewhat with cell type (Carter et al., 2005; Whitbeck et al., 2009). This phenomenon is also highlighted in this thesis, as I showed specifically that the utilisation of CSE increased as HS was deleted from the cell surface. Therefore, utilising primary epithelial cells and, as VACV is known to alter the host immune response resulting in vaccination complications (Bray, 2003), cells of the hematopoietic lineage in the binding assays presented here with the mutants viruses and with soluble GAGs would allow a more accurate and biologically relevant understanding the interaction. Comparison of the specific receptors used in different cell types would also be interesting - this could be done utilising Ligand Receptor Capture (LRC; (Frei et al., 2012)). LRC would allow us to validate the hypothesis that CSPG4 may be more important for binding in the brain and CNS (Section 5.4). Nevertheless, the data in this thesis showing compensatory mechanisms in GAG usage provides a strong foundation and themes to explore when analysing binding on primary cell lines.

Likewise, studying viral entry in relevant tissues is a next obvious step. Preliminary work has shown that VACV enter differentiated epilthelia through the ba-

solateral membrane (Vermeer et al., 2007), highlighting the fact that important information can be missed when studying cell monolayers. Studying this first step of infection at high resolution in 3D, rather than 2D, may reveal previously unknown phenomena and a clearer picture of cellular tropism could be gained. Studying spread and viral exit in tissue explants would also be extremely interesting, for example how this is mediated by actin tails (Smith et al., 2002). In this regard, as the MV and EV membranes are different, studies should now look more into EV binding due to their importance in cell to cell spread. There is precedent for this - it has been shown that MVs and EVs behave oppositely in binding to protease treated HeLa and RK13 cells: protease treatment reduced MV binding but increased EV binding (Vanderplasschen and Smith, 1997). Moreover, EV binding appears much more readily inhibited by H and HS than MV binding (Khanna et al., 2017) and deletion of heparin sulfation affects EV mediated spread (Khanna et al., 2019; Flores et al., 2020).

The binding and fusion proteins all appear to be highly conserved, however differences are known in entry mechanisms between members of the orthopox genera, notably in their use of low-pH pathways and entry inhibition by heparin (Bengali et al., 2009; Chang et al., 2010; Mercer et al., 2010b; **?**). In this thesis, I have only used the strain WR. This strain undergoes pH dependent macropinocytosis (Mercer and Helenius, 2008). Due to the extensive passage in tissue culture of WR, there was a possibility that it may have adapted to particular entry pathway. Bengali *et al.* (2012) compared the entry pathway to isolated cowpox and monkeypox strains. Gratifyingly, these strains appeared similar to WR in their entry mechanism and use of cell surface GAGs (**?**), showing that studying WR entry in the lab does have clinical relevance.

The differences between strains in terms of low-pH enhancement are intriguing (WR, monkeypox and cowpox undergo low-pH enhancement, whilst IHD-J, Copenhagen and Elstree do not) and could not be attributed to differences in the A26 protein sequence (**?**). It would now be interesting to map the binding and fusion proteins on the strains which are not enhanced by low-pH, in the same way it

has been done on WR in this thesis and in Gray *et al.* (2019), to understand if they are also polarised. If there are differences, as compared to low-pH sensitive WR, in polarisation and/or if A26 is clustered differently, this might help to explain the variability in fusion suppression ability of A26. Moreover, in this vein, analysing the ability of D8 to induce invagination, another pH dependent step found in WR entry which works cooperatively with A26 to regulate pH dependent fusion, may also be revealing.

VACV is known to have one of the most complex cellular fusion mechanisms in the virus world. Here, I have found a novel pH dependent step in entry highlighting again the complexity of this process. It seems that this step, combined with the pH dependent removal of the fusion suppressor (Chang et al., 2012), is involved, but not sufficient, to satisfy the two-step model of VACV entry (Townsley and Moss, 2007). Therefore, it remains for the fusion protein(s) to be identified and its pH dependence understood. The interplay between the members of the EFC also need to be studied in more detail. At the moment, it is known that deletion of A28, L1 or L5 allow lipid mixing without full fusion, whilst deletion of any of the others results in no lipid mixing at all (Laliberte et al., 2011). I hypothesise that there will be a conformational change and subsequent cellular membrane insertion of one or more of the EFC proteins which constitutes the remaining pH dependent step(s) in the two-step model.

6.3 Overall Conclusions

Overall, this thesis had two overarching aims: to develop a minimal model system compatible for the study of VACV binding and fusion and to unravel the complex interplay between the VACV binding proteins in host cell entry. I believe that these aims have been met and, as a consequence, a completely novel step in VACV entry was found. Only by studying binding and fusion on our bleb minimal system was this step discovered, and thus highlights the importance of developing novel tools to study familiar processes.

Bibliography

Agnello, V., Ábel, G., Elfahal, M., Knight, G. B., and Zhang, Q. X. (1999). Hepatitis C virus and other flaviviridae viruses enter cells via low density lipoprotein receptor. *Proceedings of the National Academy of Sciences of the United States of America*, 96(22):12766–12771.

Albert, M. L. (2004). Death-defying immunity: Do apoptotic cells influence antigen processing and presentation? *Nature Reviews Immunology*, 4(3):223–231.

Albertini, A. A., Baquero, E., Ferlin, A., and Gaudin, Y. (2012). Molecular and cellular aspects of rhabdovirus entry. *Viruses*, 4(1):117–139.

Aldaz-carroll, L., Whitbeck, J. C., Leon, M. P. D., Lou, H., Hirao, L., Isaacs, S. N., Moss, B., Eisenberg, R. J., and Cohen, G. H. (2005). Epitope-Mapping Studies Define Two Major Neutralization Sites on the Vaccinia Virus Extracellular Enveloped Virus. 79(10):6260–6271.

Anderson, R., King, A. D., and Innis, B. L. (1992). Correlation of E protein binding with cell susceptibility to dengue 4 virus infection. *Journal of General Virology*, 73(8):2155–2159.

Armstrong, J., Metz, D., and Young, M. (1973). The Mode of Entry of Vaccinia Virus into L Cells. *Journal of General Virology*, 21:533–537.

Ashdown, G. W., Burn, G. L., Williamson, D. J., Pandžić, E., Peters, R., Holden, M., Ewers, H., Shao, L., Wiseman, P. W., and Owen, D. M. (2017). Live-Cell Super-resolution Reveals F-Actin and Plasma Membrane Dynamics at the T Cell Synapse. *Biophysical Journal*, 112(8):1703–1713.

Ashdown, G. W., Cope, A., Wiseman, P. W., and Owen, D. M. (2014). Molecular flow quantified beyond the diffraction limit by spatiotemporal image correlation of structured illumination microscopy data. *Biophysical Journal*, 107(9):L21–L23.

Atanasiu, D., Cairns, T. M., Whitbeck, J. C., Saw, W. T., Rao, S., Eisenberg, R. J., and Cohen, G. H. (2013). Regulation of herpes simplex virus gB-induced cell-cell fusion by mutant forms of gH/gL in the absence of gD and cellular receptors. *mBio*, 4(2):1–9.

Atanasiu, D., Saw, W. T., Eisenberg, R. J., and Cohen, G. H. (2016). Regulation of Herpes Simplex Virus Glycoprotein-Induced Cascade of Events Governing Cell-Cell Fusion. *Journal of Virology*, 90(23):10535–10544.

Avirutnan, P., Zhang, L., Punyadee, N., Manuyakorn, A., and Puttikhunt, C. (2007). Secreted NS1 of Dengue Virus Attaches to the Surface of Cells via Interactions with Heparan Sulfate and Chondroitin Sulfate E. *PLoS Pathogens*, 3(11):1798–1812.

Backovic, M. and Jardetzky, T. S. (2009). Class III viral membrane fusion proteins. *current opinion in structural biology*, 2(1):189–196.

Bahar, M. W., Graham, S. C., Stuart, D. I., and Grimes, J. M. (2011). Insights into the evolution of a complex virus from the crystal structure of vaccinia virus D13. *Structure*, 19(7):1011–1020.

Banfield, B. W., Leduc, Y., Esford, L., Schubert, K., and Tufaro, F. (1995). Sequential isolation of proteoglycan synthesis mutants by using herpes simplex virus as a selective agent: evidence for a proteoglycan-independent virus entry pathway. *Journal of virology*, 69(6):3290–3298.

Baroudy, B. M. and Moss, B. (1982). Sequence homologies of diverse length tandem repetitions near ends of vaccinia virus genome suggest unequal crossing over. *Nucleic Acids Research*, 10(18):5673–5679.

Barquet, N., Barquet, N., Domingo, P., and Domingo, P. (1997). Smallpox: the triumph over the most terrible of the ministers of death. *Annals of internal medicine*, 127(8 Pt 1):635–642.

Barth, H., Schäfer, C., Adah, M. I., Zhang, F., Linhardt, R. J., Toyoda, H., Kinoshita-Toyoda, A., Toida, T., Van Kuppevelt, T. H., Depla, E., Von Weizsäcker, F., Blum, H. E., and Baumert, T. F. (2003). Cellular Binding of Hepatitis C Virus Envelope Glycoprotein E2 Requires Cell Surface Heparan Sulfate. *Journal of Biological Chemistry*, 278(42):41003–41012.

Barton, E. S., Forrest, J. C., Connolly, J. L., Chappell, J. D., Liu, Y., Schnell, F. J., Nusrat, A., Parkos, C. A., and Dermody, T. S. (2001). Junction adhesion molecule is a receptor for reovirus. *Cell*, 104(3):441–451.

Belouzard, S., Millet, J. K., Licitra, B. N., and Whittaker, G. R. (2012). Mechanisms of coronavirus cell entry mediated by the viral spike protein. *Viruses*, 4(6):1011–1033.

Bengali, Z., Townsley, A. C., and Moss, B. (2009). Vaccinia virus strain differences in cell attachment and entry. *Virology*, 389(301):132–140.

Bergefall, K., Trybala, E., Johansson, M., Uyama, T., Naito, S., Yamada, S., Kitagawa, H., Sugahara, K., and Bergstro, T. (2005). Chondroitin Sulfate Characterized by the E-disaccharide Unit Is a Potent Inhibitor of Herpes Simplex Virus Infectivity and Provides the Virus Binding Sites on gro2C Cells. *Journal of Biological Chemistry*, 280(37):32193–32199.

Bergert, M., Erzberger, A., Desai, R. A., Aspalter, I. M., Oates, A. C., Charras, G., Salbreux, G., and Paluch, E. K. (2015). Force transmission during adhesion-independent migration. *Nature Cell Biology*, 17(4):524–529.

Bermejo-Barrera, P., Fernândez-Nocelo, S., Moreda-Pineiro, A., and Bermejo-Barrera, A. (1999). Usefulness of enzymatic hydrolysis procedures based on the use of pronase E as sample pre-treatment for multi-element determination in

biological materials. *Journal of analytical atomic spectrometry*, 14(12):1893–1900.

Bertucci, C., Cimitan, S., and Menotti, L. (2003). Optical biosensor analysis in studying herpes simplex virus glycoprotein D binding to target nectin1 receptor. *Journal of Pharmaceutical and Biomedical Analysis*, 32(4-5):697–706.

Bidgood, S. R. (2019). Continued poxvirus research: From foe to friend. *PLoS Biology*, 17(1):10–13.

Bidgood, S. R. and Mercer, J. (2015). Cloak and dagger: Alternative immune evasion and modulation strategies of poxviruses. *Viruses*, 7(8):4800–4825.

Biro, M., Romeo, Y., Kroschwald, S., Bovellan, M., Boden, A., Tcherkezian, J., Roux, P. P., Charras, G., and Paluch, E. K. (2013). Cell cortex composition and homeostasis resolved by integrating proteomics and quantitative imaging. *Cytoskeleton*, 70(11):741–754.

Bisht, H., Weisberg, A. S., and Moss, B. (2008). Vaccinia virus l1 protein is required for cell entry and membrane fusion. *Journal of virology*, 82(17):8687–94.

Boden, N. and Sixl, F. (1986). Forces between phospholipid bilayers. *Faraday Discussions of the Chemical Society*, 81(19159):191–199.

Boulant, S., Stanifer, M., and Lozach, P. Y. (2015). Dynamics of virus-receptor interactions in virus binding, signaling, and endocytosis. *Viruses*, 7(6):2794–2815.

Bovellan, M., Romeo, Y., Biro, M., Boden, A., Chugh, P., Yonis, A., Vaghela, M., Fritzsche, M., Moulding, D., Thorogate, R., Jégou, A., Thrasher, A. J., Romet-Lemonne, G., Roux, P. P., Paluch, E. K., and Charras, G. (2014). Cellular control of cortical actin nucleation. *Current Biology*, 24(14):1628–1635.

Bray, M. (2003). Pathogenesis and potential antiviral therapy of complications of smallpox vaccination. *Antiviral Research*, 58(2):101–114.

Brown, E., Senkevich, T. G., and Moss, B. (2006). Vaccinia virus F9 virion membrane protein is required for entry but not virus assembly, in contrast to the related L1 protein. *Journal of virology*, 80(19):9455–64.

Bubeck, D., Filman, D. J., Cheng, N., Steven, A. C., Hogle, J. M., and Belnap, D. M. (2005). The Structure of the Poliovirus 135S Cell Entry Intermediate at 10-Angstrom Resolution Reveals the Location of an Externalized Polypeptide That Binds to Membranes. *Journal of Virology*, 79(12):7745–7755.

Bubeck, D., Filman, D. J., Kuzmin, M., Fuller, S. D., and Hogle, J. M. (2008). Post-imaging fiducial markers aid in the orientation determination of complexes with mixed or unknown symmetry. *Journal of Structural Biology*, 162(3):480–490.

Cairns, T. M., Ditto, N. T., Atanasiu, D., Lou, H., Brooks, B. D., Saw, W. T., Eisenberg, R. J., and Cohen, G. H. (2019). Surface Plasmon Resonance Reveals Direct Binding of Herpes Simplex Virus Glycoproteins gH/gL to gD and Locates a gH/gL Binding Site on gD. *Journal of Virology*, 93(15):1–21.

Cao, S. and Zhang, W. (2013). Characterization of an early-stage fusion intermediate of Sindbis virus using cryoelectron microscopy. *Proceedings of the National Academy of Sciences of the United States of America*, 110(33):13362–13367.

Cardone, G., Brecher, M., Fontana, J., Winkler, D. C., Butan, C., White, J. M., and Steven, A. C. (2012). Visualization of the Two-Step Fusion Process of the Retrovirus Avian Sarcoma / Leukosis Virus by Cryo-Electron Tomography. *Journal of Virology*, 86(22):12129–12137.

Carter, G. C., Law, M., Hollinshead, M., and Smith, G. L. (2005). Entry of the vaccinia virus intracellular mature virion and its interactions with glycosaminoglycans. *Journal of General Virology*, 86(5):1279–1290.

Cavanagh, D. (1995). The Coronavirus Surface Glycoprotein. In Siddell, S., editor, *The Coronaviridae*, chapter 5, pages 73–113. Springer US, Boston, MA.

Cepeda, V. and Esteban, M. (2014). Novel insights on the progression of intermediate viral forms in the morphogenesis of vaccinia virus. *Virus Research*, 183:23–29.

Cera, M. R., Fabbri, M., Molendini, C., Corada, M., Orsenigo, F., Rehberg, M., Reichel, C. A., Krombach, F., Pardi, R., and Dejana, E. (2009). JAM-A promotes neutrophil chemotaxis by controlling integrin internalization and recycling. *Journal of Cell Science*, 122(2):268–277.

Chahroudi, A., Chavan, R., Koyzr, N., Edmund, K., Silvestri, G., Feinberg, M. B., and Waller, E. K. (2005). Vaccinia Virus Tropism for Primary Hematolymphoid Cells Is Determined by Restricted Expression of a Unique Virus Receptor Vaccinia Virus Tropism for Primary Hematolymphoid Cells Is Determined by Restricted Expression of a Unique Virus Receptor. *Journal of Virology*, 79(16):10397–10407.

Chan, D. C. and Kim, P. S. (1998). HIV-1 entry and its inhibition. *Cell*, 93(5):681–684.

Chang, A. and Metz, D. H. (1976). Further Investigations on the Modee of Entry of Vaccinia Virus into Cells National Institute for Medical Research ,. *Journal of General Virology*, (1975):275–282.

Chang, H.-w., Yang, C.-h., Luo, Y.-c., Su, B.-g., and Cheng, Huei-yin, C. W. W. C. (2019). Vaccinia viral A26 protein is a fusion suppressor of mature virus and triggers membrane fusion through conformational change at low pH. *PLoS Pathogens*, 15(6):1–31.

Chang, S.-j., Chang, Y.-x., Izmailyan, R., Tang, Y.-l., and Chang, W. (2010). Vaccinia Virus A25 and A26 Proteins Are Fusion Suppressors for Mature Virions and Determine Strain-Specific Virus Entry Pathways into HeLa , CHO-K1 , and L Cells . 84(17):8422–8432.

Chang, S.-j., Shih, A.-c., Tang, Y.-l., and Chang, W. (2012). Vaccinia Mature Virus Fusion Regulator A26 Protein Binds to A16 and G9 Proteins of the Viral Entry

Fusion Complex and Dissociates from Mature Virions at Low pH. *Journal of Virology*, 86(7):3809–3818.

Charras, G. T. (2008). A short history of blebbing. *Journal of Microscopy*, 231(3):466–478.

Charras, G. T., Coughlin, M., Mitchison, T. J., and Mahadevan, L. (2008). Life and times of a cellular bleb. *Biophysical Journal*, 94(5):1836–1853.

Charras, G. T., Hu, C. K., Coughlin, M., and Mitchison, T. J. (2006). Reassembly of contractile actin cortex in cell blebs. *Journal of Cell Biology*, 175(3):477–490.

Chen, B. (2019). Molecular Mechanism of HIV-1 Entry. *Trends in Microbiology*, 27(10):878–891.

Chen, Y., Maguire, T., and Marks, R. M. (1996). Demonstration of binding of dengue virus envelope protein to target cells. *Journal of virology*, 70(12):8765–8772.

Cheng, C. Y., Liao, Y. H., and Hsieh, C. L. (2019). High-speed imaging and tracking of very small single nanoparticles by contrast enhanced microscopy. *Nanoscale*, 11(2):568–577.

Chermos, V. I., Vovk, T. S., Ivanova, O. N., Antonova, T. P., and Loparev, V. N. (1993). Insertion mutants of the vaccinia virus. The effect of inactivating E7R and D8L genes on the biological properties of the virus. *Molecular Genetics, Microbiology and Virology*, 2:30–34.

Chernomordik, L. V. and Kozlov, M. M. (2003). Protein-Lipid Interplay in Fusion and Fission of Biological Membranes. *Annual Review of Biochemistry*, 72(1):175–207.

Chernomordik, L. V. and Kozlov, M. M. (2008). Mechanics of membrane fusion. *Nature Structural and Molecular Biology*, 15(7):675–683.

Chernomordik, L. V., Zimmerberg, J., and Kozlov, M. M. (2006). Membranes of the world unite! *Journal of Cell Biology*, 175(2):201–207.

Cheshenko, N., Pierce, C., and Herold, B. C. (2018). Herpes simplex viruses activate phospholipid scramblase to redistribute phosphatidylserines and Akt to the outer leaflet of the plasma membrane and promote viral entry. *PLoS Pathogens*, 14(1):1–24.

Ching, Y.-C., Chung, C.-S., Huang, C.-Y., Hsia, Y., Tang, Y.-L., and Chang, W. (2009). Disulfide Bond Formation at the C Termini of Vaccinia Virus A26 and A27 Proteins Does Not Require Viral Redox Enzymes and Suppresses Glycosaminoglycan-Mediated Cell Fusion. *Journal of Virology*, 83(13):6464–6476.

Chiu, W.-L., Lin, C.-L., Yang, M.-H., Tzou, D.-L. M., and Chang, W. (2007). Vaccinia Virus 4c (A26L) Protein on Intracellular Mature Virus Binds to the Extracellular Cellular Matrix Laminin. *Journal of Virology*, 81(5):2149–2157.

Chlanda, P., Carbajal, M. A., Cyrklaff, M., Griffiths, G., and Krijnse-Locker, J. (2009). Membrane Rupture Generates Single Open Membrane Sheets during Vaccinia Virus Assembly. *Cell Host and Microbe*, 6(1):81–90.

Chlanda, P., Mekhedov, E., Waters, H., Schwartz, C. L., Fischer, E. R., Ryham, R. J., Cohen, F. S., Blank, P. S., Zimmerberg, J., Laboratories, M., Unit, E. M., and Diseases, I. (2016). The hemifusion structure induced by Influenza virus haemagglutinin is determined by physical properties of the target membranes. *Nature Microbiology*, 1(6):1–19.

Chojnacki, J., Staudt, T., Glass, B., Bingen, P., Engelhardt, J., Anders, M., Schneider, J., Müller, B., Hell, S. W., and Kräusslich, H. G. (2012). Maturation-dependent HIV-1 surface protein redistribution revealed by fluorescence nanoscopy. *Science*, 338(6106):524–528.

Chugh, P., Clark, A. G., Smith, M. B., Cassani, D. A. D., Dierkes, K., Ragab, A., Roux, P. P., Charras, G., Salbreux, G., and Paluch, E. K. (2017). Actin cortex

architecture regulates cell surface tension Europe PMC Funders Group. *Nat Cell Biol*, 19(6):689–697.

Chung, C.-S., Chen, C.-H., Ho, M.-Y., Huang, C.-Y., Liao, C.-L., and Chang, W. (2006). Vaccinia Virus Proteome: Identification of Proteins in Vaccinia Virus Intracellular Mature Virion Particles. *Journal of Virology*, 80(5):2127–2140.

Chung, C. S., Hsiao, J. C., Chang, Y. S., and Chang, W. (1998). A27L protein mediates vaccinia virus interaction with cell surface heparan sulfate. *Journal of virology*, 72(2):1577–1585.

Chung, C.-S., Huang, C.-Y., and Chang, W. (2005). Vaccinia Virus Penetration Requires Cholesterol and Results in Specific Viral Envelope Proteins Associated with Lipid Rafts. *Journal of Virology*, 79(3):1623–1634.

Churchward, M. A., Rogasevskaia, T., Brandman, D. M., Khosravani, H., Nava, P., Atkinson, J. K., and Coorssen, J. R. (2008). Specific lipids supply critical negative spontaneous curvature-an essential component of native Ca2+-triggered membrane fusion. *Biophysical Journal*, 94(10):3976–3986.

Churchward, M. A., Rogasevskaia, T., Höfgen, J., Bau, J., and Coorssen, J. R. (2005). Cholesterol facilitates the native mechanism of Ca2+-triggered membrane fusion. *Journal of Cell Science*, 118(20):4833–4848.

Clark, A. G., Wartlick, O., Salbreux, G., and Paluch, E. K. (2014). Stresses at the cell surface during animal cell morphogenesis. *Current Biology*, 24(10):R484–R494.

Clement, C., Tiwari, V., Scanlan, P. M., Valyi-Nagy, T., Yue, B. Y., and Shukla, D. (2006). A novel role for phagocytosis-like uptake in herpes simplex virus entry. *Journal of Cell Biology*, 174(7):1009–1021.

Coller, K. E., Berger, K. L., Heaton, N. S., Cooper, J. D., Yoon, R., and Randall, G. (2009). RNA interference and single particle tracking analysis of hepatitis C virus endocytosis. *PLoS Pathogens*, 5(12).

Condit, R. C., Moussatche, N., and Traktman, P. (2006). In A Nutshell: Structure and Assembly of the Vaccinia Virion. *Advances in Virus Research*, 65(February):31–124.

Cooper, R. S. and Heldwein, E. E. (2015). Herpesvirus gB: A finely tuned fusion machine. *Viruses*, 7(12):6552–6569.

Costello, D. A., Lee, D. W., Drewes, J., Vasquez, K. A., Kisler, K., Wiesner, U., Pollack, L., Whittaker, G. R., and Daniel, S. (2012). Influenza virus-membrane fusion triggered by proton uncaging for single particle studies of fusion kinetics. *Analytical Chemistry*, 84(20):8480–8489.

Crickard, L., Babas, T., Seth, S., Silvera, P., Koriazova, L., and Crotty, S. (2012). Protection of Rabbits and Immunodeficient Mice against Lethal Poxvirus Infections by Human Monoclonal Antibodies. *PLoS ONE*, 7(11).

Cureton, D. K., Harbison, C. E., Cocucci, E., Parrish, C. R., and Kirchhausen, T. (2012). Limited Transferrin Receptor Clustering Allows Rapid Diffusion of Canine Parvovirus into Clathrin Endocytic Structures. *Journal of Virology*, 86(9):5330–5340.

Cyrklaff, M., Linaroudis, A., Boicu, M., Chlanda, P., Baumeister, W., Griffith, G., and Krijnse-Locker, J. (2007). Whole cell cryo-electron tomography reveals distinct disassembly intermediates of vaccinia virus. *PLoS ONE*, 2(5).

Cyrklaff, M., Risco, C., Fernández, J. J., Jiménez, M. V., Estéban, M., Baumeister, W., and Carrascosa, J. L. (2005). Cryo-electron tomography of vaccinia virus. *Proc Natl Acad Sci U S A*, 102(8):2772–7.

da Fonseca, F. G., Wolffe, E. J., Weisberg, A., and Moss, B. (2000a). Characterization of the Vaccinia Virus H3L Envelope Protein: Topology and Posttranslational Membrane Insertion via the C-Terminal Hydrophobic Tail. *Journal of Virology*, 74(16):7508–7517.

da Fonseca, F. G., Wolffe, E. J., Weisberg, A., and Moss, B. (2000b). Effects of Deletion or Stringent Repression of the H3L Envelope Gene on Vaccinia Virus Replication. *Journal of Virology*, 74(16):7518–7528.

Daecke, J., Fackler, O. T., and Dittmar, M. T. (2004). Involvement of Clathrin-Mediated Endocytosis in Human Immunodeficiency Virus Type 1 Entry. *Journal of virology*, 79(3):1581–1594.

Dales, S., Milovanovitch, V., Pogo, B. G., Weintraub, S. B., Huima, T., Wilton, S., and McFadden, G. (1978). Biogenesis of vaccinia: Isolation of conditional lethal mutants and electron microscopic characterization of their phenotypically expressed defects. *Virology*, 84(2):403–428.

Dales, S. and Mosbach, E. H. (1968). Vaccinia as a model for membrane biogenesis. *Virology*, 35(4):564–583.

Dales, S. and Siminovitch, L. (1961). The development of vaccinia virus in Earle's L strain cells as examined by electron microscopy. *The Journal of biophysical and biochemical cytology*, 10:475–503.

Davies, D. H., McCausland, M. M., Valdez, C., Huynh, D., Hernandez, J. E., Mu, Y., Hirst, S., Villarreal, L., Felgner, P. L., and Crotty, S. (2005). Vaccinia Virus H3L Envelope Protein Is a Major Target of Neutralizing Antibodies in Humans and Elicits Protection against Lethal Challenge in Mice. *Journal of Virology*, 79(18):11724–11733.

Davies, W. A. and Stossel, T. P. (1977). Peripheral hyaline blebs (podosomes) of macrophages. *The Journal of Cell Biology*, 75:941–955.

Deepa, S. S., Umehara, Y., Higashiyama, S., Itoh, N., and Sugahara, K. (2002). Specific molecular interactions of oversulfated chondroitin sulfate E with various heparin-binding growth factors: Implications as a physiological binding partner in the brain and other tissues. *Journal of Biological Chemistry*, 277(46):43707–43716.

Dixit, R., Tiwari, V., and Shukula, D. (2008). Herpes Simplex Virus Type 1 Induces Filopodia in Differentiated P19 Neural Cells to Facilitate Viral Spread. *Neuroscience Letters*, 440(2):113–118.

Domanska, M. K., Wrona, D., and Kasson, P. M. (2013). Multiphasic effects of cholesterol on influenza fusion kinetics reflect multiple mechanistic roles. *Biophysical Journal*, 105(6):1383–1387.

Doms, R. W., Blumenthal, R., and Moss, B. (1990). Fusion of intra-and extracellular forms of vaccinia virus with the cell membrane. *Journal of virology*, 64(10):4884–4892.

Doms, R. W. and Moore, J. P. (2000). HIV-1 Membrane Fusion: Targets of Opportunity. *The Journal of Cell Biology*, 151(2):F9–F14.

Dowhan, W. and Bogdanov, M. (2012). Lipid-protein interactions as determinants of membrane protein structure and function. *Biochemical Society Transactions*, 39(3):767–774.

Dubochet, J., Adrian, M., Richter, K., Garces, J., and Wittek, R. (1994). Structure of intracellular mature vaccinia virus observed by cryoelectron microscopy. *Journal of Virology*, 68(3):1935–1941.

Dunnebacke, T. H., Levinthal, J. D., and Williams, R. C. (1969). Entry and release of poliovirus as observed by electron microscopy of cultured cells. *Journal of Virology*, 4(4):505–513.

Easterbrook, K. B. (1966). Controlled degradation of vaccinia virions in vitro: an electron microscopic study. *Journal of Ultrasructure Research*, 14(5-6):484–496.

Edinger, T. O., Pohl, M. O., and Stertz, S. (2014). Entry of influenza A virus: Host factors and antiviral targets. *Journal of General Virology*, 95(PART 2):263–277.

Endreß, T., Lampe, M., Briggs, J. A., Kräusslich, H. G., Bräuchle, C., Müller, B., and Lamb, D. C. (2008). HIV-1-cellular interactions analyzed by single virus tracing. *European Biophysics Journal*, 37(8):1291–1301.

Ennomani, H., Letort, G., Guérin, C., Martiel, J. L., Cao, W., Nédélec, F., De La Cruz, E. M., Théry, M., and Blanchoin, L. (2016). Architecture and Connectivity Govern Actin Network Contractility. *Current Biology*, 26(5):616–626.

Eppstein, D. A., Marsh, Y. V., Schreiber, A. B., Newman, S. R., Todaro, G. J., and Nestor, J. J. (1985). Epidermal growth factor receptor occupancy inhibits vaccinia virus infection. *Nature*, 318(6047):663–665.

Esparza, J., Schrick, L., Damaso, C. R., and Nitsche, A. (2017). Equination (inoculation of horsepox): An early alternative to vaccination (inoculation of cowpox) and the potential role of horsepox virus in the origin of the smallpox vaccine. *Vaccine*, 35(52):7222–7230.

Essani, K. and Dales, S. (1979). Biogenesis of vaccinia: Evidence for more than 100 polypeptides in the virion. *Virology*, 95(2):385–394.

Ewers, H. and Helenius, A. (2011). Lipid-mediated endocytosis. *Cold Spring Harbor Perspectives in Biology*, 3(8):1–14.

Ewers, H., Römer, W., Smith, A. E., Bacia, K., Dmitrieff, S., Chai, W., Mancini, R., Kartenbeck, J., Chambon, V., Berland, L., Oppenheim, A., Schwarzmann, G., Feizi, T., Schwille, P., Sens, P., Helenius, A., and Johannes, L. (2010). GM1 structure determines SV40-induced membrane invagination and infection. *Nature Cell Biology*, 12(1):11–18.

Ewers, H., Smith, A. E., Sbalzarini, I. F., Lilie, H., Koumoutsakos, P., and Helenius, A. (2005). Single-particle tracking of murine polyoma virus-like particles on live cells and artificial membranes. *Proceedings of the National Academy of Sciences of the United States of America*, 102(42):15110–15115.

Fackler, O. T. and Peterlin, B. M. (2000). Endocytic entry of HIV-1. *Current Biology*, 10(16):1005–1008.

Fenner, F. and Kerr, P. J. (1994). *The Evolutionary Biology of Viruses*. Raven Press, New York.

Fenz, S. F. and Sengupta, K. (2012). Giant vesicles as cell models. *Integrative Biology (United Kingdom)*, 4(9):982–995.

Fields, B., Knipe, D., and Howley, P. (2007). *Fields Virology*. Wolters Kluwer Health/Lippincott Williams & Wilkins, Philadelphia, fifth edition.

Fishkind, D. J., Cao, L. G., and Wang, Y.-L. (1991). Microinjection of the cataqlytic fragment of myosin light chain kinase into dividing cells: Effects on Mitosis and cytokinesis. *J. Bell Biol.*, 114(5):967–975.

Flores, E. B., Bartee, M. Y., and Id, E. B. (2020). Reduced cellular binding affinity has profoundly different impacts on the spread of distinct poxviruses. *PLoS ONE*, 15(4):1–15.

Floyd, D. L., Ragains, J. R., Skehel, J. J., Harrison, S. C., and van Oijen, A. M. (2008). Single-particle kinetics of influenza virus membrane fusion. *Proceedings of the National Academy of Sciences of the United States of America*, 105(40):15382–15387.

Foo, C. H., Lou, H., Whitbeck, J. C., Ponce-de León, M., Atanasiu, D., Eisenberg, R. J., and Cohen, G. H. (2009). Vaccinia virus L1 binds to cell surfaces and blocks virus entry independently of glycosaminoglycans. *Virology*, 385(2):368–382.

Frei, A. P., Jeon, O.-y., Kilcher, S., Moest, H., Henning, L. M., Jost, C., Pluckthun, A., Mercer, J., Aebersold, R., Carreira, E., and Wollscheid, B. (2012). Direct identification of ligand-receptor interactions on living cells and tissues. *Nature Biotechnology*, 30:997–1001.

Gallagher, J. R., Saw, W. T., Atanasiu, D., Lou, H., Eisenberg, R. J., and Cohen, G. H. (2013). Displacement of the C Terminus of Herpes Simplex Virus gD Is Sufficient To Expose the Fusion-Activating Interfaces on gD. *Journal of Virology*, 87(23):12656–12666.

Garcel, A., Fauquette, W., Dehouck, M. P., Crance, J. M., and Favier, A. L. (2012).

Vaccinia virus-induced smallpox postvaccinal encephalitis in case of blood-brain barrier damage. *Vaccine*, 30(7):1397–1405.

Geddes, A. (2006). 2006 the history of smallpox.pdf. *Clinics in Dermatology*, 24:152–157.

Geshelin, P. and Berns, K. (1974). 1981 Characterization and localization of the naturally occurring cross-links in vaccinia.pdf. *J Mol Bio*, 88:785–796.

Giroglou, T., Florin, L., Schäfer, F., Streeck, R. E., and Sapp, M. (2001). Human Papillomavirus Infection Requires Cell Surface Heparan Sulfate. *Journal of Virology*, 75(3):1565–1570.

Grasso, L., Wyss, R., Piguet, J., Werner, M., Hassaïne, G., Hovius, R., and Vogel, H. (2013). Downscaling the Analysis of Complex Transmembrane Signaling Cascades to Closed Attoliter Volumes. *PLoS ONE*, 8(8):1–9.

Gray, R. D. M., Albrecht, D., Beerli, C., Huttunen, M., Cohen, G. H., White, I. J., Burden, J. J., Henriques, R., and Mercer, J. (2019). Nanoscale polarization of the entry fusion complex of vaccinia virus drives efficient fusion. *Nature Microbiology*, 4:1636–1644.

Gray, R. D. M., Beerli, C., Pereira, P. M., Scherer, K. M., Samolej, J., Bleck, C. K. E., Mercer, J., and Henriques, R. (2016). VirusMapper: open-source nanoscale mapping of viral architecture through super-resolution microscopy. *Scientific Reports*, 6(1):29132.

Greber, U. F. (2002). Signalling in viral entry. *Cellular and Molecular Life Sciences*, 59(4):608–626.

Greening, D. W., Xu, R., Ji, H., Tauro, B. J., and Simpson, R. J. (2015). *A Protocol for Exosome Isolation and Characterization: Evaluation of Ultracentrifugation, Density-Gradient Separation, and Immunoaffinity Capture Methods*, pages 179–209. Springer New York, New York, NY.

Grove, J. and Marsh, M. (2011). The cell biology of receptor-mediated virus entry. *Journal of Cell Biology*, 195(7):1071–1082.

Gruenheid, S., Gatzke, L., Meadows, H., and Tufaro, F. (1993). Herpes simplex virus infection and propagation in a mouse L cell mutant lacking heparan sulfate proteoglycans. *Journal of Virology*, 67(1):93–100.

Gui, L., Ebner, J. L., Mileant, A., Williams, J. A., and Lee, K. K. (2016). Visualization and Sequencing of Membrane Remodeling Leading to Influenza Virus Fusion. *Journal of Virology*, 90(15):6948–6962.

Guirakhoo, F., Heinz, F. X., Mandl, C. W., Holzmann, H., and Kunz, C. (1991). Fusion activity of flaviviruses: Comparison of mature and immature (prM-containing) tick-borne encephalitis virions. *Journal of General Virology*, 72(6):1323–1329.

Gustafsson, M. G. (2000). Surpassing the lateral resolution limit by a factor of two using structured illumination microscopy. *Journal of Microscopy*, 198(2):82–87.

Hagen, G. M., Kr, P., Borkovec, J., and Ovesny, M. (2014). ThunderSTORM : a comprehensive ImageJ plug-in for PALM and STORM data analysis and super-resolution imaging. *Bioinformatics*, 30(16):2389–2390.

Haldar, S., Mekhedov, E., McCormick, C. D., Blank, P. S., and Zimmerberg, J. (2019). Lipid-dependence of target membrane stability during influenza viral fusion. *Journal of Cell Science*, 132(4).

Halldorsson, S., Li, S., Li, M., Harlos, K., Bowden, T. A., and Huiskonen, J. T. (2018). Shielding and activation of a viral membrane fusion protein. *Nature Communications*, 9(1).

Harrison, S. C. (2009). Viral membrane fusion. *Nature Structural and Molecular Biology*, 15(7):690–698.

Harrison, S. C. (2015). Viral membrane fusion. *Virology*, 479-480:498–507.

Heald-Sargent, T. and Gallagher, T. (2012). Ready, set, fuse! the coronavirus spike protein and acquisition of fusion competence. *Viruses*, 4(4):557–580.

Heldwein, E. E., Lou, H., Bender, F. C., Cohen, G. H., Eisenberg, R. J., and Harrison, S. C. (2006). Crystal structure of glycoprotein B from herpes simplex virus 1. *Science*, 313(5784):217–220.

Henson, P. M., Bratton, D. L., and Fadok, V. A. (2001). Apoptotic cell removal. *Current Biology*, 11(19):795–805.

Heuser, J. (2005). Deep-etch EM reveals that the early poxvirus envelope is a single membrane bilayer stabilized by a geodetic "honeycomb" surface coat. *Journal of Cell Biology*, 169(2):269–283.

Ho, C. S., Khadka, N. K., She, F., Cai, J., and Pan, J. (2016). Influenza M2 Transmembrane Domain Senses Membrane Heterogeneity and Enhances Membrane Curvature. *Langmuir*, 32(26):6730–6738.

Ho, Y., Hsiao, J. C., Yang, M. H., Chung, C. S., Peng, Y. C., Lin, T. H., Chang, W., and Tzou, D. L. M. (2005). The oligomeric structure of vaccinia viral envelope protein A27L is essential for binding to heparin and heparan sulfates on cell surfaces: A structural and functional approach using site-specific mutagenesis. *Journal of Molecular Biology*, 349(5):1060–1071.

Hollinshead, M., Vanderplasschen, A., Smith, G. L., and Vaux, D. J. (1999). Vaccinia virus intracellular mature virions contain only one lipid membrane. *Journal of virology*, 73(2):1503–17.

Holowczak, J. A. and Joklik, W. K. (1967). Studies on the structural proteins of vaccinia virus I. Structural proteins of virions and cores. *Virology*, 33(4):717–725.

Housawi, F. M., Roberts, G. M., Gilray, J. A., Pow, I., Reid, H. W., Nettleton, P. F., Sumption, K. J., Hibma, M. H., and Mercer, A. A. (1998). The reactivity of monoclonal antibodies against off virus with other parapoxviruses and

the identification of a 39 kDa immunodominant protein. *Archives of Virology*, 143(12):2289–2303.

Howard, A. R., Senkevich, T. G., and Moss, B. (2008). Vaccinia Virus A26 and A27 Proteins Form a Stable Complex Tethered to Mature Virions by Association with the A17 Transmembrane Protein . *Journal of Virology*, 82(24):12384–12391.

Hruby, D. E. (1990). Vaccinia virus vectors: New strategies for producing recombinant vaccines. *Clinical Microbiology Reviews*, 3(2):153–170.

Hruby, D. E., Guarino, L. a., and Kates, J. R. (1979a). Vaccinia virus replication. I. Requirement for the host-cell nucleus. *Journal of virology*, 29(2):705–15.

Hruby, D. E., Lynn, D. L., and Kates, J. R. (1979b). Vaccinia virus replication requires active participation of the host cell transcriptional apparatus. *Proc Natl Acad Sci U S A*, 76(4):1887–1890.

Hsiao, J. C., Chung, C. S., and Chang, W. (1998). Cell surface proteoglycans are necessary for A27L protein-mediated cell fusion: identification of the N-terminal region of A27L protein as the glycosaminoglycan-binding domain. *Journal of virology*, 72(10):8374–9.

Hsiao, J. C., Chung, C. S., and Chang, W. (1999). Vaccinia virus envelope D8L protein binds to cell surface chondroitin sulfate and mediates the adsorption of intracellular mature virions to cells. *Journal of virology*, 73(10):8750–8761.

Hsieh, C. L., Spindler, S., Ehrig, J., and Sandoghdar, V. (2014). Tracking single particles on supported lipid membranes: Multimobility diffusion and nanoscopic confinement. *Journal of Physical Chemistry B*, 118(6):1545–1554.

Huang, C.-Y., Lu, T.-Y., Bair, C.-H., Chang, Y.-S., Jwo, J.-K., and Chang, W. (2008). A novel cellular protein, VPEF, facilitates vaccinia virus penetration into HeLa cells through fluid phase endocytosis. *Journal of virology*, 82(16):7988–99.

Huang, Y. F., Zhuo, G. Y., Chou, C. Y., Lin, C. H., Chang, W., and Hsieh, C. L. (2017). Coherent Brightfield Microscopy Provides the Spatiotemporal Resolution to Study Early Stage Viral Infection in Live Cells. *ACS Nano*, 11(3):2575–2585.

Hughes, A. L., Irausquin, S., and Friedman, R. (2010). The evolutionary biology of poxviruses. *Infection, Genetics and Evolution*, 10(1):50–59.

Ibrahim, J., Griffin, P., Coombe, D. R., Rider, C. C., and James, W. (1999). Cell-surface heparan sulfate facilitates human immunodeficiency virus Type 1 entry into some cell lines but not primary lymphocytes. *Virus Research*, 60(2):159–169.

Ichihashi, Y. and Masayasu, O. (1983). The activation of vaccinia virus infectivity by the transfer of.pdf. *Virology*, 130:306–317.

Ichihashi, Y., Oie, M., and Tsuruhara, T. (1984). Location of DNA-binding proteins and disulfide-linked proteins in vaccinia virus structural elements. *Journal of virology*, 50(3):929–38.

Izmailyan, R., Hsao, J.-C., Chung, C.-S., Chen, C.-H., Hsu, P. W.-C., Liao, C.-L., and Chang, W. (2012). Integrin 1 Mediates Vaccinia Virus Entry through Activation of PI3K/Akt Signaling. *Journal of Virology*, 86(12):6677–6687.

Izmailyan, R. a., Huang, C.-Y., Mohammad, S., Isaacs, S. N., and Chang, W. (2006). The envelope G3L protein is essential for entry of vaccinia virus into host cells. *Journal of virology*, 80(17):8402–10.

Jacobsen, V., Stoller, P., Brunner, C., Vogel, V., and Sandoghdar, V. (2006). Interferometric optical detection and tracking of very small gold nanoparticles at a water-glass interface. *Optics Express*, 14(1):405.

Jensen, O. N., Houthaeve, T., Shevchenko, A., Mann, M., Cudmore, S., Ashford, T., Griffiths, G., and Locker, J. K. (1996). Identification of the major membrane and core proteins of vaccinia virus by two-dimensional electrophoresis. *Journal of Virology*, 70(11):7485–7497.

Johannsdottir, H. K., Mancini, R., Kartenbeck, J., Amato, L., and Helenius, A. (2009). Host Cell Factors and Functions Involved in Vesicular Stomatitis Virus Entry. *Journal of Virology*, 83(1):440–453.

Joklik, W. K. and Becker, Y. (1964). The replication and coating of vaccinia DNA. *Journal of Molecular Biology*, 10(3):452–474.

Jones, A. T. (2007). Macropinocytosis: Searching for an endocytic identity and role in the uptake of cell penetrating peptides. *Journal of Cellular and Molecular Medicine*, 11(4):670–684.

Jones, K. S., Petrow-Sadowski, C., Bertolette, D. C., Huang, Y., and Ruscetti, F. W. (2005). Heparan Sulfate Proteoglycans Mediate Attachment and Entry of Human T-Cell Leukemia Virus Type 1 Virions into CD4+ T Cells. *Journal of Virology*, 79(20):12692–12702.

Julien Lescar, Roussel, A., Wien, M. W., Navaza, J., Fuller, S. D., Wengler, G., and Rey, F. A. (2001). The Fusion glycoprotein shell of Semliki Forest virus: an icosahedral assembly primed for fusogenic activation at endosomal pH. *Cell*, 105(1):137–148.

Kamiya, K., Kobayashi, J., Yoshimura, T., and Tsumoto, K. (2010). Confocal microscopic observation of fusion between baculovirus budded virus envelopes and single giant unilamellar vesicles. *Biochimica et Biophysica Acta - Biomembranes*, 1798(9):1625–1631.

Kates, J. R. and McAuslan, B. R. (1967). Poxvirus DNA-dependent RNA polymerase. *Proc Natl Acad Sci U S A*, 58(1):134–141.

Kato, D., Era, S., Watanabe, I., Arihara, M., Sugiura, N., Kimata, K., Suzuki, Y., Morita, K., Hidari, K., and Suzuki, T. (2010). Antiviral activity of chondroitin sulphate E targeting dengue virus envelope protein. *Antiviral Research*, 88(2):236–243.

Ketter, E. and Randall, G. (2019). Virus Impact on Lipids and Membranes. *Annual Review of Virology*, 6(1):319–340.

Khanna, M., Ranasinghe, C., Browne, A. M., Li, J. P., Vlodavsky, I., and Parish, C. R. (2019). Is host heparanase required for the rapid spread of heparan sulfate binding viruses? *Virology*, 529(October 2018):1–6.

Khanna, M., Ranasinghe, C., Jackson, R., and Parish, C. R. (2017). Heparan sulfate as a receptor for poxvirus infections and as a target for antiviral agents. *Journal of General Virology*, 98(10):2556–2568.

Kielian, M. (2006). Class II virus membrane fusion proteins. *Virology*, 344(1):38–47.

Kilcher, S. and Mercer, J. (2014). Next generation approaches to study virus entry and infection. *Current Opinion in Virology*, 4:8–14.

Kochan, G., Escors, D., González, J. M., Casasnovas, J. M., and Esteban, M. (2008). Membrane cell fusion activity of the vaccinia virus A17 – A27 protein complex. *Cellular Microbiology*, 10(1):149–164.

Kociurzynski, R., Beck, S. D., Bouhon, J. B., Römer, W., and Knecht, V. (2019). Binding of SV40's Viral Capsid Protein VP1 to Its Glycosphingolipid Receptor GM1 Induces Negative Membrane Curvature: A Molecular Dynamics Study. *Langmuir*, 35(9):3534–3544.

Kozlov, M. M. and Chernomordik, L. V. (2015). Membrane tension and membrane fusion. *current opinion in structural biology*, 33(1):51–57.

Krummenacher, C., Supekar, V. M., Whitbeck, J. C., Lazear, E., Connolly, S. A., Eisenberg, R. J., Cohen, G. H., Wiley, D. C., and Carfí, A. (2005). Structure of unliganded HSV gD reveals a mechanism for receptor-mediated activation of virus entry. *EMBO Journal*, 24(23):4144–4153.

Kukura, P., Ewers, H., Müller, C., Renn, A., Helenius, A., and Sandoghdar, V. (2009). High-speed nanoscopic tracking of the position and orientation of a single virus. *Nature Methods*, 6(12):923–927.

Kuznetsov, Y., Gershon, P. D., and McPherson, A. (2008). Atomic Force Microscopy Investigation of Vaccinia Virus Structure. *Journal of Virology*, 82(15):7551–7566.

Lai, A., Moorthy, A., Li, Y., and Tamm, L. K. (2012). Fusion Activity of HIV GP41 Fusion Domain is Related to its Secondary Structure and Depth of Membrane Insertion in a Cholesterol-Dependent Fashion. *J Mol Biol*, 23(1):1–7.

Laliberte, J. P. and Moss, B. (2009). Appraising the apoptotic mimicry model and the role of phospholipids for poxvirus entry. *Proceedings of the National Academy of Sciences of the United States of America*, 106(41):17517–17521.

Laliberte, J. P., Weisberg, A. S., and Moss, B. (2011). The membrane fusion step of vaccinia virus entry is cooperatively mediated by multiple viral proteins and host cell components. *PLoS Pathogens*, 7(12).

Lazear, E., Carfi, A., Whitbeck, J. C., Cairns, T. M., Krummenacher, C., Cohen, G. H., and Eisenberg, R. J. (2008). Engineered Disulfide Bonds in Herpes Simplex Virus Type 1 gD Separate Receptor Binding from Fusion Initiation and Viral Entry. *Journal of Virology*, 82(2):700–709.

Lazear, E., Whitbeck, J. C., Ponce-de Leon, M., Cairns, T. M., Willis, S. H., Zuo, Y., Krummenacher, C., Cohen, G. H., and Eisenberg, R. J. (2012). Antibody-Induced Conformational Changes in Herpes Simplex Virus Glycoprotein gD Reveal New Targets for Virus Neutralization. *Journal of Virology*, 86(3):1563–1576.

Lee, D. W., Hsu, H. L., Bacon, K. B., and Daniel, S. (2016). Image restoration and analysis of influenza virions binding to membrane receptors reveal adhesion-strengthening kinetics. *PLoS ONE*, 11(10).

Lee, K. K. (2010). Architecture of a nascent viral fusion pore. *EMBO Journal*, 29(7):1299–1311.

Lehmann, M. J., Sherer, N. M., Marks, C. B., Pypaert, M., and Mothes, W. (2005). Actin- and myosin-driven movement of viruses along filopodia precedes their entry into cells. *Journal of Cell Biology*, 170(2):317–325.

Levet, F., Hosy, E., Kechkar, A., Butler, C., Beghin, A., Choquet, D., and Sibarita, J. B. (2015). SR-Tesseler: A method to segment and quantify localization-based super-resolution microscopy data. *Nature Methods*, 12(11):1065–1071.

Li, L., Jose, J., Xiang, Y., Kuhn, R. J., and Rossmann, M. G. (2010). Structural Changes of Envelope Proteins During Alphavirus Fusion. *Nature*, 468(7324):705–708.

Li, L., Wan, T., Wan, M., Liu, B., Cheng, R., and Zhang, R. (2015). The effect of the size of fluorescent dextran on its endocytic pathway. *Cell Biology International*, 39(5):531–539.

Li, Y., Carroll, D. S., Gardner, S. N., Walsh, M. C., Vitalis, E. A., and Damon, I. K. (2007). On the origin of smallpox: Correlating variola phylogenics with historical smallpox records. *Proceedings of the National Academy of Sciences*, 104(40):15787–15792.

Lin, C. L., Chung, C. S., Heine, H. G., and Chang, W. (2000). Vaccinia virus envelope H3L protein binds to cell surface heparan sulfate and is important for intracellular mature virion morphogenesis and virus infection in vitro and in vivo. *Journal of virology*, 74(7):3353–3365.

Lin, Y. L., Lei, H. Y., Lin, Y. S., Yeh, T. M., Chen, S. H., and Liu, H. S. (2002). Heparin inhibits dengue-2 virus infection of five human liver cell lines. *Antiviral Research*, 56(1):93–96.

Lindenbach, B. D. and Rice, C. M. (2007). Flaviviridae: The Viruses and Their Replication. *Fields Virology*, pages 1101– 1151.

Liu, H. Y., Grant, H., Hsu, H. L., Sorkin, R., Bošković, F., Wuite, G., and Daniel, S. (2017). Supported Planar Mammalian Membranes as Models of in Vivo Cell Surface Architectures. *ACS Applied Materials and Interfaces*, 9(41):35526–35538.

Liu, K. N. and Boxer, S. G. (2020). Target Membrane Cholesterol Modulates Single Influenza Virus Membrane Fusion Efficiency but Not Rate. *Biophysical Journal*, 118(10):2426–2433.

Liu, S.-w., Wyatt, L. S., Orandle, M. S., and Minai, M. (2014). The D10 Decapping Enzyme of Vaccinia Virus Contributes to Decay of Cellular and Viral mRNAs and to Virulence in Mice. *Journal of Virology*, 88(1):202–211.

Lobigs, M. and Garoff, H. (1990). Fusion function of the Semliki Forest virus spike is activated by proteolytic cleavage of the envelope glycoprotein precursor p62. *Journal of Virology*, 64(3):1233–1240.

Locker, J. K., Kuehn, a., Schleich, S., Rutter, G., Hohenberg, H., Wepf, R., and Griffiths, G. (2000). Entry of the two infectious forms of vaccinia virus at the plasma membane is signaling-dependent for the IMV but not the EEV. *Molecular biology of the cell*, 11(7):2497–511.

Macleod, D. T., Nakatsuji, T., Wang, Z., Richard, L., Jolla, L., and Diego, S. (2015). Vaccinia virus binds to the scavenger receptor MARCO on the surface of keratinocytes. *Journal of Investigative Dermatology*, 135(1):142–150.

Maginnis, M. S., Forrest, J. C., Kopecky-Bromberg, S. A., Dickeson, S. K., Santoro, S. A., Zutter, M. M., Nemerow, G. R., Bergelson, J. M., and Dermody, T. S. (2006). 1 Integrin Mediates Internalization of Mammalian Reovirus. *Journal of Virology*, 80(6):2760–2770.

Mammen, M., Choi, S.-K., and Whitesides, G. M. (1998). Polyvalent Interactions in Biological Systems: Implications for Design and Use of Multivalent Ligands and Inhibitors. *Angewandte Chemie (International ed.)*, 37(20):2754–2794.

Mårdberg, K., Trybala, E., Tufaro, F., and Bergström, T. (2002). Herpes simplex virus type 1 glycoprotein C is necessary for efficient infection of chondroitin sulfate-expressing gro2C cells. *Journal of General Virology*, 83(2):291–300.

Marks, R. M., Lu, H., Sundaresan, R., Toida, T., Suzuki, A., Imanari, T., Hernáiz, M. J., and Linhardt, R. J. (2001). Probing the interaction of dengue virus envelope protein with heparin: Assessment of glycosaminoglycan-derived inhibitors. *Journal of Medicinal Chemistry*, 44(13):2178–2187.

Marsh, M. and Helenius, A. (2006). Virus entry: Open sesame. *Cell*, 124(4):729–740.

Martyna, A., Bahsoun, B., Badham, M. D., Srinivasan, S., Howard, M. J., and Rossman, J. S. (2017). Membrane remodeling by the M2 amphipathic helix drives influenza virus membrane scission. *Scientific Reports*, 7(February):1–12.

Mary, H. and Brouhard, G. (2019). Kappa (κ): Analysis of Curvature in Biological Image Data using B-splines. *bioRxiv*.

Matho, M. H., Maybeno, M., Benhnia, M. R.-e.-i., Becker, D., Meng, X., and Xiang, Y. (2012). Structural and Biochemical Characterization of the Vaccinia Virus Envelope Protein D8 and Its Recognition by the Antibody LA5. *Journal of Virology*, 86(15):8050–8058.

Matho, M. H., Val, N. D., Miller, G. M., Brown, J., Schlossman, A., Meng, X., Crotty, S., Peters, B., Xiang, Y., Hsieh-wilson, L. C., Ward, A. B., and Zajonc, D. M. (2014). Murine Anti-vaccinia Virus D8 Antibodies Target Different Epitopes and Differ in Their Ability to Block D8 Binding to CS-E. *PLoS Pathogens*, 10(12).

Matson, J., Chou, W., Ngo, T., and Gershon, P. D. (2014). Static and dynamic protein phosphorylation in the Vaccinia virion. *Virology*, 452-453:310–323.

Maurin, T., Fenard, D., Lambeau, G., and Doglio, A. (2007). An Envelope-determined Endocytic Route of Viral Entry Allows HIV-1 to Escape from

Secreted Phospholipase A2 Entry Blockade. *Journal of Molecular Biology*, 367(3):702–714.

McFadden, G. (2005). Poxvirus tropism. *Nature Reviews Microbiology*, 3(3):201–213.

Meher, G., Sinha, S., Pattnaik, G. P., Ghosh Dastidar, S., and Chakraborty, H. (2019). Cholesterol Modulates Membrane Properties and the Interaction of gp41 Fusion Peptide to Promote Membrane Fusion. *Journal of Physical Chemistry B*, 123(33):7113–7122.

Meng, X., Zhong, Y., Embry, A., Yan, B., Lu, S., Zhong, G., and Xiang, Y. (2011). Generation and characterization of a large panel of murine monoclonal antibodies against vaccinia virus. *Virology*, 409(2):271–279.

Mercer, J. and Helenius, A. (2008). Vaccinia Virus Uses Macropinocytosis and Apoptotic Mimicry to Enter Host Cells. *Science*, 320(5875):531–535.

Mercer, J. and Helenius, A. (2009). Virus entry by macropinocytosis. *Nature Cell Biology*, 11(5):510–520.

Mercer, J. and Helenius, A. (2010). Apoptotic mimicry: Phosphatidylserine-mediated macropinocytosis of vaccinia virus. *Annals of the New York Academy of Sciences*, 1209(1):49–55.

Mercer, J., Knebel, S., Schmidt, F. I., Crouse, J., Burkard, C., and Helenius, A. (2010a). Vaccinia virus strains use distinct forms of macropinocytosis for host-cell entry. *Proceedings of the National Academy of Sciences*, 107(20):9346–9351.

Mercer, J., Schelhaas, M., and Helenius, A. (2010b). Virus Entry by Endocytosis. *Annual Review of Biochemistry*, 79(1):803–833.

Mills, J. C., Stone, N. L., Erhardt, J., and Pittman, R. N. (1998). Blebbing Is Regulated Apoptotic Membrane by Myosin Light Chain Phosphorylation. *Cell*, 140(3):627–636.

Mim, C. and Unger, V. M. (2012). Membrane curvature and its generation by BAR proteins. *Trends in Biochmical Science*, 37(12):526–533.

Mirzakhanyan, Y. and Gershon, P. (2019). The Vaccinia virion: Filling the gap between atomic and ultrastructure. *PLoS Pathogens*, 15(1):1–41.

Mitsuhashi, W., Kawakita, H., Murakami, R., Takemoto, Y., Saiki, T., Miyamoto, K., and Wada, S. (2007). Spindles of an Entomopoxvirus Facilitate Its Infection of the Host Insect by Disrupting the Peritrophic Membrane. *Journal of Virology*, 81(8):4235–4243.

Morgan, C. (1976). The insertion of DNA into vaccinia virus. *Science*, 193(4253):591–592.

Moser, T. S., Jones, R. G., Thompson, C. B., Coyne, C. B., and Cherry, S. (2010). A Kinome RNAi Screen Identified AMPK as Promoting Poxvirus Entry through the Control of Actin Dynamics. *PLoS Pathogens*, 6(6).

Moss, B. (2006). Poxvirus entry and membrane fusion. *Virology*, 344(1):48–54.

Moss, B. (2012). Poxvirus cell entry: How many proteins does it take? *Viruses*, 4(5):688–707.

Moss, B. (2018). Origin of the poxviral membrane: A 50-year-old riddle. *PLoS Pathogens*, 14(6):1–6.

Nagler, F. P. and Rake, G. (1948). The use of the electron microscope in diagnosis of variola, vaccinia,. *Journal of bacteriology*, 55(1):45–51.

Nelson, G. E., Wagenaar, T. R., and Moss, B. (2008). A Conserved Sequence within the H2 Subunit of the Vaccinia Virus Entry/Fusion Complex Is Important for Interaction with the A28 Subunit and Infectivity. *Journal of Virology*, 82(13):6244–6250.

Ngo, T., Mirzakhanyan, Y., Moussatche, N., and Gershon, P. D. (2016). Protein Primary Structure of the Vaccinia Virion at Increased Resolution. *Journal of Virology*, 90(21):9905–9919.

Nicola, A. V., Aguilar, H. C., Mercer, J., Ryckman, B., and Wiethoff, C. M. (2013). Virus entry by endocytosis. *Advances in Virology*, 2013.

Nikolaus, J., Scolari, S., Bayraktarov, E., Jungnick, N., Engel, S., Plazzo, A. P., Stöckl, M., Volkmer, R., Veit, M., and Herrmann, A. (2010). Hemagglutinin of influenza virus partitions into the nonraft domain of model membranes. *Biophysical Journal*, 99(2):489–498.

Novy, K., Kilcher, S., Omasits, U., Bleck, C. K. E., Beerli, C., Vowinckel, J., Martin, C. K., Syedbasha, M., Maiolica, A., White, I., Mercer, J., and Wollscheid, B. (2018). Proteotype profiling unmasks a viral signalling network essential for poxvirus assembly and transcriptional competence. *Nature Microbiology*, 3(5):588–599.

Oh, J. and Broyles, S. S. (2005). Host Cell Nuclear Proteins Are Recruited to Cytoplasmic Vaccinia Virus Replication Complexes. *Society*, 79(20):12852–12860.

Ojeda, S., Domi, A., and Moss, B. (2006a). Vaccinia virus G9 protein is an essential component of the poxvirus entry-fusion complex. *Journal of virology*, 80(19):9822–30.

Ojeda, S., Senkevich, T. G., and Moss, B. (2006b). Entry of vaccinia virus and cell-cell fusion require a highly conserved cysteine-rich membrane protein encoded by the A16L gene. *Journal of Virology*, 80(1):51–61.

Olety, B., Veatch, S. L., and Ono, A. (2016). Visualization of HIV-1 Gag Binding to Giant Unilamellar Vesicle (GUV) Membranes. *Journal of visualized experiments : JoVE*, 41(113):135–49.

Ortega Arroyo, J., Cole, D., and Kukura, P. (2016). Interferometric scattering microscopy and its combination with single-molecule fluorescence imaging. *Nature Protocols*, 11(4):617–633.

Orynbayeva, Z., Kolusheva, S., Groysman, N., Gavrielov, N., Lobel, L., and Jelinek, R. (2007). Vaccinia Virus Interactions with the Cell Membrane Studied by New

Chromatic Vesicle and Cell Sensor Assays. *Journal of Virology*, 81(3):1140–1147.

Paluch, E., Piel, M., Prost, J., Bornens, M., and Sykes, C. (2005). Cortical actomyosin breakage triggers shape oscillations in cells and cell fragments. *Biophysical Journal*, 89(1):724–733.

Patel, M., Yanagishita, M., Roderiquez, G., Bou-Habib, D. C., Oravecz, T., Hascall, V. C., and Norcross, M. A. (1993). Cell-Surface Heparan Sulfate Proteoglycan Mediates HIV-1 Infection of T-Cell Lines. *AIDS Research and Human Retroviruses*, 9(2):167–174.

Payne, L. (1978). Polypeptide composition of extracellular enveloped vaccinia virus. *Journal of Virology*, 27(1):28–37.

Payne, L. G. (1979). Identification of the vaccinia hemagglutinin polypeptide from a cell system yielding large amounts of extracellular enveloped virus. *Journal of Virology*, 31(1):147–155.

Pedersen, K., Snijder, E. J., Schleich, S., Roos, N., Griffiths, G., and Locker, J. K. (2000). Characterization of Vaccinia Virus Intracellular Cores: Implications for Viral Uncoating and Core Structure. *Journal of Virology*, 74(8):3525–3536.

Peerboom, N., Schmidt, E., Trybala, E., Block, S., Bergstro, T., Pace, H. P., and Bally, M. (2018). Cell Membrane Derived Platform To Study Virus Binding Kinetics and Di ff usion with Single Particle Sensitivity. *Infecious Diseases*, 4(1):944–953.

Perino, J., Crouzier, D., Spehner, D., Debouzy, J. C., Garin, D., Crance, J. M., and Favier, A. L. (2011). Lung surfactant DPPG phospholipid inhibits vaccinia virus infection. *Antiviral Research*, 89(1):89–97.

Peters, D. and Muller, G. (1963). The Fine Structure of the DNA-Containing Core of Vaccinia Virus. *Virology*, 21(2):266–269.

Pezeshkian, W., Hansen, A. G., Johannes, L., Khandelia, H., Shillcock, J. C., Kumar, P. B., and Ipsen, J. H. (2016). Membrane invagination induced by Shiga toxin B-subunit: From molecular structure to tube formation. *Soft Matter*, 12(23):5164–5171.

Pezeshkian, W., Nåbo, L. J., and Ipsen, J. H. (2017). Cholera toxin B subunit induces local curvature on lipid bilayers. *FEBS Open Bio*, 7(11):1638–1645.

Pick, H., Schmidt, E. L., Tairi, A. P., Ilegems, E., Hovius, R., and Vogel, H. (2005). Investigating cellular signaling reactions in single attoliter vesicles. *Journal of the American Chemical Society*, 127(9):2908–2912.

Pinon, J. D., Klasse, P. J., Jassal, S. R., Welson, S., Weber, J., Brighty, D. W., and Sattentau, Q. J. (2003). Human T-Cell Leukemia Virus Type 1 Envelope Glycoprotein gp46 Interacts with Cell Surface Heparan Sulfate Proteoglycans. *Journal of Virology*, 77(18):9922–9930.

Postigo, A., Ramsden, A. E., Howell, M., and Way, M. (2017). Cytoplasmic ATR Activation Promotes Vaccinia Virus Genome Replication. *Cell Reports*, 19(5):1022–1032.

Prescott, D., Kates, J., and Kirkpatrick, J. (1971). 1971 Replication of vaccinia virus DNA in enucleated L-cells.pdf. *J Mol Biol*, 59:505–508.

Przybylo, M., Sýkora, J., Humpolíčová, J., Benda, A., Zan, A., and Hof, M. (2006). Lipid diffusion in giant unilamellar vesicles is more than 2 times faster than in supported phospholipid bilayers under identical conditions. *Langmuir*, 22(22):9096–9099.

Purushothaman, A., Fukuda, J., Mizumoto, S., Ten Dam, G. B., Van Kuppevelt, T. H., Kitagawa, H., Mikami, T., and Sugahara, K. (2007). Functions of chondroitin sulfate/dermatan sulfate chains in brain development: Critical roles of E and iE disaccharide units recognized by a single chain antibody GD3G7. *Journal of Biological Chemistry*, 282(27):19442–19452.

Rankl, C., Kienberger, F., Wildling, L., Wruss, J., Gruber, H. J., Blaas, D., and Hinterdorfer, P. (2008). Multiple receptors involved in human rhinovirus attachment to live cells. *Proceedings of the National Academy of Sciences of the United States of America*, 105(46):17778–83.

Resch, W., Hixson, K. K., Moore, R. J., Lipton, M. S., and Moss, B. (2007). Protein composition of the vaccinia virus mature virion. *Virology*, 358(1):233–247.

Risco, C., Rodriguez, J. R., Lopez-Iglesias, C., Carrascosa, J. L., Esteban, M., and Rodriguez, D. (2002). Endoplasmic Reticulum-Golgi Intermediate Compartment Membranes and Vimentin Filaments Participate in Vaccinia Virus Assembly. *Journal of Virology*, 76(4):1839–1855.

Rizopoulos, Z., Balistreri, G., Kilcher, S., Martin, C. K., Syedbasha, M., Helenius, A., and Mercer, J. (2015). Vaccinia Virus Infection Requires Maturation of Macropinosomes. *Traffic*, 16(8):814–831.

Roberts, K. L. and Smith, G. L. (2008). Vaccinia virus morphogenesis and dissemination. *Trends in Microbiology*, 16(10):472–479.

Roche, S., Bressanelli, S., Rey, F., and Gaudin, Y. (2006). Crystal structure of the low-pH form of the vesicular stomatis virus glycoprotein G. *Science*, 313(July):187–192.

Roos, N., Cyrklaff, M., Cudmore, S., Blasco, R., Krijnse-Locker, J., and Griffiths, G. (1996). A novel immunogold cryoelectron microscopic approach to investigate the structure of the intracellular and extracellular forms of vaccinia virus. *The EMBO Journal*, 15(10):2343–2355.

Rossman, J. S., Jing, X., Leser, G. P., and Lamb, R. A. (2010). Influenza Virus M2 Protein Mediates ESCRT-Independent Membrane Scission. *Cell*, 142(6):902–913.

Rydell, G. E., Svensson, L., Larson, G., Johannes, L., and Römer, W. (2013). Human GII.4 norovirus VLP induces membrane invaginations on giant unilamel-

lar vesicles containing secretor gene dependent α1,2-fucosylated glycosphingolipids. *Biochimica et Biophysica Acta - Biomembranes*, 1828(8):1840–1845.

Sakry, D. and Trotter, J. (2016). The role of the NG2 proteoglycan in OPC and CNS network function. *Brain Research*, 1638:161–166.

Salbreux, G., Charras, G., and Paluch, E. (2012). Actin cortex mechanics and cellular morphogenesis. *Trends in Cell Biology*, 22(10):536–545.

Sánchez-Sampedro, L., Perdiguero, B., Mejías-Pérez, E., García-Arriaza, J., Di Pilato, M., and Esteban, M. (2015). The evolution of poxvirus vaccines. *Viruses*, 7(4):1726–1803.

Sanderson, C. M., Hollinshead, M., and Smith, G. L. (2000). The vaccinia virus A27L protein is needed for the microtubule-dependent transport of intracellular mature virus particles. *Journal of General Virology*, 81(1):47–58.

Sandgren, K. J., Wilkinson, J., Miranda-saksena, M., Mcinerney, G. M., Byth, K., Robinson, P. J., and Cunningham, A. L. (2010). A Differential Role for Macropinocytosis in Mediating Entry of the Two Forms of Vaccinia Virus into Dendritic Cells. *PLoS Pathogens*, 6(4).

Sarov, I. and Joklik, W. K. (1972). Studies on the nature and location of the capsid polypeptides of vaccinia virions. *Virology*, 50(2):579–592.

Satheshkumar, P. S. and Moss, B. (2009). Characterization of a newly identified 35-amino-acid component of the vaccinia virus entry/fusion complex conserved in all chordopoxviruses. *Journal of virology*, 83(24):12822–32.

Schelhaas, M., Ewers, H., Rajamäki, M. L., Day, P. M., Schiller, J. T., and Helenius, A. (2008). Human papillomavirus type 16 entry: Retrograde cell surface transport along actin-rich protrusions. *PLoS Pathogens*, 4(9).

Schiffer, D., Mellai, M., Boldorini, R., Bisogno, I., Grifoni, S., Corona, C., Bertero, L., Cassoni, P., Casalone, C., and Annovazzi, L. (2018). The significance of

chondroitin sulfate proteoglycan 4 (CSPG4) in human gliomas. *International Journal of Molecular Sciences*, 19(9).

Schindelin, J., Arganda-carreras, I., Frise, E., Kaynig, V., Pietzsch, T., Preibisch, S., Rueden, C., Saalfeld, S., Schmid, B., Tinevez, J.-y., White, D. J., Hartenstein, V., Tomancak, P., and Cardona, A. (2019). Fiji - an Open Source platform for biological image analysis. 9(7).

Schink, K. O., Tan, K. W., Martorana, D., Campsteijn, C., Raiborg, C., and Stenmark, H. (2017). The PtdIns3P-binding protein Phafin2 escorts macropinosomes through the cortical actin cytoskeleton. *bioRxiv*, page 180760.

Schmidt, F. I., Bleck, C. K. E., Helenius, A., and Mercer, J. (2011). Vaccinia extracellular virions enter cells by macropinocytosis and acid-activated membrane rupture. *The EMBO Journal*, 30(17):3647–3661.

Schmidt, F. I., Bleck, C. K. E., and Mercer, J. (2012). Poxvirus host cell entry. *Current Opinion in Virology*, 2(1):20–27.

Schmidt, F. I., Bleck, C. K. E., Reh, L., Novy, K., Wollscheid, B., Helenius, A., Stahlberg, H., and Mercer, J. (2013a). Vaccinia virus entry is followed by core activation and proteasome-mediated release of the immunomodulatory effector VH1 from lateral bodies. *Cell Reports*, 4(3):464–476.

Schmidt, F. I., Kuhn, P., Robinson, T., Mercer, J., and Dittrich, P. S. (2013b). Single-virus fusion experiments reveal proton influx into vaccinia virions and hemifusion lag times. *Biophysical Journal*, 105(2):420–431.

Schroeder, N., Chung, C.-S., Chen, C.-H., Liao, C.-L., and Chang, W. (2012). The Lipid Raft-Associated Protein CD98 Is Required for Vaccinia Virus Endocytosis. *Journal of Virology*, 86(9):4868–4882.

Scott, R. E. (1976). Plasma membrane vesiculation: A new technique for isolation of plasma membranes. *Science*, 194(4266):743–745.

Seet, B. T., Johnston, J., Brunetti, C. R., Barrett, J. W., Everett, H., Cameron, C., Sypula, J., Nazarian, S. H., Lucas, A., and McFadden, G. (2003). Poxviruses and Immune evasion. *Annual Review of Immunology*, 21(1):377–423.

Selgelid, M. J. (2004). Bioterrorism and smallpox planning: Information and voluntary vaccination. *Journal of Medical Ethics*, 30(6):558–560.

Senkevich, T. G. and Moss, B. (2005). Vaccinia Virus H2 Protein Is an Essential Component of a Complex Involved in Virus Entry and Cell-Cell Fusion Vaccinia Virus H2 Protein Is an Essential Component of a Complex Involved in Virus Entry and Cell-Cell Fusion. *Journal of Virology*, 79(8):4744–4754.

Senkevich, T. G., Ojeda, S., Townsley, A., Nelson, G. E., and Moss, B. (2005). Poxvirus multiprotein entry-fusion complex. *Proceedings of the National Academy of Sciences of the United States of America*, 102(51):18572–7.

Senkevich, T. G., Ward, B. M., and Moss, B. (2004). Vaccinia virus A28L gene encodes an essential protein component of the virion membrane with intramolecular disulfide bonds formed by the viral cytoplasmic redox pathway. *Journal of virology*, 78(5):2348–56.

Senkevich, T. G., Weisberg, A. S., and Moss, B. (2000). Vaccinia virus E10R protein is associated with the membranes of intracellular mature virions and has a role in morphogenesis. *Virology*, 278(1):244–252.

Senkevich, T. G., White, C. L., Weisberg, A., Granek, J. A., Wolffe, E. J., Koonin, E. V., and Moss, B. (2002). Expression of the vaccinia virus A2.5L redox protein is required for virion morphogenesis. *Virology*, 300(2):296–303.

Shieh, M. T., WuDunn, D., Montgomery, R. I., Esko, J. D., and Spear, P. G. (1992). Cell surface receptors for herpes simplex virus are heparan sulfate proteoglycans. *Journal of Cell Biology*, 116(5):1273–1281.

Silver, M., McFadden, G., Wilton, S., and Dales, S. (1979). Biogenesis of poxviruses: Role for the DNA-dependent RNA polymerase II of the host during

expression of late functions. *Proceedings of the National Academy of Sciences of the United States of America*, 76(8):4122–4125.

Skehel, J. and Wiley, D. (2000). Receptor binding and membrane fusion in virus entry: the influenza hemagglutinin. *Annual Reviews in Biochemistry*, pages 777–810.

Smith, G. L., Vanderplasschen, A., and Law, M. (2002). The formation and function of extracellular enveloped vaccinia virus. *Journal of General Virology*, 83(12):2915–2931.

Sodeik, B., Doms, R. W., Ericsson, M., Hiller, G., Machamer, C. E., Van't Hof, W., Van Meer, G., Moss, B., and Griffiths, G. (1993). Assembly of vaccinia virus: Role of the intermediate compartment between the endoplasmic reticulum and the Golgi stacks. *Journal of Cell Biology*, 121(3):521–542.

Stanford, M. M., Barrett, J. W., Nazarian, S. H., Werden, S., and McFadden, G. (2007). Oncolytic Virotherapy Synergism with Signaling Inhibitors: Rapamycin Increases Myxoma Virus Tropism for Human Tumor Cells. *Journal of Virology*, 81(3):1251–1260.

Stein, B. S., Gowda, S. D., Lifson, J. D., Penhallow, R. C., Bensch, K. G., and Engleman, E. G. (1987). pH-independent HIV entry into CD4-positive T cells via virus envelope fusion to the plasma membrane. *Cell*, 49(5):659–668.

Stern, W. and Dales, S. (1976). Biogenesis of vaccinia: Isolation and characterization of a surface component that elicits antibody suppressing infectivity and cell-cell fusion. *Virology*, 75(1):232–241.

Stiasny, K. and Heinz, F. X. (2004). Effect of Membrane Curvature-Modifying Lipids on Membrane Fusion by Tick-Borne Encephalitis Virus. *Journal of Virology*, 78(16):8536–8542.

Stiefel, P., Schmidt, F. I., Dorig, P., Behr, P., Zambelli, T., Vorholt, J. A., and Mercer,

J. (2012). Cooperative vaccinia infection demonstrated at the single-cell level using fluiDFM. *Nano Letters*, 12(8):4219–4227.

Sugiura, N., Jinno-oue, A., Tanaka, A., Shimizu, N., Mori, T., Kimata, K., Isomura, H., and Hoshino, H. (2013). Inhibitory Effect of Chondroitin Sulfate Type E on the Binding Step of Human T-Cell Leukemia Virus Type 1. *AIDS Research and Human Retroviruses*, 29(3):621–629.

Swanson, J. A. (2008). Shaping cups into phagosomes and macropinosomes. *Nature Reviews Molecular Cell Biology*, 9(8):639–649.

Sypula, J., Wang, F., Ma, Y., Bell, J., and Mcfadden, G. (2004). Myxoma virus tropism in human tumor cells. *Gene Therapy and Molecular Biology*, 8:103–114.

Szajner, P., Weisberg, A. S., Lebowitz, J., Heuser, J., and Moss, B. (2005). External scaffold of spherical immature poxvirus particles is made of protein trimers, forming a honeycomb lattice. *Journal of Cell Biology*, 170(6):971–981.

Takahashi, T., Kawagishi, S., Masuda, M., and Suzuki, T. (2013). Binding kinetics of sulfatide with influenza a virus hemagglutinin. *Glycoconjugate Journal*, 30(7):709–716.

Tamm, L. K., Crane, J., and Kiessling, V. (2003). Membrane fusion: A structural perspective on the interplay of lipids and proteins. *Current Opinion in Structural Biology*, 13(4):453–466.

Thorley, J. A., McKeating, J. A., and Rappoport, J. Z. (2010). Mechanisms of viral entry: Sneaking in the front door. *Protoplasma*, 244(1):15–24.

Tolonen, N., Doglio, L., Schleich, S., and Krijnse Locker, J. (2001). Vaccinia virus DNA replication occurs in endoplasmic reticulum-enclosed cytoplasmic mininuclei. *Molecular Biology of the Cell*, 12(7):2031–2046.

Townsley, A. C. and Moss, B. (2007). Two Distinct Low-pH Steps Promote Entry of Vaccinia Virus. *Journal of Virology*, 81(16):8613–8620.

Townsley, A. C., Senkevich, T. G., and Moss, B. (2005a). The product of the vaccinia virus L5R gene is a fourth membrane protein encoded by all poxviruses that is required for cell entry and cell-cell fusion. *Journal of virology*, 79(17):10988–10998.

Townsley, A. C., Senkevich, T. G., and Moss, B. (2005b). Vaccinia Virus A21 Virion Membrane Protein Is Required for Cell Entry and Fusion. *Allergy*, 79(15):9458–9469.

Townsley, A. C., Weisberg, A. S., Wagenaar, T. R., and Moss, B. (2006). Vaccinia Virus Entry into Cells via a Low-pH-Dependent Endosomal Pathway. *Journal of Virology*, 80(18):8899–8908.

Trinkaus, J. P. (1973). Activity and Locomotion Blastula of Funduhs Stages Deep Cells During and Gastrula The Fun-. *Developmental Biology*, 103:68–103.

Tsai, F. C., Stuhrmann, B., and Koenderink, G. H. (2011). Encapsulation of active cytoskeletal protein networks in cell-sized liposomes. *Langmuir*, 27(16):10061–10071.

Turner, P. and Moyer, R. (2008). The vaccinia virus fusion inhibitor proteins SPI-3 (K2) and HA (A56) expressed by infected cells reduce the entry of superinfecting virus. *Virology*, 380(2):226–233.

Ueoka, C., Kaneda, N., Okazaki, I., Nadanaka, S., Muramatsu, T., Sugahara, K., and Chem, K. J. B. (2000). Neuronal Cell Adhesion, Mediated by the Heparin-binding Neuroregulatory Factor Midkine, Is Specifically Inhibited by Chondroitin Sulfate E. *The Journal of Biological Chemistry*, 275(48):37407–37413.

Vanderplasschen, A. and Smith, G. L. (1997). A novel virus binding assay using confocal microscopy: demonstration that the intracellular and extracellular vaccinia virions bind to different cellular receptors. *Journal of virology*, 71(5):4032–41.

Vázquez, M. I., Esteban, M., Va, A.-i., and Esteban, M. (1999). Identification of functional domains in the 14-kilodalton envelope protein (A27L) of vaccinia virus. *Journal of virology*, 73(11):9098–9109.

Vermeer, P. D., McHugh, J., Rokhlina, T., Vermeer, D. W., Zabner, J., and Welsh, M. J. (2007). Vaccinia virus entry, exit, and interaction with differentiated human airway epithelia. *Journal of Virology*, 81(18):9891–9899.

Vicente-Manzanares, M., Ma, X., Adelstein, R. S., and Horwitz, A. R. (2009). Non-muscle myosin II takes centre stage in cell adhesion and migration. *Nature Reviews Molecular Cell Biology*, 10(11):778–790.

Voss, J. E., Vaney, M. C., Duquerroy, S., Vonrhein, C., Girard-Blanc, C., Crublet, E., Thompson, A., Bricogne, G., and Rey, F. A. (2010). Glycoprotein organization of Chikungunya virus particles revealed by X-ray crystallography. *Nature*, 468(7324):709–712.

Wagenaar, T. R., Ojeda, S., and Moss, B. (2008). Vaccinia Virus A56/K2 Fusion Regulatory Protein Interacts with the A16 and G9 Subunits of the Entry Fusion Complex. *Journal of Virology*, 82(11):5153–5160.

Walls, A. C., Tortorici, M. A., Snijder, J., Xiong, X., Bosch, B. J., Rey, F. A., and Veesler, D. (2017). Tectonic conformational changes of a coronavirus spike glycoprotein promote membrane fusion. *Proceedings of the National Academy of Sciences of the United States of America*, 114(42):11157–11162.

Ward, B. M. (2005). Visualization and Characterization of the Intracellular Movement of Vaccinia Virus Intracellular Mature Virions. *Journal of Virology*, 79(8):4755–4763.

Weisberg, A. S., Maruri-Avidal, L., Bisht, H., Hansen, B. T., Schwartz, C. L., Fischer, E. R., Meng, X., Xiang, Y., and Moss, B. (2017). Enigmatic origin of the poxvirus membrane from the endoplasmic reticulum shown by 3D imaging of vaccinia virus assembly mutants. *Proceedings of the National Academy of Sciences of the United States of America*, 114(51):E11001–E11009.

Wessels, L., Elting, M. W., Scimeca, D., and Weninger, K. (2007). Rapid membrane fusion of individual virus particles with supported lipid bilayers. *Biophysical Journal*, 93(2):526–538.

Whitbeck, J. C., Foo, C. H., Ponce de Leon, M., Eisenberg, R. J., and Cohen, G. H. (2009). Vaccinia virus exhibits cell-type-dependent entry characteristics. *Virology*, 385(2):383–391.

White, C. L., Senkevich, T. G., and Moss, B. (2002). Vaccinia Virus G4L Glutaredoxin Is an Essential Intermediate of a Cytoplasmic Disulfide Bond Pathway Required for Virion Assembly. *Journal of Virology*, 76(2):467–472.

White, J., Matlin, K., and Helenius, A. R. I. (1981). Cell Fusion by Semliki Forest , Influenza , and Vesicular Stomatitis Viruses. *The Journal of Cell Biology*, 89(June):1–6.

White, J. M., Delos, S. E., Brecher, M., and Schornberg, K. (2008). Structures and Mechanisms of Viral Membrane Fusion Proteins. *Critical Reviews in Biochemistry and Molecular Biology*, 43(3):189–219.

Wilton, S., Gordon, J., and Dales, S. (1986). Identification of antigenic determinants by polyclonal and hybridoma antibodies induced during the course of infection by vaccinia virus. *Virology*, 148(1):84–96.

Wolfe, C. L. and Moss, B. (2011). Interaction between the G3 and L5 proteins of the vaccinia virus entry-fusion complex. *Virology*, 412(2):278–283.

Wolfe, C. L., Ojeda, S., and Moss, B. (2012). Transcriptional Repression and RNA Silencing Act Synergistically To Demonstrate the Function of the Eleventh Component of the Vaccinia Virus Entry-Fusion Complex. *Journal of Virology*, 86(1):293–301.

World Health Organization (1980). The Global Eradication of Smallpox. Final Report of the Global Commission for the Certification of Smallpox Eradication.

WuDunn, D. and Spear, P. G. (1989). Initial interaction of herpes simplex virus with cells is binding to heparan sulfate. *Journal of Virology*, 63(1):52–58.

Yakimovich, A., Huttunen, M., Zehnder, B., Coulter, L. J., Gould, V., Schneider, C., Kopf, M., McInnes, C. J., Greber, U. F., and Mercer, J. (2017). Inhibition of Poxvirus Gene Expression and Genome Replication by Bisbenzimide Derivatives. *Journal of virology*, 91(18):1–15.

Yamauchi, Y. and Helenius, A. (2013). Virus entry at a glance. *Journal of Cell Science*, 126(6):1289–1295.

Yang, S. T., Kreutzberger, A. J., Kiessling, V., Ganser-Pornillos, B. K., White, J. M., and Tamm, L. K. (2017). HIV virions sense plasma membrane heterogeneity for cell entry. *Science Advances*, 3(6):1–13.

Yang, S. T., Kreutzberger, A. J., Lee, J., Kiessling, V., and Tamm, L. K. (2016). The role of cholesterol in membrane fusion. *Chemistry and Physics of Lipids*, 199:136–143.

Yang, Z. and Moss, B. (2009). Interaction of the Vaccinia Virus RNA Polymerase-Associated 94-Kilodalton Protein with the Early Transcription Factor. *Journal of Virology*, 83(23):12018–12026.

Yaping, C., Maguire, T., Hileman, R. E., Fromm, J. R., Esko, J., Linhardt, R., and Marks, R. M. (1997). Dengue virus infectivity depends on envelope protein binding to target heparan sulfate. *Nature Medicine*, 3(11):866–871.

Yoder, J. D., Chen, T. S., Gagnier, C. R., Vemulapalli, S., Maier, C. S., and Hruby, D. E. (2006). Pox proteomics: Mass spectrometry analysis and identification of Vaccinia virion proteins. *Virology Journal*, 3:1–16.

Young, J. T. (2001). *Fields virology*. Lippincott-Raven Publishers, Philadelphia ; London, 4th ed. edition.

Zhang, Y., Ahn, B. Y., and Moss, B. (1994). Targeting of a multicomponent transcription apparatus into assembling vaccinia virus particles requires RAP94, an RNA polymerase-associated protein. *Journal of Virology*, 68(3):1360–1370.

Zinoviev, V. V., Tchikaev, N. A., Chertov, O. Y., and Malygin, E. G. (1994). Identification of the gene encoding vaccinia virus immunodominant protein p35. *Gene*, 147(2):209–214.